UCL Université catholique de Louvain

École polytechnique de Louvain (EPL)

epl

Modeling of harmonics in the frequency range 2-150 kHz

Dissertation presented by
Guillaume SCHMIT , Louis MARION

for obtaining the Master's degree in
Electrical Engineering

Supervisor(s)
Emmanuel DE JAEGER

Reader(s)
Marc BEKEMANS , Caroline LEROI

Academic year 2016-2017

ACKNOWLEDGMENTS

These few lines to express our gratitude to all people who took part in any way to the realization of this thesis. It was a wonderful subject in which we learned a lot. Without the help of these people, we would not be able to reach my goals.

Foremost we wish to thank **Prof. Emmanuel De Jaeger** for his supervision. His knowledge and comments guiding us along the work. The comments on our work was very instructive.

We wish to thank **Caroline Leroi** for her help along the year and for correcting our report so many times.

We also would like to thank **Prof. Marc Bekemans** for giving us some help when we needed it.

Finally, we would like to express a special thanks to our families and friends who encouraged and supported us until the end.

ABSTRACT

Disturbances in the frequency range 2-150 kHz become more and more important every day. Many experiments have been done to observe and record them but less work has been done toward the modeling of these disturbances.

This work describes the implementation of a CFL (*Compact Fluorescent Lamp*) model. In order to start from its input connection, the model is composed of: EMI filter, rectifier, APFC (boost converter), half-bridge, tank circuit and finally CFL load. Three implementations are proposed:

1. A complete model in *Simulink*, simulating in the time-domain the APFC, its controller and the other components.

2. The data of interest is the current harmonics at the device input. The device current is periodic with a period imposed by the grid frequency (T = 1/50) and therefore the Fourier series of this current can be computed over this period. The EMI filter must be kept to simulate the interactions with other devices in parallel, but the rest of the model is replaced by one equivalent Fourier series.
   It enables fast computation of the current harmonics for one device, but at this stage the Simulink simulation must still be executed to compute the harmonics for several devices in parallel.

3. The last model represents the devices interactions (previously done in Simulink) based on their Kirchhoff's current equations. The system of equation is then resolved in matlab with everything after the rectifier represented again by a current source. This enables fast computation time and current harmonics can now be defined everywhere in the circuit.

The error ratio between this last simplified model and the ideal complete model are bounded between 0.9 and 1.1 allowing us to validate our model.

GLOSSARY

CFL	Compact Fluorescent Lamp
PLC	Power Line Communication
TDL	Touch Dimmer Lamp
AMR	Automatic Meter Reading
SMPS	Switched-mode Power Supply
PV	Photovoltaics
THD	Total Harmonic Distortion
PF	Power Factor
PFC	Power Factor Correction
APFC	Active Power Factor Correction
RMS	Root Mean Square
ZCS	Zero Current Switching
EMI	Electromagnetic Interference
DM	Differential Mode
CM	Common Mode
d	Duty-Cycle
ESR	Equivalent Series Resistance
PWM	Pulse Width Modulation
BW	Bandwidth
PI	Proportional-Integral
CCM	Continuous Conduction Mode
LISN	Line Impedance Stabilization Network
FFT	Fast Fourier Transform

CONTENTS

CHAPTER 1

INTRODUCTION

The power grid can be subject to all kind of disturbances (harmonics, dips, unbalance,...) caused by faults and different components in the installation. These disturbances make standardization essential to keep the grid working correctly. This work will focus on harmonic disturbances in the frequency range between 2 and 150 kHz which are often referred by the term *supraharmonics*. They are mainly generated by power electronics whose usage increases more and more every day, therefore the supraharmonics increase as well.

So far, supraharmonics have been mostly observed over very local ranges (within a house or between a couple of houses). These usually cause issues on a signal level: communication through the power grid, dimmer control,...
A couple experiments have already been led to observe and measure supraharmonics, trying to quantify their actual impact on the grid. General results obtained so far will be summarized in the *State of the Art*.

This work will try to develop a modeling procedure of equipment emitting supraharmonics to help quantify them. This procedure will be done for one kind of equipment, having a very generic structure. Simulations have been performed with Matlab Simulink environment and more specifically the SimPowerSystems toolbox .

Modeling is usually a trade-off between complexity/accuracy and time-consumption. This is the reason why the modeling procedure comes in 2 main steps:

- Complete model of the device running with Simulink
- Simplification to speed up the simulation while keeping a certain accuracy level

The structure of the overall work is divided in 4 main chapters:

1. Presentation of the studied piece of equipment and general description of its different building blocks
2. Complete model: actual design of the building blocks
3. Simplified model: replacement of the supraharmonics source by its Fourier series
4. Interaction between several equipments (primary, secondary emissions) on a grid. A frequency-based approach is used to compute the harmonics in the system theoretically enabling a fast computation time compared to the simulation with the full equipment models.

CHAPTER 2

STATE OF THE ART

This section will give an overview of what is known about harmonics in the frequency range 2-150 kHz, grouped in 5 main categories:

- Particularity of this frequency range
- Disturbance definition
- Standards and standardization
- Summary of observed and recorded disturbances
- Previous experiments

2.1 Particularity of this frequency range

Below 2 kHz: the European power grid works at a frequency of 50Hz and it was previously considered that no significant harmonics were produced above the 40th order (i.e. 2 kHz).This is why main restrictions and standardization were done below this frequency.

Above 150 kHz: standards above 150 kHz were introduced to protect telecommunication services and prevent interference produced by the grid itself.

2 - 150 kHz: as it does not belong to any of the two previous categories, no complete limitation has been done for this frequency range yet. Standards existing currently will be described in section 2.4 and examples of disturbances are given in section 2.5.

2.1.1 Purpose of the 2-150 kHz band

***Power Line Communication* (PLC):** it uses the grid installation to transmit data. It has the advantage of being easy to deploy wherever an electric installation is already present with no additional infrastructure necessary.
But as it works on usual power cables which are not always isolated and well designed for communications, there are limiting factors preventing to reach very high data rates. In a more general manner, there are 3 frequency band used for PLC system [18]:

- Ultra narrow band (UNB): below 2 kHz, very low data rate (less than 1 kbps), mostly used for smart meter readings.
- Narrow band (NB): between 2 and 500 kHz, this band is the most used one by energy companies for smart meter readings.

- Broadband (BB): also called *Broadband over Power Lines* (BPL), it goes from 500 kHz up to 30 or 50 MHz. They can reach data rates of several dozens of Mbps and they are used to bring internet to homes and small business.

NB-PLC (in the frequency band of interest) shall be further explained and subdivided in section 2.4.

In Europe today, there is an increased use of Smart meters to determine automatically the power consumption of the customers. An important number of these meters will use power line communication in the 9 to 95kHz frequency range to transmit the readings of the meters.[31]
The PLC signals are intentional emissions and are often much higher than the emissions of the equipments connected to the grid. Thus, immunity levels have to be determined for the PLC (see section 2.4).
Figure 2.1 shows the model of a communication channel from the transmitter of the PLC signal to the receiver [31]. The signal is damped by the wiring and has to cope with other signal present in the grid (see section 2.2).
A last interference is the shunting of the transmitted signal due to the low high-frequency impedance of the devices connected to the grid (EMI filter,).

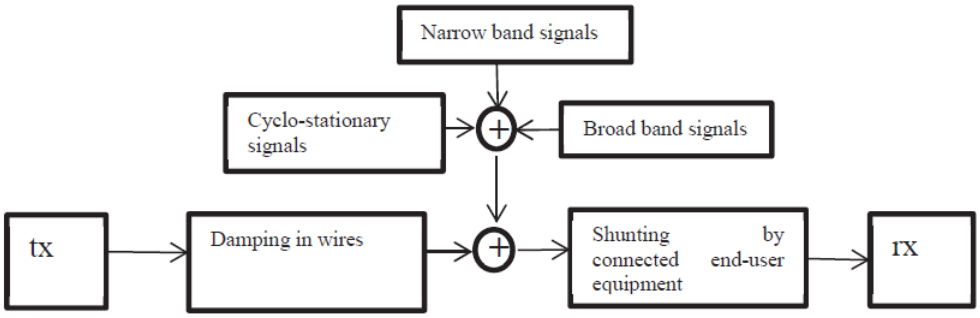

Figure 2.1: Communication channel model for a PLC signal [31]

Power electronics control: PWM (Pulse Width Modulation) control is often active in this frequency band. It is used in PV-inverters to transmit the power from the DC to the AC (grid) side.
Moreover more and more equipments (CFL > 25W), computer chargers,... use what is called an active power factor correction (APFC) to lower the low-frequency harmonic content (below 2kHz) and thus meet the standards and also to reduce the losses, weight and size [22].

A high-frequency ballast of a compact fluorescent lamp is shown in Figure 2.2. A boost APFC is used to increase the voltage to feed the lamp but for other equipments other DC/DC converter are used depending on the load (buck, buck-boost, flyback,...). The output stage of the model is a half-bridge driven resonant tank and working at switching frequencies from 30 to 90kHz. Except at the start of an equipment, the output stage can be considered as a constant load.
A detailed analysis and implementation of such a model will be done in this work.

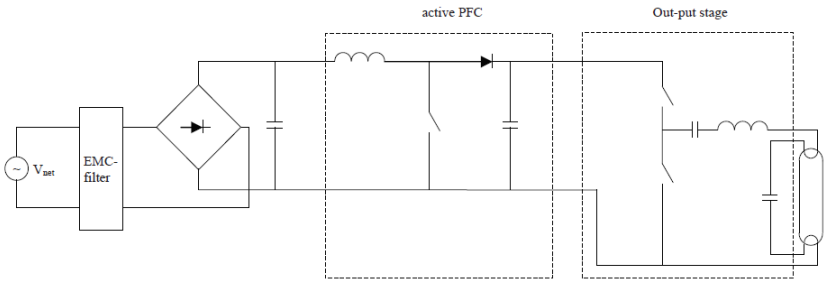

Figure 2.2: CFL model [22]

2.2 High-frequency components

A lot of measurements have been performed in low-voltage networks and in the 2-150kHz range the three following frequency components can be observed [22]:

Narrowband components : Signals with a small bandwidth (smaller than 4 or 5 kHz depending on the definition). These components are present due to power-line communication.

Broadband components : Signals with a larger bandwidth due to the electronic ballast in end-user equipments: Solar panels, APFCs,... .

Recurrent oscillations: Damped oscillations that occur repeatedly due for example to "dead-beat" near the zero crossing as shown in Figure 2.3 . These oscillations are also due to the power electronics of the equipments.

The two last signals are illustrated in Figure 2.3. The broadband signal comes from the ripple observed on the peak of the input current. The recurrent oscillations are due to the "deadbeat" near the zero crossing and will add a large frequency band in the lower frequency range.
Of course, the frequency components will depend on the APFC type (converter type, controller mode,...) and are not always as described in Figure 2.3.

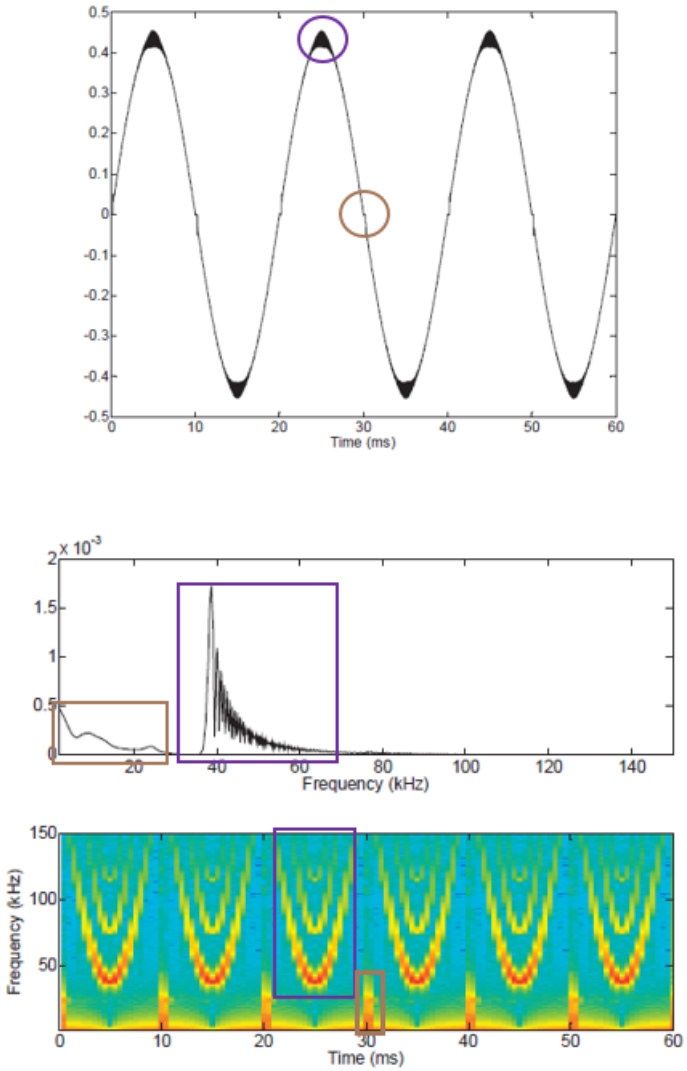

Figure 2.3: Signal in time-domain (first graph), in frequency domain (next one) and spectrogram of the signal (last graph) showing the broadband components (purple) and recurrent oscillations (brown) [22]

2.3 Disturbances definition

Tolerance to disturbances will depend on electromagnetic compatibility (EMC) of an equipment. The following definition of EMC is given in [40] and based on IEC-60050 standard:

EMC is the ability of a device, unit of equipment, or system to function satisfactorily in its electromagnetic environment without introducing intolerable electromagnetic disturbances to anything in that environment.

This means that EMC is a combination of both *emission limit* and *immunity limit*.

Emission limit: a piece of equipment cannot introduce electromagnetic disturbances at a higher level than its *emission limit*.

Immunity limit: a piece of equipment must be able to tolerate electromagnetic disturbances at lower level than its *immunity level*.

All of this is synthesized in figure 2.4.

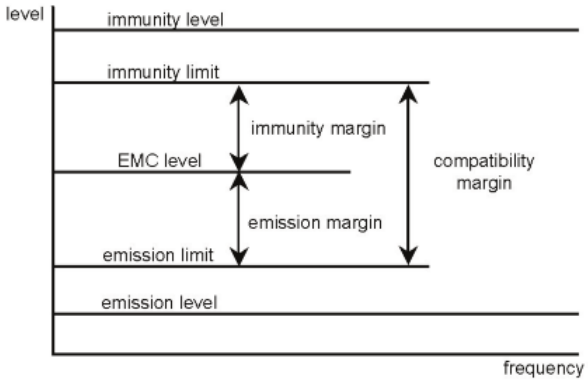

Figure 2.4: EMC summary [25]

2.4 Standards and standardization

Standards and regulation about EMC are given by IEC (*International Electrotechnic Commission*), CISPR (*Comité International Spécial des Perturbations Radioélectriques*) and CENELEC (Comité Européen de Normalisation Electrotechnique) which delivers EN (European Normalization). There are different measurement methods depending on the detector type:

- **Peak detector:** *its output voltage is the peak value of an applied signal.* [4]
- **Quasi-peak detector:** *a detector having specified electrical time constants which, when regularly repeated identical pulses are applied to it, delivers an output voltage which is a fraction of the peak value of the pulses, the fraction increasing towards unity as the pulse repetition rate is increased.* [4]
- **Root-mean-square detector:** *its output voltage is the r.m.s. value of an applied signal.* [4]
- **Average detector:** *its output voltage is the average value of the envelope of an applied signal.* [4]

2.4.1 Global regulation

IEC 61000-3

Part 2: Limits for harmonic current emissions.
Part 3: Limitation of voltage changes, voltage fluctuations and flicker in public low-voltage supply systems, for equipment with rated current $\leq$ 16 A per phase and not subject to conditional connection

2.4.2 Emission regulation

EN 50065-1

CENELEC standard authorizing PLC communication in the frequency band 3-148.5 kHz (see limits in figure 2.6). As stated earlier, this band corresponds to a part of the Narrowband PLC (NB_PLC). It is further sub-divided in 4 bands:

	Frequency [kHz]	Description
Band A	3 - 95	Usage limited to energy provider (for smart-meter,...)
Band B	95 - 125	For customers, no application specified
Band C	125 - 140	For customers, local network with *CSMA/CA* protocol (Carrier Sense Multiple Access/ Collision Avoidance)
Band D	140 - 148.5	For customers, security systems

Table 2.1: Cenelec Band ([3])

N.B: this standard is for Europe. Outside of Europe, the standard IEC 61000-3-8 allows frequencies up to 525 kHz.

CISPR 11 / EN-55011 [5]

Limits non-intentional emissions for industrial, scientific, medical and household equipment in the frequency range below 400 GHz (see figure 2.6).

This limitation was separated for 2 groups of equipments depending on the frequency:

- Group 1: Devices emitting in the range below 9kHz
- Group 2: Devices emitting above this range

Each group was then subdivided into 2 classes depending on the power:

- Class A: Industrial devices, not directly connected to a low power supply voltage which supplies domestic environment.
- Class B: Domestic devices, directly connected to a low power supply voltage.

The EN-55011 standard limits the disturbances above 150kHz that could interfere with the radio communication. Figure 2.5 shows the Quasi-peak limits for conducted emissions (150kHz-30MHz) for Class A and Class B devices.
Requirements for the radiated emissions in the 30MHz-1GHz range have also to be met.

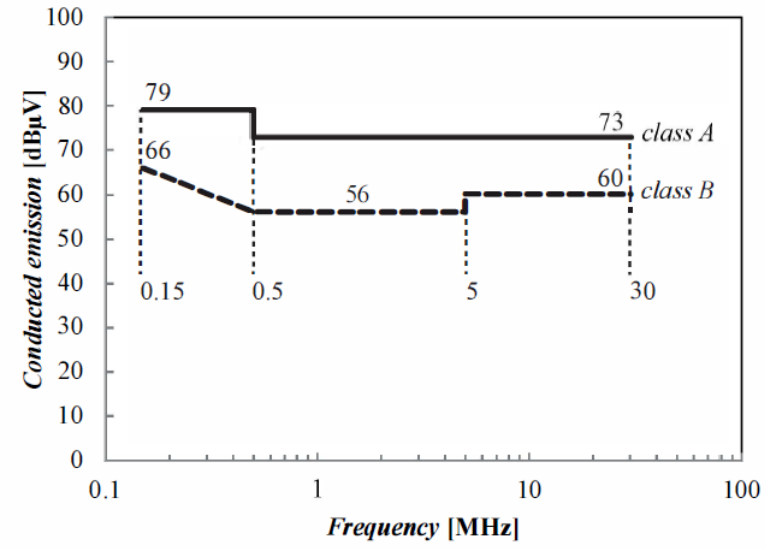

Figure 2.5: Quasi-peak limits for conducted emissions (EN-55011) [27]

CISPR 15 / EN-55015 [6]

Limits for non-intentional emissions from lighting equipment (see figure 2.6) in the 9kHz-300MHz band.
This standard covers a part of the 2-150kHz band that is considered in this work, but is only valid for lightning equipments.
The following devices can be cite as example:
Street LED lighting devices, table lamps, office lighting equipment, etc. .

There is no classification for covered devices, but there are requirement for the frequency ranges:

- Conducted emissions for main ports: limits in frequency range 9kHz-30MHz
- Conducted emissions for load terminals and controls terminals: limits in frequency range 50kHz-30MHz
- Radiated emission: limits in frequency range 9kHz-300MHz

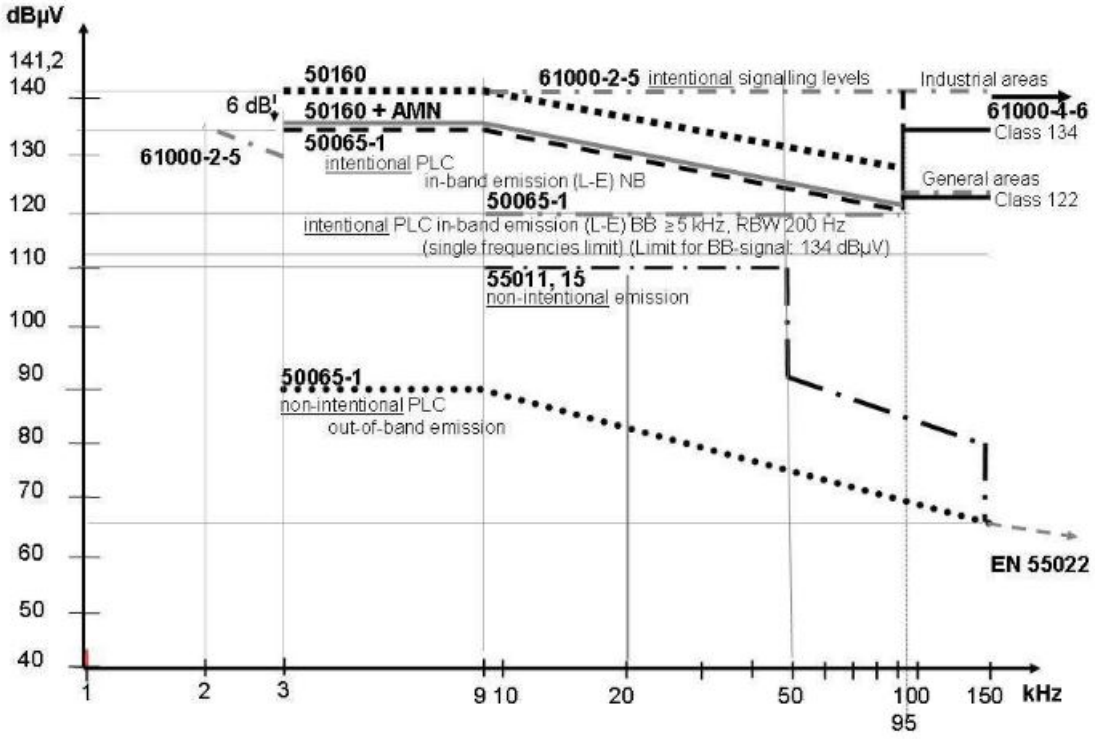

Figure 2.6: Emission limits [16]

2.4.3 Immunity regulation

IEC 61000-4-16 [8]

It provides test methods for immunity requirements to common mode disturbances up to 150 kHz. Defined elements are:

- Test voltage and current waveforms
- Range of test levels
- Test equipment
- Test set-up
- Test procedures

These disturbances are usually produced by the power distribution system and power electronic equipments.

IEC 61000-4-19 [9]

In addition to *IEC 61000-4-16*, this standard provides test methods for immunity requirements to differential mode disturbances in the range 2kHz to 150kHz.

The tests are done with a sweep of continuous waves pulses at different frequencies.

2.5 Summary of observed and recorded disturbances

Here is non-exhaustive list of recorded malfunctioning equipment due to supraharmonics from *CENELEC* report on Electromagnetic Interference [16]:

- Germany:
  - Source of interference: Smart meter
  - Victim: Touch dimmer lamp (TDL)

  After the installation of smart meter in a test area, a customer complained because two touch dimmer lamps were switching on and off in an uncontrolled manner.
  Some laboratory test have been conducted verifying this complained EMI case.

- Germany:
  - Source of interference: PV-inverter
  - Victim: Smart meter reading

  Some measurements tests in a plant as well as in laboratory showed that the electronic meters displayed an energy level of $\approx 18.5\%$ below the real energy fed into the grid by the PV-inverter.

- Finland:
  - Source of interference: Automatic meter reading using PLC for data transmission
  - Victim: street lighting and traffic light control

- Finland:
  - Source of interference: frequency converters of small industrial plant
  - Victim: AMR (*Automatic Meter Reading*) control

  In this case, the transformer station was not able to communicate with all smart meters due to the frequency converters (PWM switching impulse disturbances) of the small industrial plant located next to the station.

- EM interactions between AMR-PLC and household equipment:
  - Ceramic hob: faster clock (+15 min/day)
  - Coffee machine: unwanted signal for filter change
  - Washing machine: re-start of washing program

In a more general manner, equipment acting as sources or victims of these interference are listed in table 2.2.

Sources	Victims
Inverter	AMR-PLC
SMPS	Electronic control
Lighting equipment	Communication systems
Household equipment (induction cooker, washing machine,...)	Contactless magnetic card readers
AMR-PLC	Road vehicle smart keys
...	...

Table 2.2

2.6 Previous simulations and experiments

Many experiments have already been realized in the domain of HF harmonics and here are listed the main observations up to now:

2.6.1 PV-inverters

Inverter on one phase [24]

The inverter model chosen in this paper uses a Pulse Width Modulation (PWM) control. It is a common method that decreases the low-harmonic frequency content but on the other hand increases the high harmonics (>2kHz) .
The model is shown in 2.7 and uses a L filter at the AC side to reduce the 2-150kHz frequency disturbances.

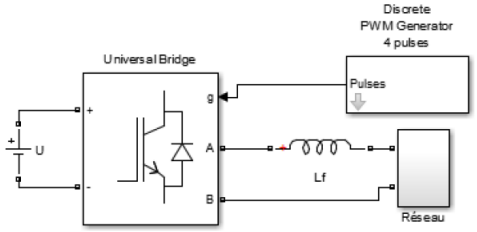

Figure 2.7: Inverter Model [24]

To analyze the high frequency content, a high frequency (HF) model has to be used for the lines. It has two big differences with the low frequency model:

- Capacitors are not neglected

- The resistances are higher due to the skin effect

The commercially available PV inverter have their commutation frequency that ranges between 15 and 20kHz. Therefore a 17.5kHz switching frequency has been chosen.
For a 2-arms inverter, the harmonic frequencies will be at $2m \pm 1$, $2m \pm 3$, $4m \pm 1, etc.$. The highest harmonic will thus be the 34.95kHz harmonic. This harmonic measured at the transformer terminal phase and depending on the feeder length is shown in Figure 2.8 .
The feeder length has an important impact on the harmonic level and the worst case seems to be for a 750 meter length for this converter (17.5kHz switching frequency and L filter of a given value).

It has to be noted that the 34.95kHz harmonic is not always the highest one due to resonance that can amplify the further harmonics.

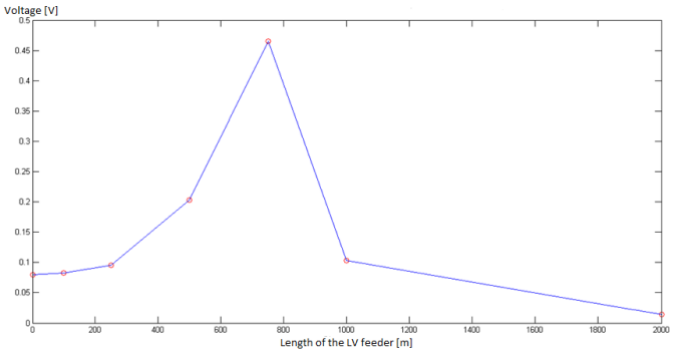

Figure 2.8: 34.95kHz harmonic voltage at the transformer terminal [24]

Several inverters on the same line [24]

Interaction between disturbances from several inverters has also been studied.
The following points have been observed:

- *For several inverters connected not far away from each other, the disturbances can become quiet high.* [24]
- *The most unfavorable case happens when all inverters are located at the same place. However, if the inverters have different commutation frequencies, we will obtain harmonics due to each commutation frequency whose magnitudes are the same order of magnitude as the case of one inverter.* [24]

Interaction between a PV-inverter and a device [32]

In this paper ([24]), the interaction between a PV panel and a TV connected to the grid has been simulated. The model used for the PV is a current source in parallel with a capacitor (capacitor of the EMI filter at the grid side).

The transfer function of the grid voltage compared to the PV current has been computed and a resonance appears at a given frequency. The resonant frequency can vary greatly (many kHz) depending on the cable length as it can be seen in figure 2.9.

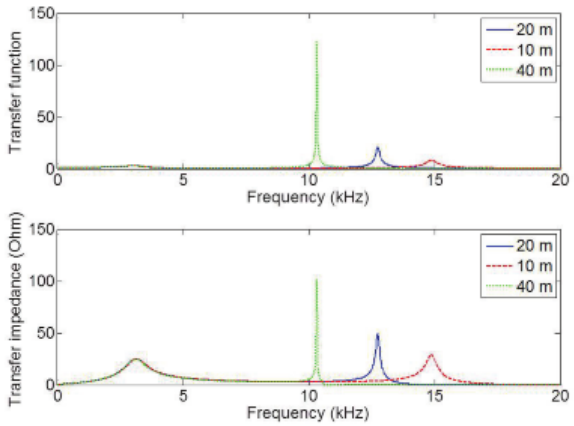

Figure 2.9: Resonance frequency relative to cable length

It has also been shown in [26] that common mode resonance is likely to occur in the frequency range of interest between parallel connected EMC-filters.

2.6.2 Lamps

In paper [30] , the effect of the replacements of incandescent lamps with energy saving lamps such that compact fluorescent lamps (CFL) and LEDs have been analyzed. The tests were conducted in a laboratory with ordinary household equipments (TV, computers, heating and kitchen equipment). This change from a resistive to a more complex electronic load will have the following impacts [30]:

+) Reduction in active power consumption and in distribution-system losses.

-) Increase of the harmonic current distortion but this increase is rather small. The other bigger equipments like the heat pump and the dish washer, impacts much more the harmonic distortion than the replacement of the incandescent lamps.

Finally the high frequency currents emitted by the energy saving lamps (CFL, LED's) seems to flow more between equipments than into the grid.

2.6.3 Peak ripple and zero-crossing

As presented in section 2.2, two main non-idealities are produced by an APFC: HF ripple and zero-crossing distortion, but these disturbances evolve differently with the number of devices.

HF ripple: its highest value is around peak voltage of the fundamental. The ripple value seen by the grid decreases with the number of devices because there is a variety in spectrum between individual devices resulting in cancellation between them.

Zero-crossing distortion: it increases almost linearly with the number of devices because the timing for zero-crossing is set by the grid and is therefore the same for every device [23]

2.6.4 Subdivision of the frequency band: below and above 9 kHz

Emission measurements of multiple fluorescent lamps with high-frequency ballasts have shown that the Total Harmonic Distortion (THD) reduces for frequency above 9kHz relatively to the number of lamps while the THD for frequency between 2kHz and 9kHz remains constant relatively to the number of lamps[21].

CHAPTER 3

GENERAL DESCRIPTION

As stated before, the goal is to model supraharmonics created by power electronics, but focusing only on one kind of device. A *Compact Fluorescent Lamp* (CFL) was chosen for its generic type whose model can be found in Figure 3.1 .
A lot of other devices as for example induction cooker, car charger (with a full-bridge instead of a half-bridge),... have a similar model.

This model is constituted of 3 main blocks:

EMI filter: passive filter to guarantee enough attenuation of harmonics higher than 150 kHz. Well-defined standardization already exists providing the necessary degree of attenuation for these harmonics to ensure the proper functioning of telecommunications services.

AC-DC converter/ Power factor correction: the CFL must be fed by a high-frequency current, but it is better to first convert the 50Hz voltage from the grid into a DC voltage before converting it back to a higher frequency voltage. Otherwise a big transformer is needed to transform from the line frequency to a higher frequency (increased size and cost).
This conversion is done through a 4-diode bridge rectifier followed by a boost converter. This boost converter is also there to get a power factor as close as possible to unity, leading to a reduction of the low-frequency harmonics.

CFL block (DC-AC converter): taking the DC-voltage provided by the boost converter, it converts it into a high-frequency sinusoidal voltage to feed the CFL represented by a resistive load.

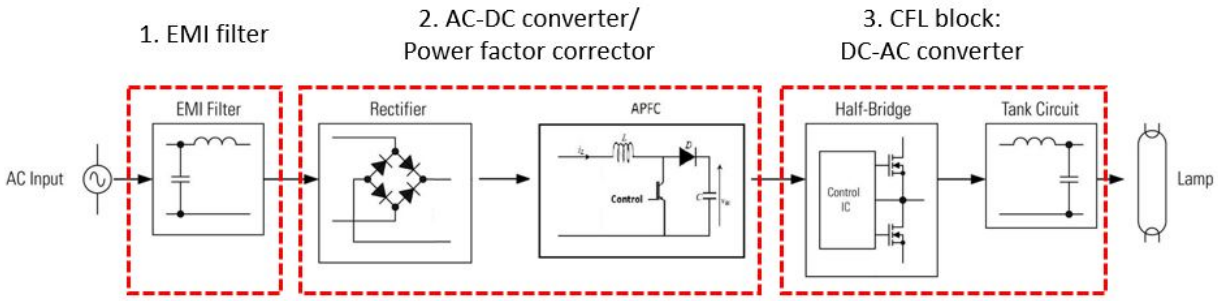

Figure 3.1: Complete model of a CFL lamp

The rest of this chapter will consist in a more accurate description of these 3 blocks and the role they must play in the device.

3.1 DC-AC converter

Combination of half-bridge and tank circuit are used to create a high-frequency pulse voltage and sinusoïdal current from the DC voltage to feed the lamp.

3.1.1 Half-bridge

A half-bridge is composed of two transistors working in reciprocation controlled through PWM (Pulse Width Modulation) to create a pulse voltage between 0V and V_{out} from the APFC. Working in reciprocation means it will switch between both situations seen in figures 3.2 and 3.3.

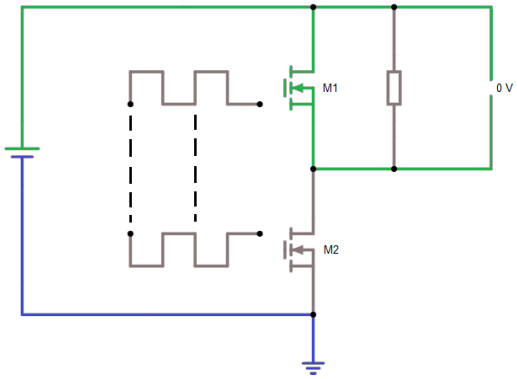

Figure 3.2: M1 closed and M2 open
$\Rightarrow \Delta V_{out} = 0V$

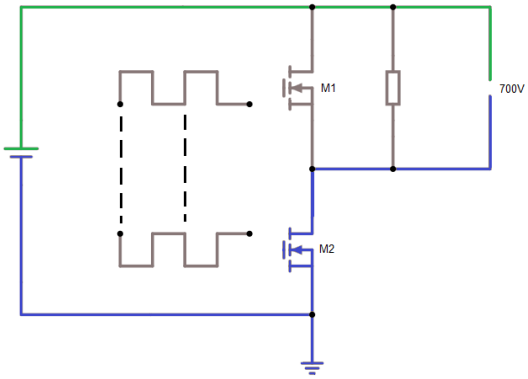

Figure 3.3: M1 open and M2 closed
$\Rightarrow \Delta V_{out} = 700V$

Half-bridges are usually not used by themselves because it asks for a lot of power to make such pulses. To prevent peak power consumption during commutations, a tank circuit is added after the half-bridge.

3.1.2 Tank circuit

The main idea of the tank circuit is to create a resonance effect at the switching frequency of the half bridge to transform the square pulse current to a sinusoidal one. This will the advantage of a current almost equal to 0 at transition (transistors closing or opening) leading to low commutation losses.
This is known as *Zero Current Switcthing* (ZCS).

A simple one can be implemented with an LC circuit and its transfer function gives a maximum gain at the switching frequency of the half-bridge (see figure 3.4).

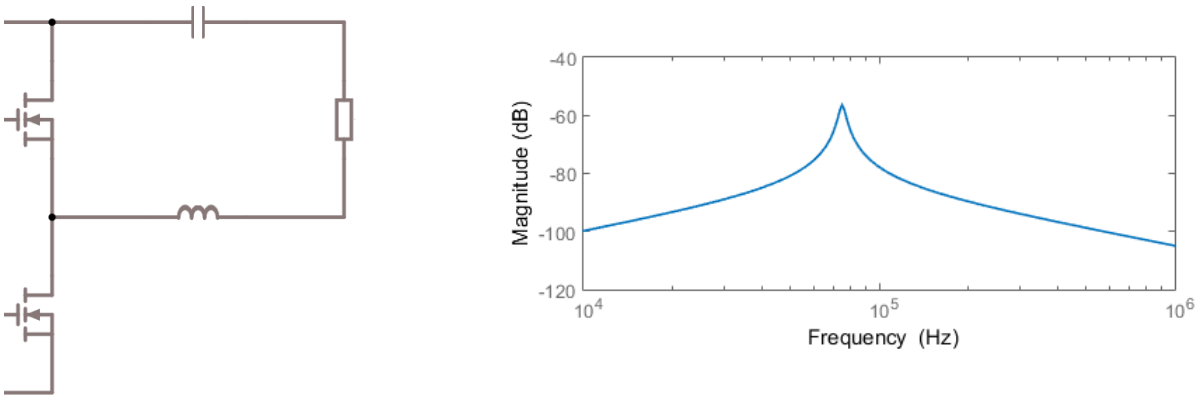

Figure 3.4: Tank circuit implementation (left), transfer function ($\frac{I}{V}$) (right)

3.1.3 Importance of the CFL in the model

Even though the DC-AC converter feeding the CFL might produce harmonics in the range of this study, their effect can be considered as negligible when measured at the device input because they will be attenuated through the APFC. This hypothesis will be proven later on (see section 5.1.2) after the APFC model has been developed. This means that the CFL block could be replaced by a constant load asking for the same mean current for general modeling.

3.2 AC-DC converter

The basic idea to obtain a DC voltage is to use a rectifier followed by a capacitor but this creates current peaks at connection times, when $V_{in} > V_C$ (see figure 3.5).
A bigger capacitor will discharge slower and lead to a more constant DC voltage, but it will reduce the connection times and creates stronger current peaks.

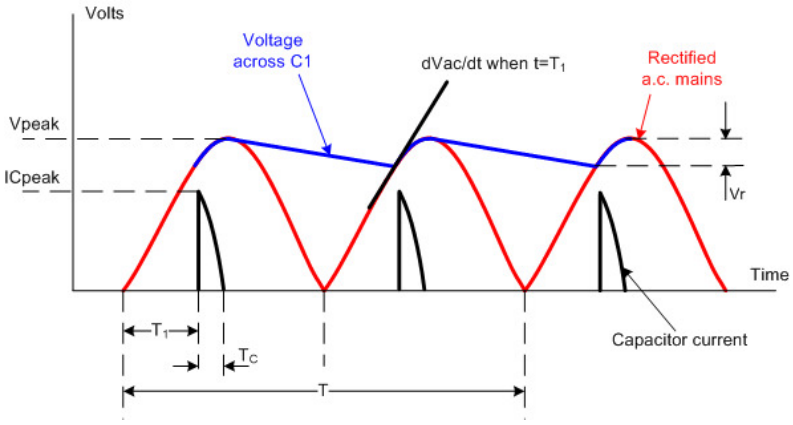

Figure 3.5: Voltage and current wave for a rectifier with only a capacitor at the output[1]

The issue is that strong current peaks create lots of low-frequency harmonics that cannot be tolerated. So a trade-off is necessary between limiting the voltage ripple on the capacitor and limiting the peak currents.
Other circuits called power factor correction can be used to increase the power factor, therefore reducing the low-harmonic pollution while maintaining a low voltage ripple.

Power Factor: The difference between voltage and current shape is characterized by the power factor and its general definition is given by [19] [36]:

$$PF = \frac{\text{Active power (P)}}{\text{Apparent power (S)}} = \frac{P}{V_{RMS}\ I_{RMS}} \tag{3.1}$$

with $P = \frac{1}{T} \cdot \int_T v \cdot i\ dt$,
and the RMS values defined as $V_{RMS} = \sqrt{\frac{1}{T} \int_T v^2\ dt}$ and $I_{RMS} = \sqrt{\frac{1}{T} \int_T i^2\ dt}$
For a sinusoidal input *voltage*, Equation 3.1 can be simplified [19]:

$$PF = \frac{V_{1,RMS} \cdot I_{1,RMS} \cdot cos(\Phi_1)}{V_{1,RMS} \cdot I_{RMS}} = \frac{I_{1,RMS}}{I_{RMS}} cos(\Phi_1) \tag{3.2}$$

where V_1 and I_1 are the fundamental components of the voltage and the current.
The first factor ($\frac{I_{1,RMS}}{I_{RMS}}$) is named the **distortion factor** and $cos(\Phi_1)$ the **displacement factor**.
The effect of both factors are shown in Figure 3.6.

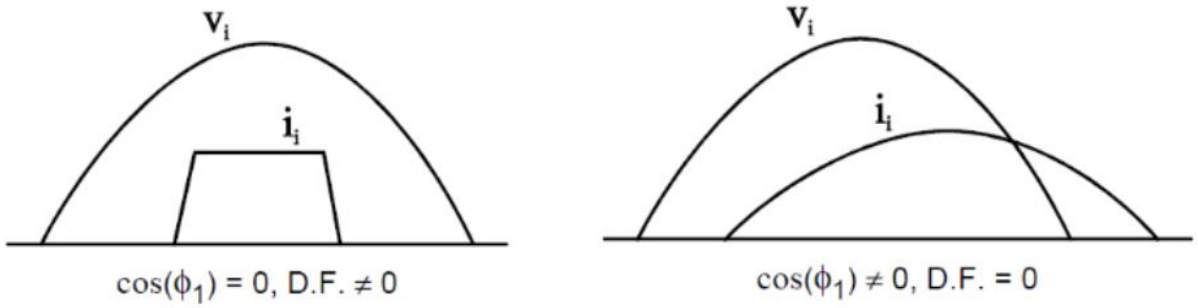

Figure 3.6: Effect of the distortion (D.F.) and displacement factor ($cos(\Phi_1)$) [19]

A power factor of 1 (best case) implies [19] :

- $cos(\Phi_1) = 1 \Rightarrow \Phi_1 = 0°$: no phase shift between current and voltage fundamental component.
- $\frac{I_{1,RMS}}{I_{RMS}} = 1 \Rightarrow I_{RMS} = I_{1,RMS}$: no harmonic content (except fundamental) for the current waveform.

It can be mentioned that the distortion factor is linked to the total harmonic distortion (THD) by [36]:

$$DF = \frac{1}{\sqrt{1 + \left(\frac{THD(\%)}{100}\right)^2}} \tag{3.3}$$

Note: When the input voltage and current are in phase (displacement factor = 1), this link can be applied to the power factor (PF).

It is important to have a good power factor to reduce the low-frequency harmonic pollution and to be compliant with the standards. This harmonic pollution can cause overheating in the transformers and in the neutral line in three-phase systems.[2]
Moreover for a given source, the available active power is higher when the power factor increases.

Several techniques are used to correct the power factor. They can be divided into two big classes: **Passive** Power Factor Correction and **Active** Power Factor Correction (APFC).

In our model, an APFC is used and more precisely, an APFC based on a **boost converter**. The converter and its controller designs will be described in chapter 4.

The end of this section consist in a classification of the different types of *active* and *passive* PFC (see figure 3.7) as well as a few examples of passive PFC circuits.

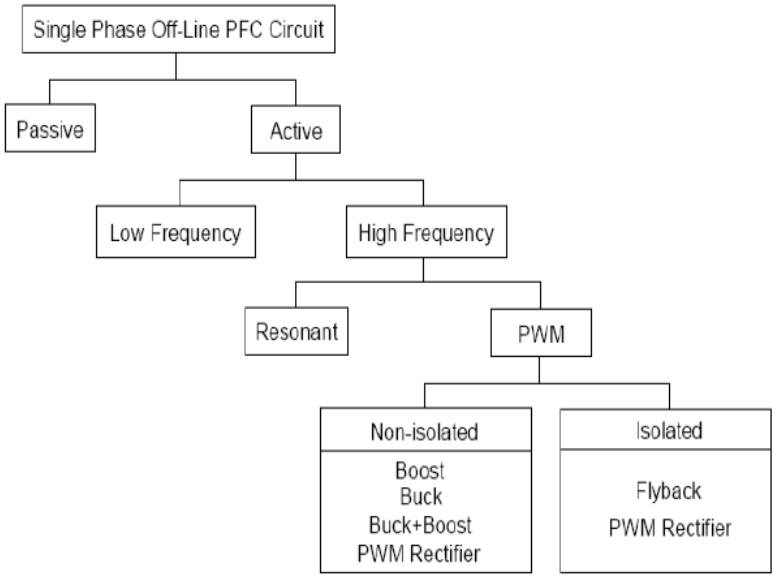

Figure 3.7: Single-phase PFC topologies [36]

3.2.1 Passive power factor correction [36]

In this section several passive PFC circuits are described to give an overview of these power factor correction methods.

One of the simplest method is to use an inductor on the AC side (before the rectifier) as described in Figure 3.8 . With this method a maximum power factor of 0.76 can be obtained.

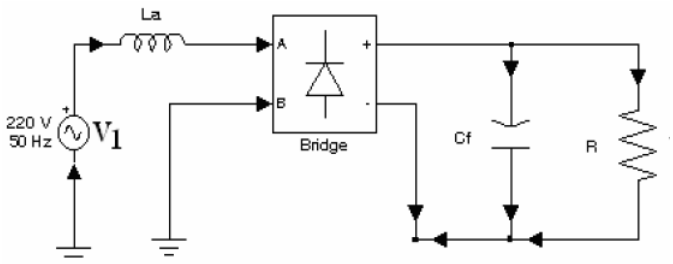

Figure 3.8: Passive PFC with AC-side inductor [36]

Another possibility is to place the inductor on the DC side (after the rectifier).
When the inductance becomes very large, the current passing through it becomes constant and the current waveform seen on the AC-side will have a square shape . Thus a theoretical power factor of 0.9 can be achieved.
For smaller inductances, the current becomes discontinuous and the maximum power factor will be the same as in the previous case (around 0.76). However adding a capacitor on the AC-side, as described in figures 3.9 and 3.10, improves the displacement factor and a maximum power

factor of 0.905 can be obtained.

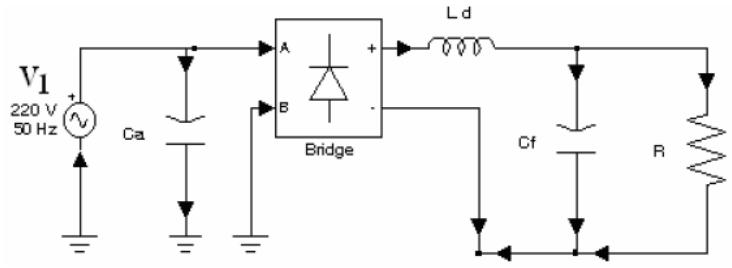

Figure 3.9: Passive PFC with DC-side inductor [36]

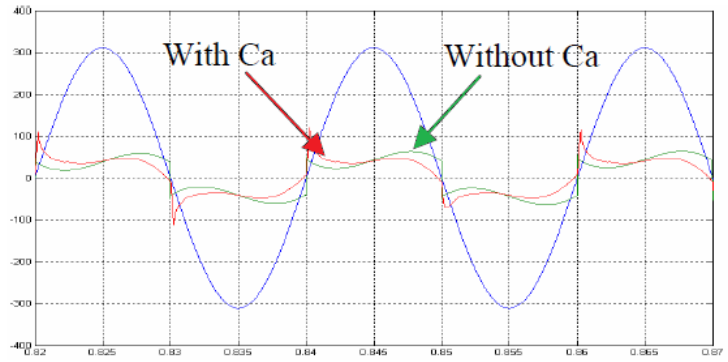

Figure 3.10: Voltage and current waveforms without C_a (PF=0.839) and with C_a (PF=0.904) ($L_d = 275mH$, $C_a = 4.8\mu F$, $R = 500\Omega$, $C_f = 470\mu F$, $V_1 = 220V_{RMS}$) [36]

Another set of methods use passive input filters to improve the power factor.
A series-resonant band-pass filter tuned at the line frequency is used in Figure 3.11. It filters out the higher harmonics but at the line frequency big passive elements are needed.
A band-stop filter tuned at the third harmonic can also be used (see figure 3.12), lowering the component sizes compared to the band-pass filter.

As simulated in [36], power factors higher than 0.9 can be obtained (0.969 for the first one and 0.918 for the second one).

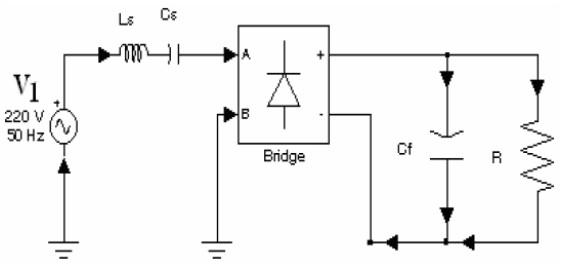

Figure 3.11: Passive PFC with band-pass filter [36]

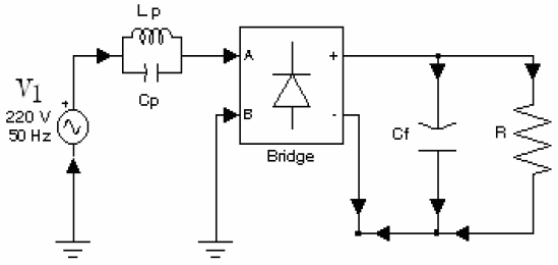

Figure 3.12: Passive PFC with band-stop filter [36]

Finally the PF can be improved using harmonic trap filters, that filters out some given harmonics. In the figure below (3.13), 2 harmonic filters are tuned at the 3^{rd} and 5^{th} harmonic aking it possible for a power factor of 0.99 to be obtained.

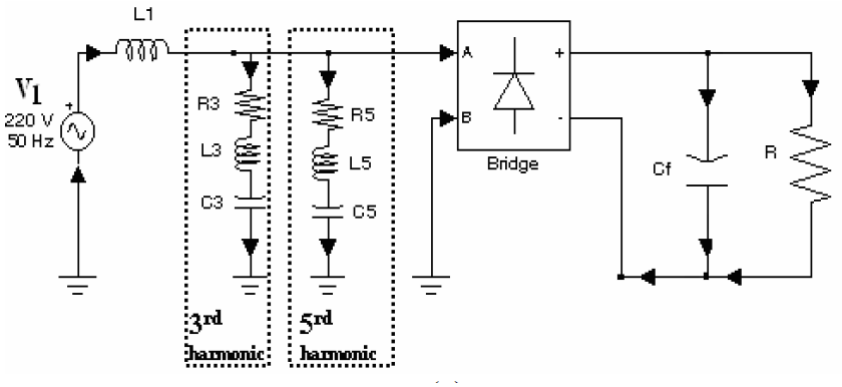

Figure 3.13: Passive PFC using trap filters [36]

As described in this section, different passive PFC circuits can be used and a power factor close to 1 can be achieved.
The advantages of passive PFC's is the simplicity and the reliability. However, the main drawback is the size (and so the cost and the area) of the reactive elements, because their value depends on the line frequency (50Hz).
Moreover, the current shape and so the power factor will depend on the load.

Nowadays more and more active power correction circuits (APFC) are used due to their efficiency and the decreasing price of such circuits. This leads to more disturbances and explains the interest of modeling their harmonics production.

3.3 EMI Filter

The EMI (Electromagnetic Interference) filter is an important part of a power electronic system. Its purpose is to reduce the noise and harmonic content above 150kHz, therefore limiting the disturbances with the radio communications.
There are two types of electromagnetic interference [35]:

- Radiated EMI: radiated by an equipment and measured in the far field using antennas.

- Conducted EMI: present in the conductors and measured at the input of the equipment using a line impedance stabilization network (LISN).

3.3.1 Conducted emissions

Only the conducted EMI will be considered for this work.
For those, a standard in the 150kHz-30MHz frequency band (CISPR 22) has to be fulfilled. As introduced in 2.4, the equipments are divided into 2 classes:

- Class A: equipments used in an industrial environment.

- Class B: equipments used in a residential environment.

There are two kind of conducted noise sources: common mode and differential mode noise. Figure 3.14 shows a typical EMI filter topology filtering both types of noise sources.

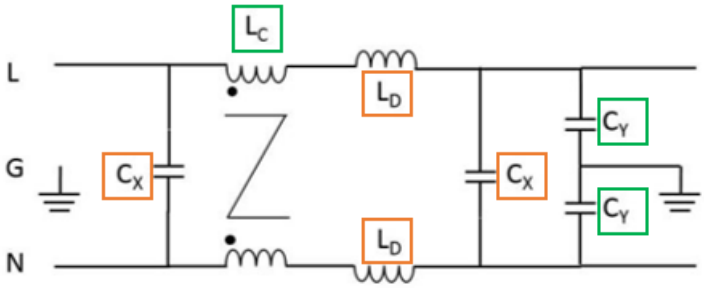

Figure 3.14: Typical EMI topology (modified from [34])
Green: common mode, Orange: differential mode

Common mode noise

Noise between the line, neutral and the ground. The noise in the line and in the neutral flows in the same direction and comes among others from the parasitic capacitors of the equipment with the ground on PCB, ...

This noise is filtered out by the L_c inductor and both C_y capacitors. The coupled inductors L_c work like an inductor for the common mode noise and like simple wires for the differential noise due to the cancellation of the magnetic fluxes [10]. This is explained in the figure below where a choke is used (fig. 3.15).

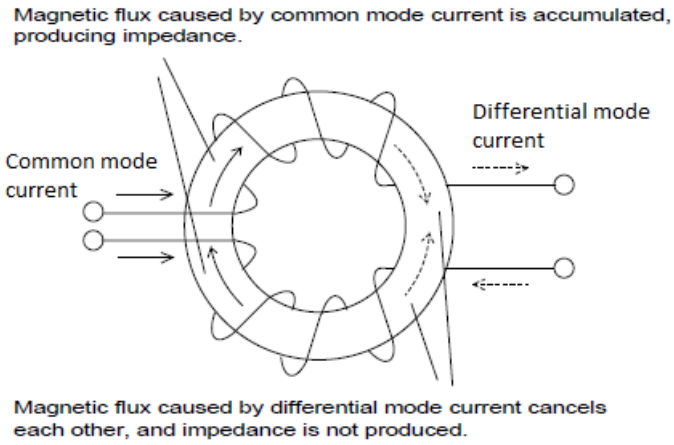

Figure 3.15: Common and differential mode noise through a choke [10]

Differential mode noise

Noise between the line and the neutral. The noise in the line and in the neutral flows in opposite directions and essentially comes from the high switching frequencies of the equipment (APFC, half-bridge, ...).

This noise is filtered out by the L_d inductors and C_x capacitors. The leakage inductance of L_c and the C_y capacitors will also have an effect but for usual sizing values, C_y is negligible. L_{leak} might also be negligible depending on the coupling factor, otherwise it must be evaluated and taken into account.

CHAPTER 4

COMPLETE MODEL

This section will provide a complete design methodology for the entire device: CFL block, APFC/rectifier and EMI filter. The boost functioning principle will also be described and its variations relative to a couple of non-idealities.

The purpose is to show the Simulink implementations, find the sizing of all passive elements alongside the coefficients and constants for the APFC controller.

4.1 CFL

4.1.1 Tank circuit: sizing

First, the resistance (output load) has to be determined for a given output power P_o (this power is equal to the input power minus the losses between the input and the tank circuit). For a good resonant circuit, the fundamental component of the square signal will be kept and the higher harmonics removed or highly attenuated. Moreover at the resonant frequency the impedance of the resonant tank is simply equal to the resistance.
We have therefore:

$$R = \frac{V_{1_{hb}}^2}{P_o} \tag{4.1}$$

For a square wave between 0 and V_{DC}, the fundamental component of the voltage is equal to (RMS value):

$$V_{1_{hb}} = \frac{1}{2} \cdot \frac{4}{\pi} \cdot \frac{1}{\sqrt{2}} \cdot V_{DC} \tag{4.2}$$

For a $150W$ device and an output voltage of the boost APFC of $V_{DC} = 700V$ we get $R = 662\ \Omega$.

Now, the tank inductor and capacitor have to be determined. The following relation links both component for a given resonance frequency:

$$2\pi f_r = \frac{1}{\sqrt{L_{tank} C_{tank}}} \tag{4.3}$$

Another important characteristic of a resonant tank circuit is its quality factor Q: measure of sharpness of the resonance (see figure 4.1). Because the resistance is fixed, the maximal amplitude (at the resonant frequency) is the same for the different Q factors. Only the bandwidth will decrease when the quality factor increases.
The quality factor can be defined as [12]:

$$Q = \frac{f_0}{\Delta f|_{-3dB}} \tag{4.4}$$

where $\Delta f|_{-3dB}$ is the bandwidth at half of the maximum amplitude(see figure 4.2).

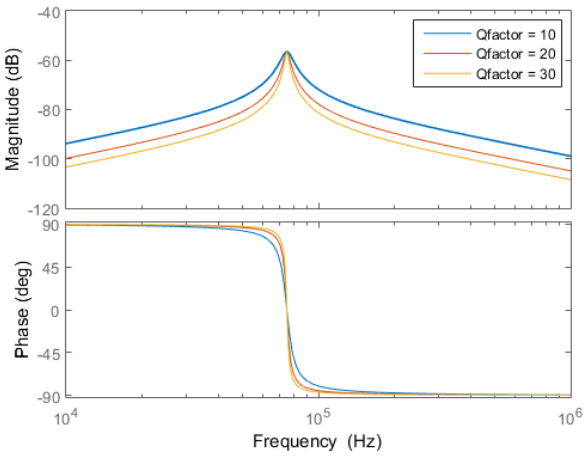

Figure 4.1: Transfer function $I_{tank}/V_{1_{tank}}$ depending on the quality factor

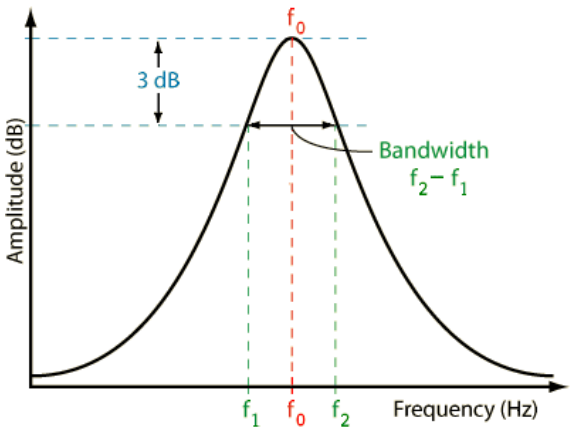

Figure 4.2: Definition of the quality factor: illustration of $\Delta f|_{-3dB}$ [11]

For a series resonant tank circuit [12]:

$$Q = \frac{2\pi f_r \cdot L_{tank}}{R} \tag{4.5}$$

A Q-factor is usually greater than 10 and was set to 20 for our design. From equation 4.5, we get an inductance of 28.1 mH for a resonant frequency of $f_r = f_{hb} = 75kHz$.

Finally the capacitor can be calculated using equation 4.3: $C_{tank} = \frac{1}{(2\pi f_{hb})^2 L_{tank}} = 16\ nF$.

4.1.2 Input voltage and current

As it was described in section 3.1.2, the tank circuit enables *Zero Current Switching* to reduce power consumption due to commutations. This can be observed at the red circles in figure 4.3, where the current is close to 0 at voltage commutation times.

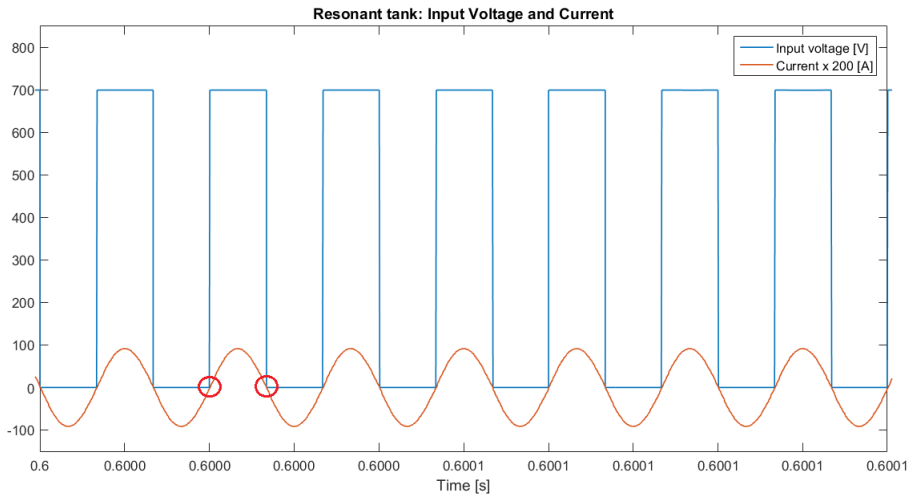

Figure 4.3: Tank circuit: input voltage and current (peak current)

4.2 APFC: boost converter

APFC: Active Power Factor Correction
The APFC used here is a boost converter and there will be first a short description of its functioning principle, an approximation of the waveforms in the circuit and what are the hypothesis necessary to make these approximations. Moreover a few non-idealities will be introduced while making sure the previous hypothesis are still met.

The boost converter works in 2 steps (3 if discontinuous) over one period which are illustrated in figure 4.4.

- Step 1: transistor is ON; inductance is charging (positive voltage); capacitor is disconnected from input because of diode and slowly discharging while feeding the load.
- Step 2: transistor is OFF; inductance is discharging (negative voltage because $V_{out} > V_{in}$); capacitor is charging.

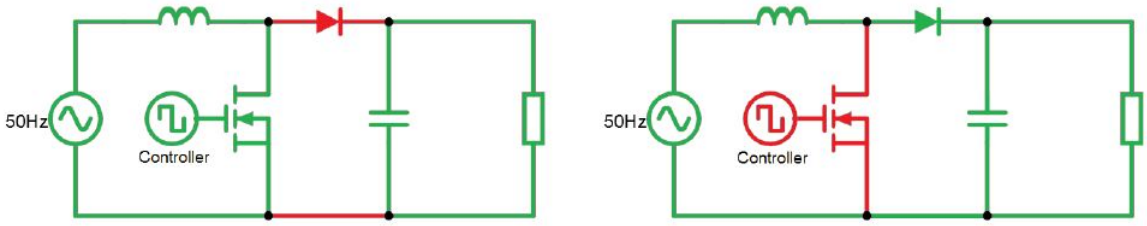

Figure 4.4: Step 1 (left) , Step 2 (right)

The inductance current increases during step 1 (inductance charging) and decreases during step 2 (inductance discharging). The time constant for the inductance is relatively high compared to the switching frequency, so the current variation can be considered to stay in its linear state.

The transfer function from V_{in} to V_{out} can be defined in a first approximation only as a function of d (duty-cycle). In average, the voltage ripple on the inductance is zero, meaning that:

$$\begin{aligned} < u_L > &= \frac{1}{T}\int_0^T u_L \, dt = \frac{1}{T}\left[\int_0^{dT} u_L \, dt + \int_{dT}^{T} u_L \, dt\right] \\ &= \frac{1}{\cancel{T}}\left[d\cancel{T} \, V_{in} + \cancel{T}(1-d)(V_{in} - V_{out})\right] \\ &= V_{in} - (1-d)V_{out} = 0 \qquad (4.6) \\ \Rightarrow \frac{V_{out}}{V_{in}} &= \frac{1}{1-d} \quad \Rightarrow \quad d = 1 - \frac{V_{in}}{V_{out}} \qquad (4.7) \end{aligned}$$

4.2.1 Sizing

Sizing method is described below and numerical values will be given for $V_{out} = 700V$, $V_{in,RMS} = 230V$, $f_{pfc} = 30kHz$ and $P_{load} = 150W$ ($\Rightarrow R = 662\Omega$).

Voltages

In this case, the boost is not used as a DC-DC converter, but more as an AC-DC converter. Indeed, V_{out} is kept almost constant, but V_{in} is the grid voltage brought through a rectifier and therefore still varying from 0V to V_{peak}. This will add some complexity to the controller (see section 4.3) because the duty-cycle value cannot be kept constant anymore to respect the transfer function in equation 4.7.

Duty-cycle

The duty-cycle will have an inversely proportional relationship with V_{in} as it is represented in figure 4.5.

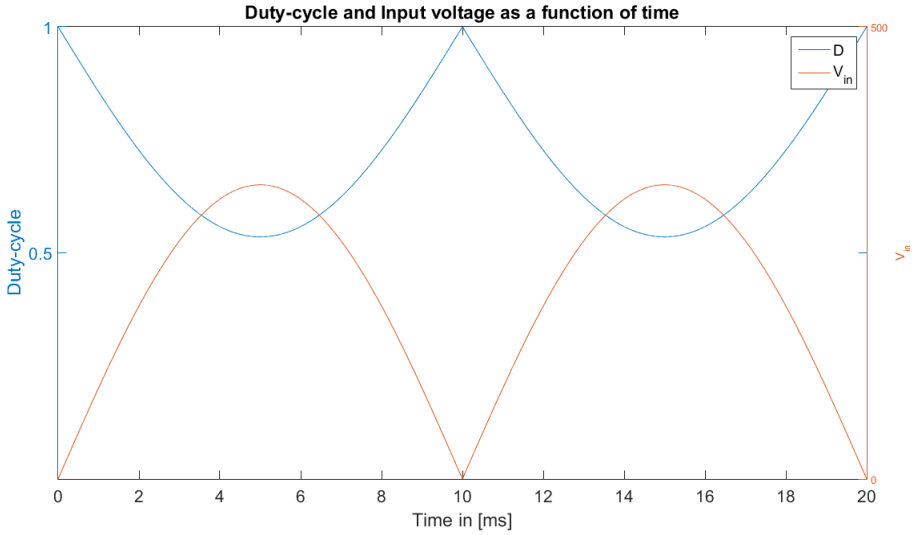

Figure 4.5: Relation between duty-cycle and input voltage

$$V_{in} \text{ max} \quad \Rightarrow \quad \frac{V_{out}}{V_{in}} \text{ min} \quad \Rightarrow \quad d \text{ min}$$

In this case, both duty-cycle and ripple amplitude will follow this relationship, but it will be shown in chapter 5 that the ripple might not be proportional to d all the time if V_{out} is too low.

Inductance

The most important factor to define the inductance value is the maximal admitted current ripple. The ripple current is the current variation during step 1 (inductance charging).

$$\begin{aligned} L\frac{di_L}{dt} &= V_{in} \\ i_L(dT) &= \frac{1}{L}\int_0^{dT} V_{in}\ dt \\ i_L(dT) &= i_L(0) + \frac{V_{in}dT}{L} \\ \Rightarrow \Delta i_L &= i_L(dT) - i_L(0) = \frac{V_{in}d}{Lf_s} \end{aligned} \tag{4.8}$$

The current ripple was arbitrarily defined as 15% of the maximal current (and maximal current is found for minimal input voltage, which is 230V - 10%).

$$\begin{aligned} \Delta I_{L,max} &= \frac{0,15\ \sqrt{2}P_o}{V_{in,min}} \\ \frac{V_{in}d}{Lf_s} &= \frac{0,15\ \sqrt{2}P_o}{V_{in,min}} \\ \Rightarrow L &= \frac{d\ V_{in,min}^2}{0,15\sqrt{2}\ P_o f_s} = 40,6mH \end{aligned} \tag{4.9}$$

Capacitance

The main criterium for capacitance sizing is the voltage ripple authorized or more directly the capacitor hold-up time which depends on the capacitor discharge time [1] defined as:

$$V(t) = \exp\left(\frac{-t}{\tau}\right) = \exp\left(\frac{-t}{RC}\right) = \exp\left(\frac{-tP_o}{V(t=0)^2 C}\right). \tag{4.10}$$

Expand the development further would be quite complex whereas a pretty accurate result can be found through the following simplified criterium (P.C.Tedd [37]):

$$C = \frac{2P_{out}\Delta t}{V_o^2 - V_{o,min}^2} = 160\mu F \tag{4.11}$$

with Δt set to 45 ms.

Moreover, an AC component appears on V_{out} due to the variation of V_{in}. In fact, it was first considered that the average voltage on the inductance was zero, which is not true as the main current is varying. This varying voltage difference around the inductance leads to a variation of V_{out} at 2 times the fundamental frequency (see figure 4.6).
It can also be seen on this figure that $V_{out} = V_{ref}$ when the fundamental of inductance current is not varying.

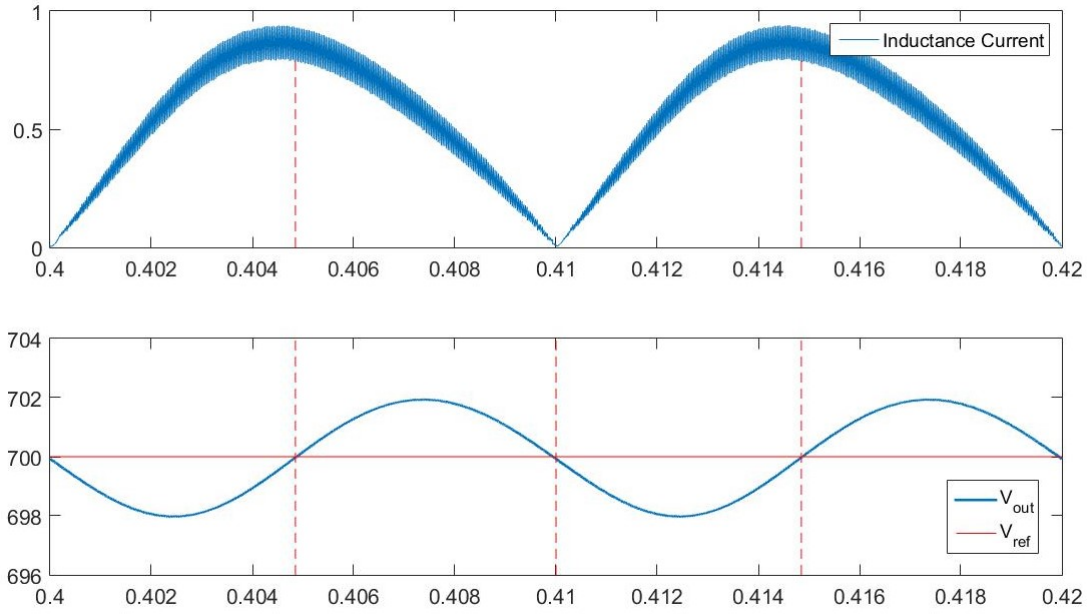

Figure 4.6: Output voltage ac component at 2 times fundamental frequency

[1] expressed here for a resistive load

4.2.2 Non-idealities

A. Diode voltage drop

If V_d (diode voltage drop) is injected directly in equation 4.6, the new function of d becomes:

$$V_{in} - (1-d)(V_{out} + V_d) = 0$$
$$\Rightarrow \quad d = 1 - \frac{V_{in}}{V_{out} + V_d}$$

So a higher d is needed to find the same gain $\frac{V_{out}}{V_{in}}$. And as d cannot increase indefinitely, the maximal gain $\frac{V_{out}}{V_{in}}$ will be reduced because of the diode.

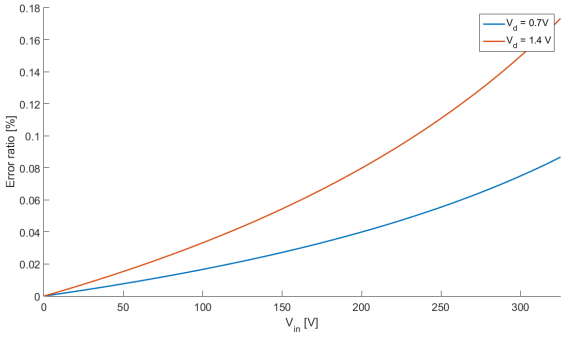

Figure 4.7: Duty-cycle error when V_d is considered

Fortunately, it can be considered negligible because V_d is much smaller than V_{out}. The actual error is given in the right figure.

B. Inductance: internal resistance

Duty-cycle: r_L (internal resistance) adds non-linearity for high values of duty-cycle and the gain $\frac{V_{out}}{V_{in}}$ becomes finite. Equation 4.6 becomes:

$$V_{in} - r_L i_L - (1-d)V_{out} = 0$$

where i_L is a function of the load current and the load impedance (Z_L):
$< i_L >= \frac{i_{LD}}{1-d} = \frac{V_{out}}{Z_L(1-d)}$

This leads to the result in figure 4.8: error ratio between ideal duty-cycle and duty-cycle with $r_L \neq 0$. But when d comes close to 1, its value becomes complex and it does not represent correctly the error. So it is more explicit to display the value of the transfer function V_{out}/V_{in} as a function of d (see figure 4.9).

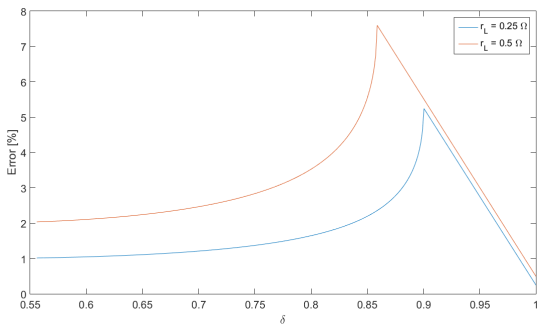

$$V_{in} - V_{out}\left[\frac{r_L}{Z_L(1-d)} + (1-d)\right] = 0$$
$$V_{out}(1-d)^2 - V_{in}(1-d) + \frac{r_L}{Z_L}V_{out} = 0$$
$$\Delta = V_{in}^2 - 4V_{out}^2\frac{r_L}{Z_L}$$
$$(1-d) = \frac{V_{in} + \sqrt{\Delta}}{2V_{out}}$$
$$\Rightarrow \quad d = 1 - \frac{V_{in} + \sqrt{\Delta}}{2V_{out}}$$

Figure 4.8: Duty-cycle error when r_L is considered

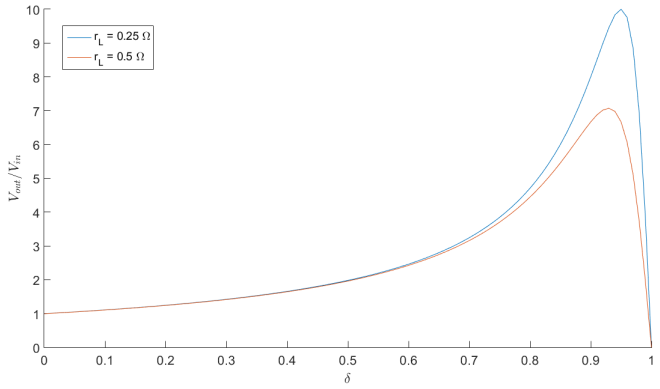

Figure 4.9: $\frac{V_{out}}{V_{in}}$ as a function of d

Ripple amplitude: Due to the voltage drop on the resistance, this also induces a voltage drop around the inductor and therefore a lower ripple amplitude:

$$\begin{aligned} i_L &= \frac{1}{L}\int_0^{dT} V_{in} - r_L i_L \, dt \\ \Rightarrow \Delta i_L &= \frac{V_{in} d}{L f_s + r_L d} \end{aligned} \tag{4.12}$$

Current harmonic ratio: Harmonic ratio relative to different powers can be seen in tables 4.1 and 4.2. This is the ratio between current harmonic in the ideal model and in the model with internal resistance in the inductor.
Common values of r_L are between 2Ω and 5Ω [20].

Cases with a resistance $r_L = 5\Omega$ and $r_L = 10\Omega$ have been tested. Results provided with $r_L = 5\Omega$ seem to give results quite close to the ideal model whereas results for $r_L = 10\Omega$ are already a lot more inaccurate. It can also be observed that the error spreads more for higher power.

Frequency [kHz]	30	60	90	120	150
$P_o = 50$ W	[1.002 1.016]	[0.985 1.018]	[0.956 1.014]	[0.939 1.023]	[0.942 1.027]
$P_o = 150$ W	[1.006 1.045]	[0.956 1.044]	[0.889 1.041]	[0.839 1.066]	[0.856 1.079]
$P_o = 200$ W	[1.007 1.072]	[0.941 1.063]	[0.859 1.056]	[0.81 1.095]	[0.835 1.113]

Table 4.1: Error range for different powers, $r_L = 5\Omega$ and constant frequencies: F_{pfc}=30kHz, F_{hb}=75kHz

Frequency [kHz]	30	60	90	120	150
$P_o = 50$ W	[1.027 1.036]	[1.025 1.033]	[1.013 1.016]	[0.985 1.041]	[0.945 1.043]
$P_o = 150$ W	[1.011 1.101]	[0.903 1.106]	[0.776 1.1]	[0.696 1.175]	[0.712 1.188]
$P_o = 200$ W	[0.926 2.244]	[0.946 1.186]	[1.11 1.27]	[1.116 1.493]	[1.025 1.802]

Table 4.2: Error range for different powers, $r_L = 10\Omega$ and constant frequencies: F_{pfc}=30kHz, F_{hb}=75kHz

C. Capacitance: internal resistance

Often called ESR (*Equivalent Series Resistance*), it represents mostly the connection soldering and losses in the dielectric.

This resistance will not affect the average output voltage but can drastically increase its ripple. Indeed, every time current is asked by the CFL load, this produces a voltage drop on the ESR. In the same way, every time the inductance is discharging into the capacitor, this also produces a voltage drop.

Current harmonic ratio: ratio between current harmonic in the complete ideal model and in the complete model with ESR is given in table 4.3 for the same device, but with different output powers.
Common values of ESR are around 1.5Ω [20].

The equipment was tested for an extreme ESR value of 5 Ω: the ratio is quite alright for low frequencies and low power combined and then it start increasing.

Frequency [kHz]	30	60	90	120	150
P_o = 50 W	[1.006 1.216]	[1.012 1.126]	[1 1.159]	[1 2.628]	[1.07 2.57]
P_o = 150 W	[1.009 1.403]	[1.004 1.498]	[1.035 1.658]	[0.987 1.867]	[0.95 2.097]
P_o = 200 W	[1.008 1.289]	[1.002 1.685]	[1.082 1.947]	[0.852 1.939]	[0.878 1.294]

Table 4.3: Error range for different powers, ESR = 5Ω and constant frequencies: F_{pfc}=30kHz, F_{hb}=75kHz

Further observations: The actual harmonic content is given in figure 4.10. It seems that the harmonics of the CFL are modulated around the harmonics of the APFC as we can observe harmonic peaks at frequencies $m \cdot f_s \pm k \cdot f_{hb}$.

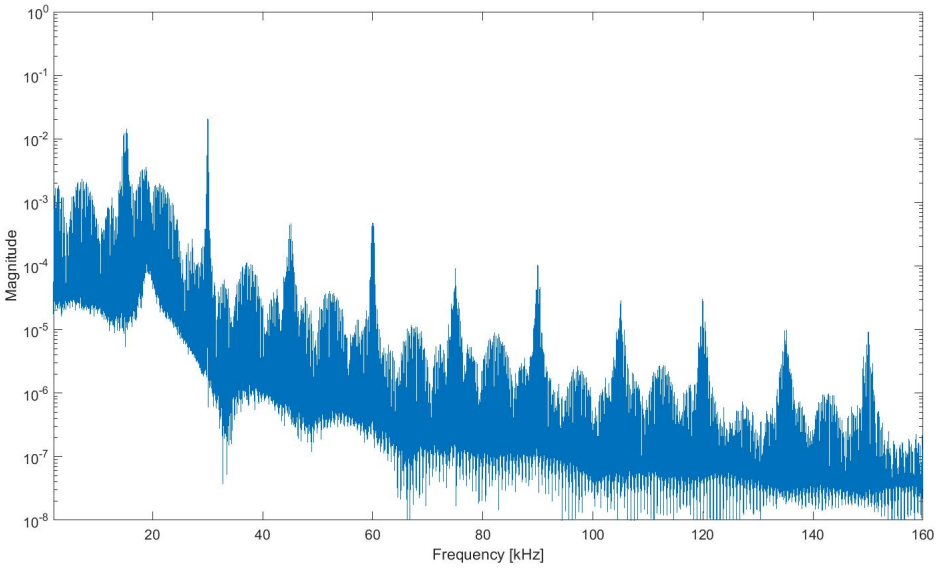

Figure 4.10: Input signal FFT (with ESR)
Characteristics: F_{pfc}=30kHz, F_{hb}=75kHz, ESR=5Ω, P_o=150W

D. Decision

As the impact of these non-idealities is not negligible, they will not be used for the procedure development. But the final model will be tested against with these non-idealities to see what are their impact at this point.

4.3 APFC: Controller design

In this section the design of the entire APFC controller will be described.
It is largely based on the document "Design and Implementation of Single-Phase Boost PFC Converter" [28] that describes the design and implementation of an average current mode controller (ACM) working in continuous conduction mode (CCM).
Such a controller is represented in Figure 4.11.

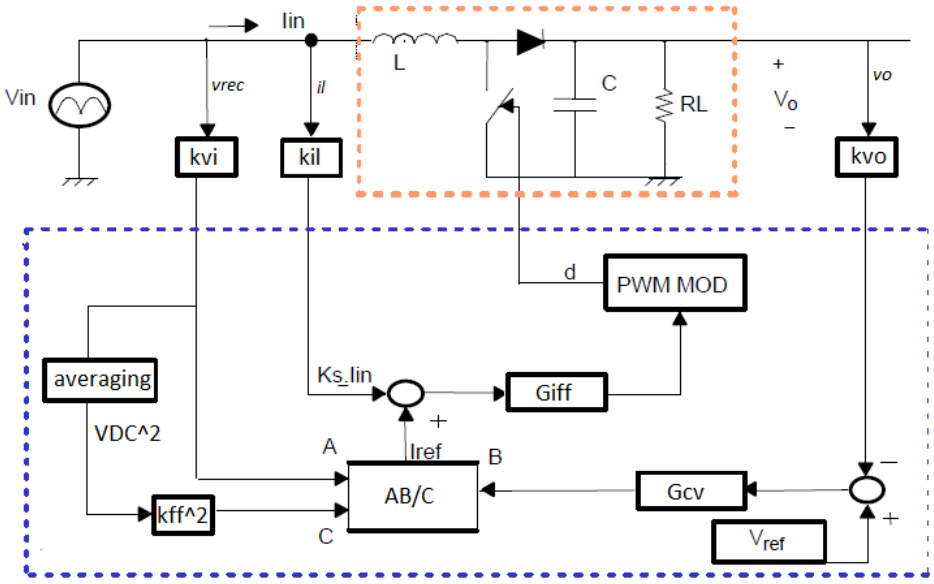

Figure 4.11: Block diagram of the APFC (modified from [17])

As we can see, there are two different loops: one current loop to have the input current that follows the rectified input voltage (fast control loop) and one to have the output voltage of the boost converter at the correct reference voltage V_{ref}.

Due to the fact that the current loop is faster than the voltage loop, we can design both loops independently.

The input mean voltage (V_{DC}) term is there to remove the mean variation of the input voltage ($230V \pm 10\%$).
Finally `kvi`, `kil`, `kvo` and `kff` are the gain factors of the different sensors. For simplicity and clarity we will consider unit factors.
The current controller can be enhanced, adding a command feed-forward controller as shown in the figure below (fig. 4.12). The idea is to pre-compute the duty-cycle to alleviate the "work" of the current controller [15]. The power factor is improved and the zero-crossing distortion reduced.

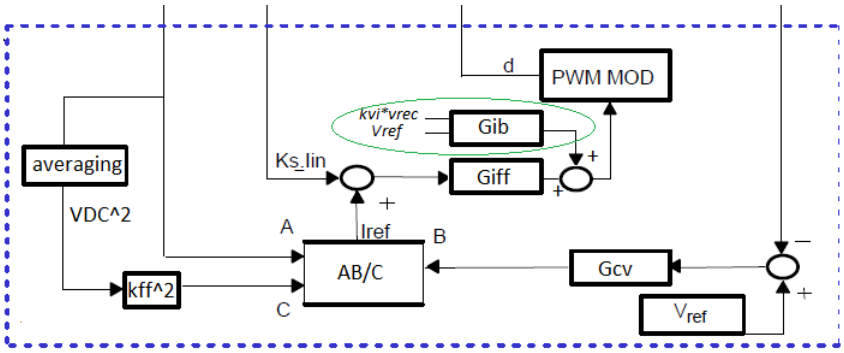

Figure 4.12: Improved APFC controller

4.3.1 Current loop

The current loop is represented in Figure 4.13.

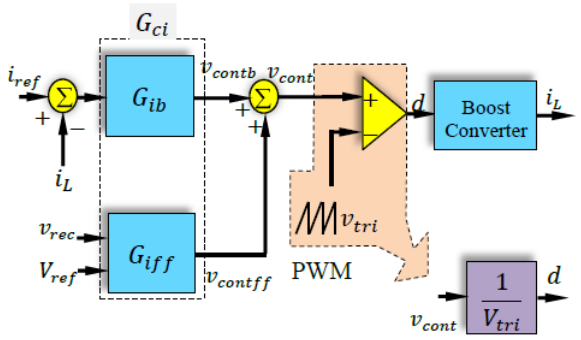

Figure 4.13: Current control scheme [28]

As shown in Figure 4.11, the reference current I_{ref} will depend on three different terms: The rectified input voltage v_{rec} such that the current is in phase with the voltage (high power factor), the amplified output voltage error to control the output voltage at V_{ref} and finally the average input voltage (V_{DC}) to counter average input voltage variations. For a single-phase full-wave rectifier, it is defined as: $V_{DC} = \frac{2 \cdot V_{in,peak}}{\pi}$ where $V_{in,peak} = 230 \cdot \sqrt{2}$.

The current will be controlled, acting on the duty-cycle of the boost controller.
The PWM (pulse width modulator) can be represented by a gain $\frac{1}{V_{tri}}$ with V_{tri} the amplitude of the triangular or sawtooth signal depending on the PWM type.
Using the state space average model of a boost converter, we can compute the duty-cycle in function of the inductor current variation:

$$L\frac{di_L}{dt} = \int_0^{d \cdot T} v_{rec} + \int_{d \cdot T}^{T} (v_{rec} - V_{ref}) \tag{4.13}$$

$$\iff L\frac{di_L}{dt} = d \cdot v_{rec} + (1-d) \cdot (v_{rec} - V_{ref}) \tag{4.14}$$

$$\iff \quad d = \frac{\frac{di_L}{dt} - v_{rec} + V_{ref}}{V_{ref}} \tag{4.15}$$

From figure 4.13,

$$d = \frac{v_{cont}}{V_{tri}} = \frac{v_{contb} + v_{contff}}{V_{tri}} \tag{4.16}$$

where v_{cont} is the controlled voltage at the input of the PWM and v_{contff} the feedforward control voltage defined as:

$$v_{contff} = V_{tri}\left(1 - \frac{v_{rec}}{V_{ref}}\right) \tag{4.17}$$

By putting the three equations together, we finally get (in the Laplace domain):

$$i_L(s) = \frac{V_{ref}}{sLV_{tri}} v_{contb} \tag{4.18}$$

The bloc diagram can thus be simplified as shown in figure 4.14.

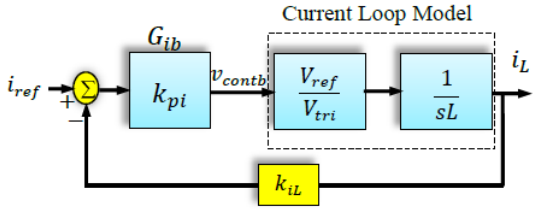

Figure 4.14: Simplified current control scheme [28]

The open loop transfer function can now be simply expressed as:

$$G_{oL} = \frac{k_{pi}V_{ref}}{LV_{tri}s} \tag{4.19}$$

The unity gain cross-over frequency defined as $\omega_c : |G(j\omega_c)| = 1$ is equal to:

$$f_{ci} = \frac{k_{pi}V_{ref}}{2\pi LV_{tri}} \tag{4.20}$$

The cross-over frequency determines the response time of the system.
To follow the rectified line frequency ($2f_{line}$), the gain cross-over frequency should be » 2 f_{line} with $f_{line} = 50Hz$. If f_{ci} is too close to $2f_{line}$, a zero-crossing distortion of the current waveform appears [28].
Moreover, f_{ci} should not be higher than 1/5 of the PWM switching frequency. We will choose $f_{ci} = \frac{1}{6}f_s$.
Thus the proportional gain can be determined:

$$k_{pi} = \frac{2\pi Lf_sV_{tri}}{6 \cdot V_{ref}} \tag{4.21}$$

In our system we have the following parameters:

- $L = 40.6mH$ (see section 4.2.1)
- $f_s = 30kHz$
- $V_{ref} = 700V$
- $V_{tri} = 1$

According to equation (4.21) we finally get:

$$\boxed{k_{pi} = 1.8233} \tag{4.22}$$

4.3.2 Voltage loop

As mentioned before, the voltage loop regulates the output voltage V_o at a given reference voltage V_{ref}. Since the voltage loop will be much slower than the current loop, we can assume that $i_L = i_{ref}$ at any time.
Using again the state space average model of a boost converter, we can compute the output voltage (V_o) in function of the average current passing through the inductor (i_L):

$$V_o = \frac{V_{rms}}{V_o} \frac{R}{2 + RCs} \cdot i_L \tag{4.23}$$

The voltage control scheme of the voltage loop is represented in Figure 4.15 with the **controller stage** ($G_{cv}(s)$) and the **power stage** (boost converter).

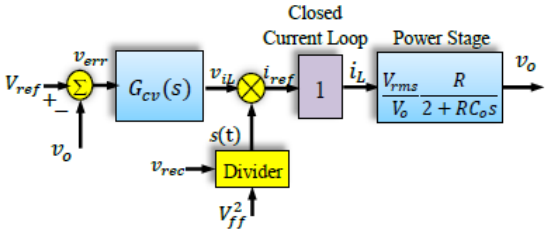

Figure 4.15: Voltage control scheme [28]

The control-to-output voltage transfer function can be expressed as:

$$G_{pv} = \frac{v_o}{v_{iL}} = \frac{k_{vi} k_f^2}{k_{vff}^2 k_{iL} V_o} \frac{R}{2 + RCs} \tag{4.24}$$

with $k_f = \frac{V_{rms}}{V_{DC}} = \frac{\pi}{2\sqrt{2}}$.

To have a zero steady-state error, a PI (proportional-integral) controller is used:

$$G_{cv}(s) = K_p + \frac{K_i}{s} = K_p \cdot \frac{s + \omega_z}{s} \tag{4.25}$$

with $\omega_z = \frac{K_i}{K_p}$.

The open loop transfer function can now be expressed as:

$$G_{vOL} = G_{cv} \cdot G_{pv} = K \cdot \frac{RK_p(s + \omega_z)}{RCs^2 + 2s} \tag{4.26}$$

with the constant $K = \frac{k_{vi} k_f^2 k_{vo}}{k_{vff}^2 k_{iL} V_o}$.
The voltage controller parameters K_p and K_i have to be determined.

First the voltage loop should have a narrow bandwidth such that $BW << 2 \cdot f_{fline}$ [14]. This is because there is always a ripple at twice the line frequency (100 Hz) on the output capacitor (see section 4.2.1). And if the bandwidth is too large (fast response time), the controller will try to counter this voltage ripple introducing distortion in the input current as illustrated in the Figure below (fig. 4.16) .

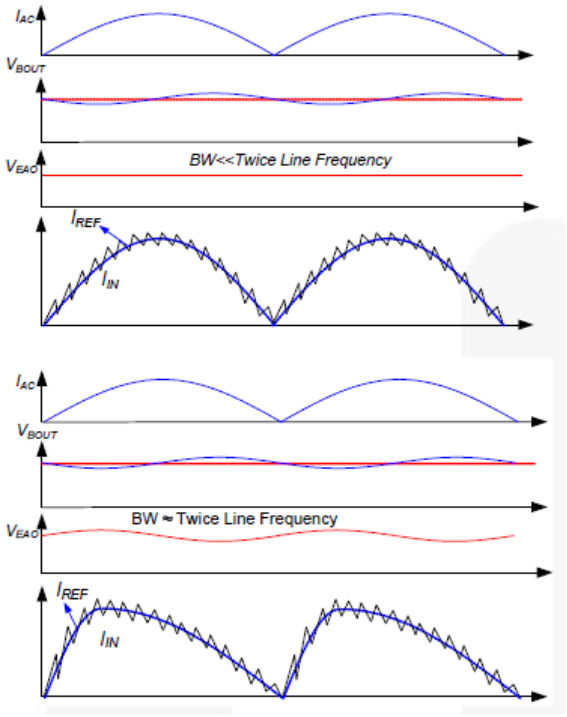

Figure 4.16: Input current waveform depending on the bandwidth [14]

We can observe that for a bandwidth « $2f_{line}$, the voltage error V_{EAO} do not vary contrary to the case where the bandwidth $\approx 2f_{line}$. This voltage error variation causes a current input distortion.
In the paper [14], the cross-over frequency should be around 1/10 to 1/5 of the line frequency (between 5 and 10Hz).
This gives a first condition that links K_p and K_i:

$$K_p = \sqrt{\frac{\omega_{cv}^2(\omega_{cv}^2 C^2 R^2 + 4) - K^2 R^2 K_i^2}{K^2 R^2 \omega_{cv}^2}} \tag{4.27}$$

The details of equation 4.27 can be found in appendix A .
In our system we chose $f_{cv} = 10Hz$.
K_i can now be chosen to satisfy other requirements [28]:

- Phase margin $> 45°$.
- Overshoot is less than 20%.
- Settling time is below 125ms.

The second condition depends also on the phase margin. A higher phase margin will decrease the overshoot.
The K_i parameter is changed until the different requirements are met and we finally get:

$$K_p = 5.44 \tag{4.28}$$
$$K_i = 150 \tag{4.29}$$

The open loop frequency response is shown in Figure 4.17 .
The cross-over frequency is at 10Hz as wanted.
Figure 4.18 represents the step response in closed loop. The overshoot and settling time (determined on Matlab) are respectively 3.5% and 0.11s.

Finally the phase margin is equal to 83°.

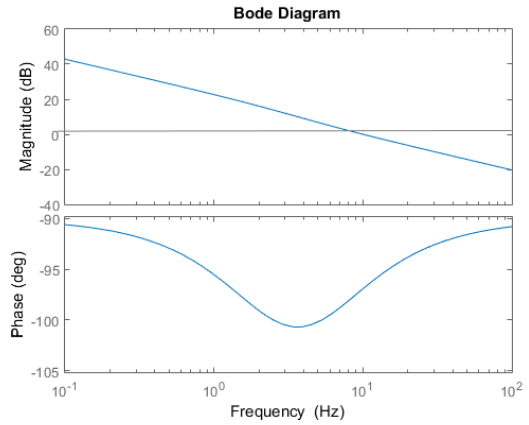

Figure 4.17: Open loop frequency response of the voltage loop

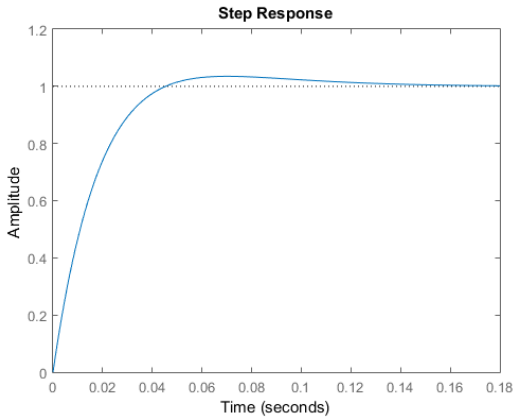

Figure 4.18: Step response of the voltage loop

4.3.3 Simulink implementation

Using the sizing of the previous section, the model can be implemented in Simulink. The model of rectifier, APFC and CFL block combined can be seen in figure 4.19 with the controller as a black box. The controller itself is represented in Figure 4.20 .

Because an ideal input voltage source is considered, no averaging function (see fig. 4.11) has been implemented. Instead the average input voltage has been precomputed as: $V_{DC} = \frac{2 \cdot 230\sqrt{2}}{\pi}$.

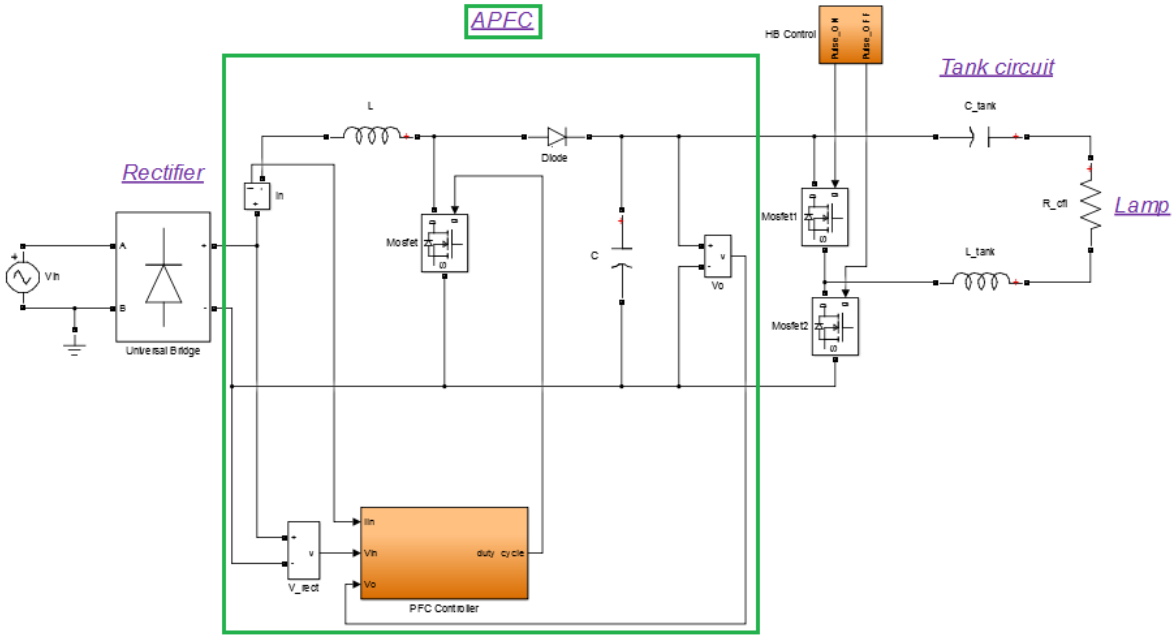

Figure 4.19: Simulink implementation of a device

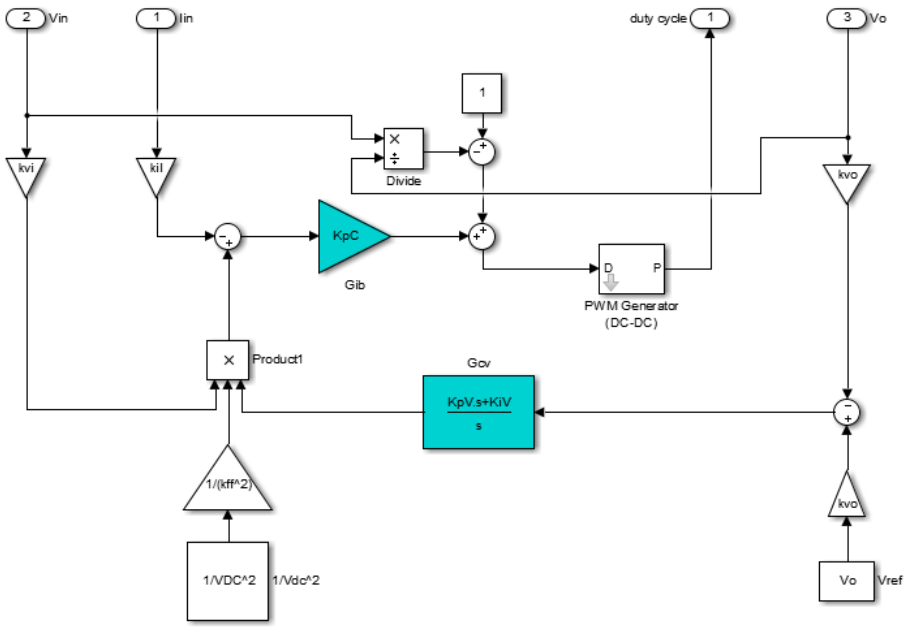

Figure 4.20: Simulink implementation the APFC controller

The controlled input current and output voltage of the APFC are shown in Figure 4.21 .
A power factor of 0.997 is obtained and as wanted,

- The current waveform follows the rectified input voltage.

- The output voltage is controlled at the reference value (700V).

The transient evolution of the waveforms at the beginning of the simulation is not analyzed in this work. In practice a start circuit is used in some devices.
For compact fluorescent lamps for example, at start, it is necessary to provide a higher voltage than in steady-state mode to produce internal arcs. [7].

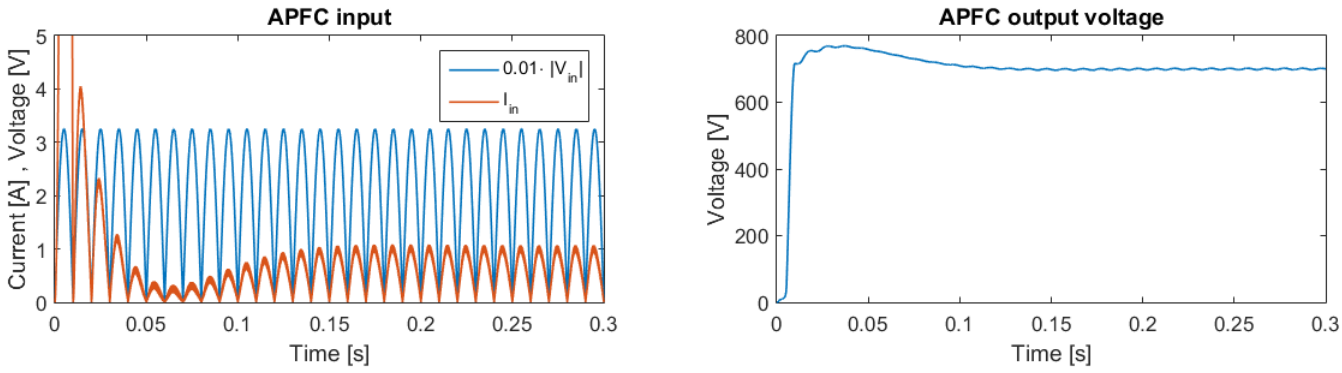

Figure 4.21: APFC Simulink implementation: waveforms

Finally a zoom on the inductance current over one period of the fundamental frequency gives the waveform observed in figure 4.22 . The frequency spectrum contains harmonic peak at multiples of the boost switching frequency (set to 30 kHz) as seen in figure 4.23.

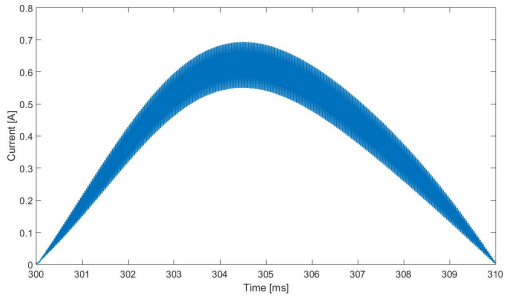

Figure 4.22: Inductance current over one period of 1/50 s

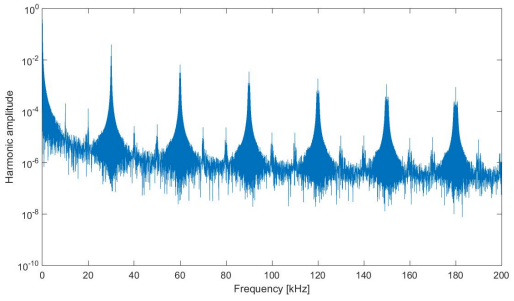

Figure 4.23: Harmonic content of the inductance current

4.4 EMI filter

As introduced in section 3.3, to isolate the noise at the input of an equipment, a LISN is used. Such a circuit is shown in Figure 4.24. The 50Ω resistances represent the matched input impedance of the EMI receiver to measure the noise.
The high frequency components coming from the equipment are blocked by the inductor and bypassed by the capacitors. These components are thus "captured" by the LISN.
The low frequency components pass through the inductors and are blocked by the capacitors and so the LISN is "transparent" to these components and they are not measured by the receiver.

N.B: Capacitors should also be used at the source side to suppress the high frequency noise coming from the source [35].

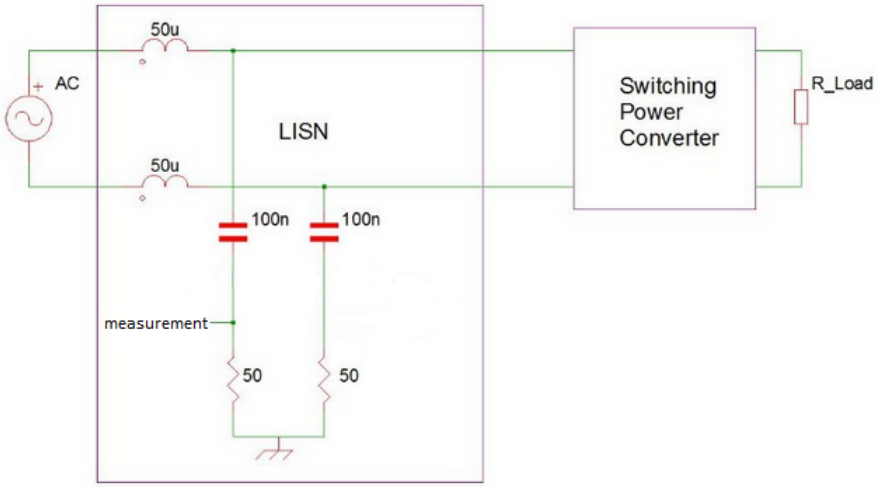

Figure 4.24: Line impedance stabilization network

The receiver filter used to measure the EMI can be of different types [35] : peak detector, quasi-peak detector or averaging. In the method described below, a quasi-peak detector is

considered.

Our equipment, being only simulated in Simulink, there is no integrated EMI measuring tool. To avoid an implementation of a receiver that has to fulfill some standards as well as the use of a spectrum analyzer that has to be well parametrized, a simple general method described in [29] will be used for the DM filter.

4.4.1 DM filter [29], [34]

It is based on the assumption that the RMS noise current at high frequency is an acceptable estimation of the quasi-peak detection voltage at the EMI test receiver.
The input current of our equipment is composed of a fundamental component (50Hz) and a high frequency component due to the switching frequency f_s of the APFC. The frequency component coming from the switching frequency of the half-bridge can be neglected as demonstrated in section 5.1.2.
As described in the figure below (fig. 4.25), it is assumed that the total noise RMS current only occurs at the switching frequency f_s.

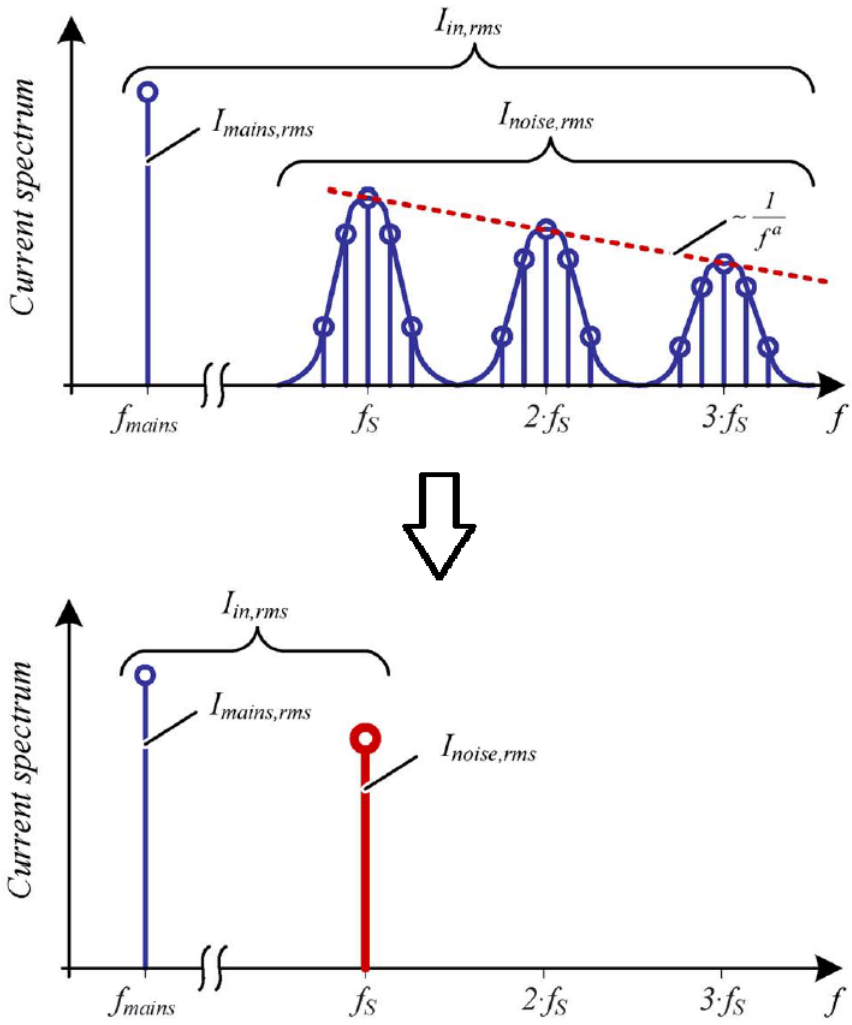

Figure 4.25: Main assumption: total RMS noise only present at the switching frequency [29]

For a continuous conduction mode (CCM) boost APFC, the total RMS noise current can be

expressed as:

$$I^2_{noise,RMS} = \frac{1}{\pi} \cdot \frac{V^2_{in}}{12 L^2_{boost} f^2_s} \left(\frac{\pi}{2} + \alpha^2 \cdot \frac{3\pi}{8} - \alpha \frac{8}{3} \right) \quad with \quad \alpha = \frac{V_{in}}{V_o} \tag{4.30}$$

The details of this result can be found in the appendix B.

The measured RMS noise voltage U_{LISN} is then simply given by:

$$U_{LISN} \approx 50\Omega \cdot I_{noise,RMS} \tag{4.31}$$

The next step, is to find the design frequency f_d, that is the first multiple of f_s that is higher or equal to 150kHz. It will be the highest noise amplitude in the $150kHz - 30MHz$ band.
The design frequency can be determined as:

$$f_d = m \cdot n \cdot f_s \tag{4.32}$$

with n the number of identical filter stages: (we will consider $n = 1$ for simplicity) and m the multiple factor of f_s that lies in the frequency band[2]:

$$m = ceil \left(\frac{150 \text{ kHz}}{n \cdot f_s} \right) \tag{4.33}$$

Finally the estimated measured peak voltage at the design frequency (f_d) expressed in $dB\mu V$ is given by:

$$U_{est}(f_d)[dB\mu V] = 20 \cdot log \left(\frac{U_{LISN}}{m^a} \cdot \frac{1}{10^{-6}} \right) \tag{4.34}$$

The decay of the harmonic value with the frequency, will depend on the current waveform. For a square wave, $a = 1$ and for a symmetrical triangular wave, $a = 2$.
In our case, the input current has a triangular wave but with slopes depending on the duty-cycle. For simplicity, the worst case will be considered ($a = 1$), but as explained in the Fourier series analyses section, the EMI filter design could be improved knowing the exact decay of the input current of an APFC with the frequency.

To meet the CISPR11/EN-55011 standard the required attenuation (including a security margin) at the design frequency will be [3]:

$$\boxed{Att_{req}(f_d)[dB] = U_{est}(f_d)[dB\mu V] - Limit(f_d)[dB\mu V] + Margin[dB]} \tag{4.35}$$

Note: For lighting equipments the CISPR15/EN-55015 standard specifies limits starting at 9kHz. However to model general equipments (TV, computer charger,...) we will only consider the CISPR11 standard (that specifies limits starting at 150kHz).

The required attenuation is represented in Figure 4.26 .

Once the required attenuation is calculated, the differential mode EMI can be implemented. The circuit including the LISN and the noise source can be simplified in a simple LC circuit as shown below (fig. 4.27).

[2] *ceil*: round-up function
[3] [dBuV] - [dBuV] = [dB]

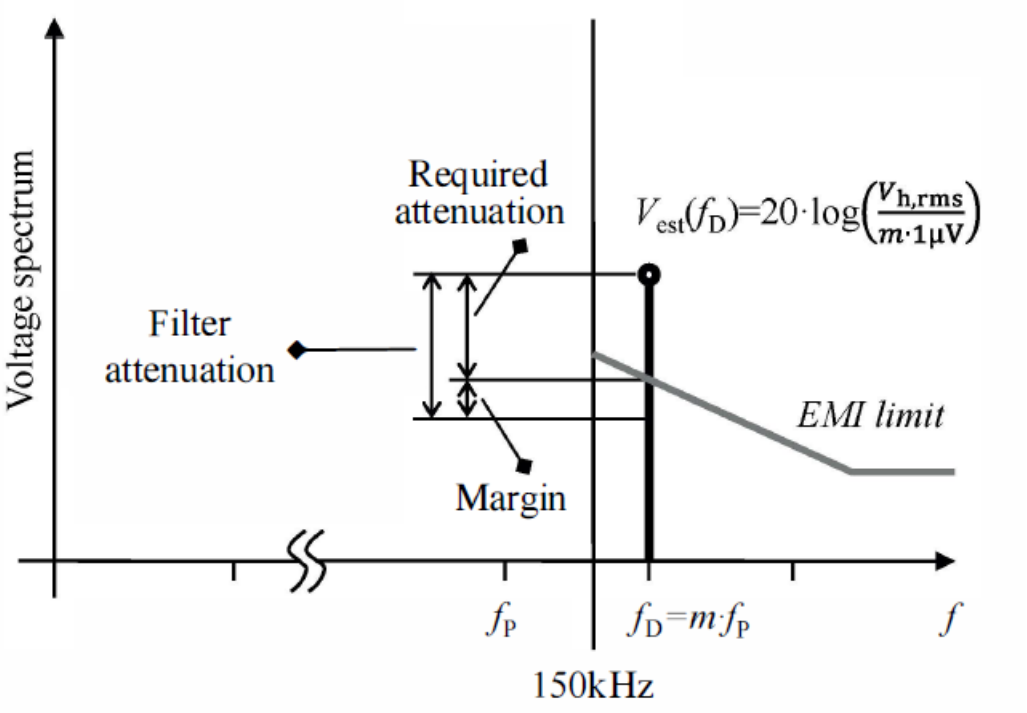

Figure 4.26: Required attenuation at the design frequency f_d [27]

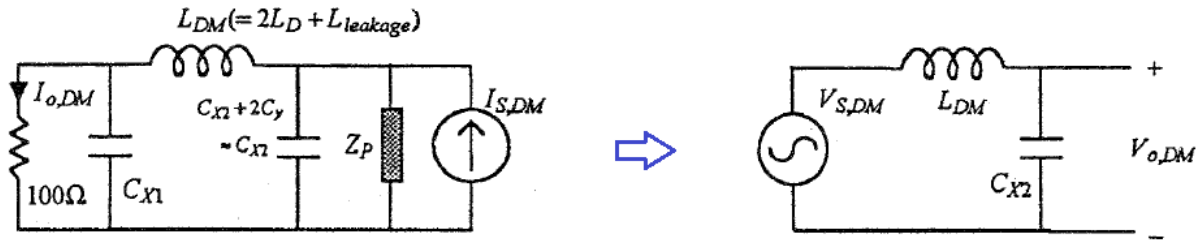

Figure 4.27: Simplification of the differential mode EMI filter [34]

Knowing the cut-off frequency of the filter, the inductance and capacitance of the LC filter can be easily calculated. The link between the design frequency (frequency where an attenuation of Att_{req} is needed) and the cut-off frequency of an LC filter (-40dB/dec slope) can be given by:

$$f_c = \frac{f_d}{10^{\frac{Att_{req}}{40}}} \tag{4.36}$$

Finally, inductance and capacitance values are obtained using the cut-off frequency equation [34]:

$$f_c = \frac{1}{2\pi} \cdot \sqrt{L_{DM} C_{DM}} \tag{4.37}$$

$$= \frac{1}{2\pi} \cdot \sqrt{(2L_D + L_{leak})\ C_X} \tag{4.38}$$

L_{leak} is the leakage inductance of the coupled inductors L_c (see fig. 3.14) . It is typically in the range 0.5-2% of L_c (1% was chosen for this design)[4].
L_c is the value of one of the coupled inductors by itself (no coupling).

[4] L_{leak} represents the leakage summation for both inductors L_c

Now there is a degree of freedom in the choice of L_D and C_X but the following points should be considered:

- Size of the components → Size of the filter. Could determine the optimal filter volume like in [29] .

- Available components in the market.

We will choose a default capacitance of $0.47\mu F$ (a commonly available capacitor value) and will check if the inductance value is not too high. Otherwise the capacitance has to be increased.
In table 4.4, the inductance and capacitance values relative to a device (f_s, $power$, V_o,...) are shown. Their value have been calculated using the methodology described above.

$Power[W]$	$V_o[V]$	$f_s[kHz]$	$L_{boost}[mH]$	$f_c[kHz]$	$\mathbf{L_D}[\mu\mathbf{H}]$	$\mathbf{C_X}[\mu\mathbf{F}]$
150	700	30	40.6	20.66	51.36	0.47
150	400	30	18.7	18.8	64.43	0.47
150	700	70	17.4	22.4	41.9	0.47
150	700	10	121.9	35.78	9.25	0.47
300	700	30	20.3	14.61	114.52	0.47
80	700	30	76.2	28.28	21.88	0.47

Table 4.4: Differential mode filter values depending on the power, output voltage and switching frequency of the boost converter. ($L_{leak} = 23.6\mu H$) [5]

Plotting the transfer function on LTSpice of the EMI filter of the first line of the table is given in figure 4.28 (top) :

As expected, the cut-off frequency is around 20kHz and the EMI filter do not affect the low frequency components especially the fundamental frequency (50Hz).
However, because a pure LC circuit is modeled, a resonance at the cut-off frequency is observed. This cannot be tolerated: harmonics around the cut-off frequency of the equipment or coming from the grid would be too much amplified. In practice, the peak is damped using the complex reactivity of the selfs that increases with the frequency, giving the self a resistive behavior only at high frequencies (thus the losses at low frequencies are small).

In this work, we do not consider the losses, so the damping will simply be modeled by a resistance R_d in series with the inductances L_d.
Using a 8Ω resistance gives a peak value of only $2dB$ that can be tolerated (see fig. 4.28 (bottom)).

[5] L_{leak} constant because L_c is fixed in our design (see CM filter)

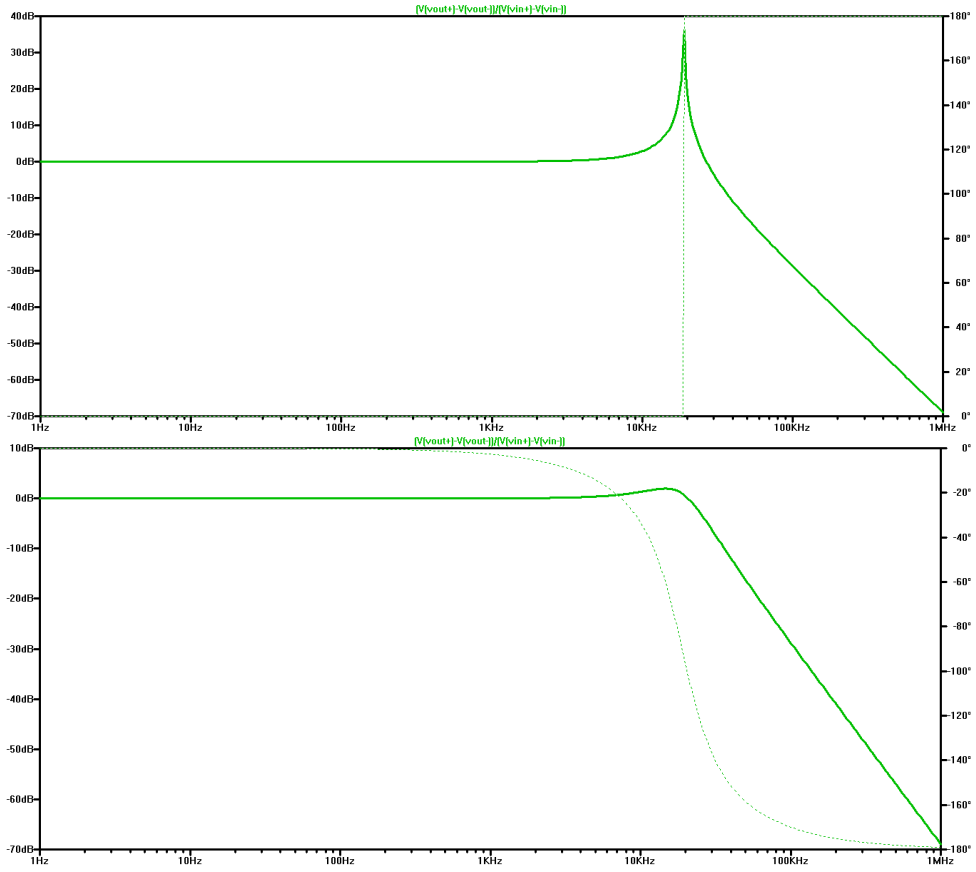

Figure 4.28: DM transfer function for $P = 150W$, $V_o = 700V$ and $f_s = 30kHz$ without (top) and with damping (bottom)

4.4.2 CM filter [34]

The CM noise depends on the parasitic elements on the equipment, PCB,... . Because no physical circuit has been produced or measured, some default values have been chosen for the design of the filter.

As for the DM filter, it can also be simplified:

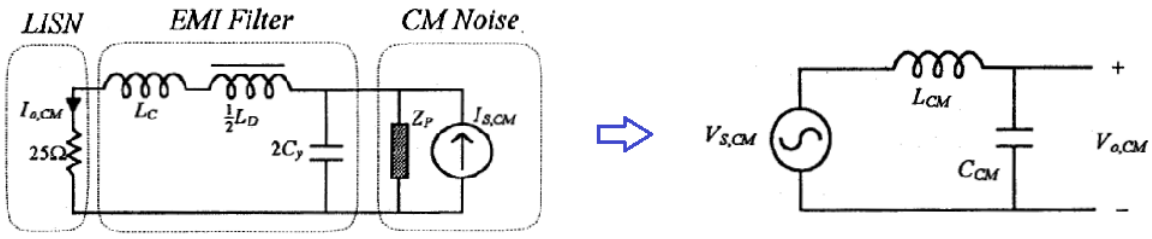

Figure 4.29: Simplification of the differential mode EMI filter [34]

Once the CM noise has been measured or simulated (knowing the parasitic elements), the same approach than the differential mode filter can be used using the equation that links f_d and

f_c and :

$$f_c = \frac{1}{2\pi} \cdot \sqrt{L_{CM} C_{CM}} \tag{4.39}$$

$$= \frac{1}{2\pi} \cdot \sqrt{(L_C + \frac{1}{2} L_D) \cdot 2C_Y} \tag{4.40}$$

$$\approx \frac{1}{2\pi} \cdot \sqrt{L_C \cdot 2C_Y} \quad if \quad L_C >> \frac{1}{2} L_D \tag{4.41}$$

As explained before, for the CM filter design some default values given in [34] will be used for our design:

- $L_c = 2.4mH$
- $C_y = 3.3nF$

4.5 Complete model conclusion

This chapter gave us a complete implementation of the model to be able to perform simulation in Simulink.

But simulations must be done with a very low time-step to obtain a correct interpolation of high-frequency signals. A time-step of $0.5\mu s$ was used for our computations.
Therefore computation time is relatively high, already a couple of minutes to simulate only a few devices in parallel for 1 second.

The next chapter will introduce simplifications to replace the APFC model. A summary of the computation times for the different models and for 1 or several devices in parallel will be given in the global conclusion.

CHAPTER 5

SIMPLIFIED MODEL

This chapter means to simplify the model described in the previous chapter to increase the computation speed of the simulation. It will focus on the simplification of the components themselves while the next chapter will describe the simplification of the all system (devices and connections between them).

First, an equivalent model will be presented for the half-bridge in the CFL block, then the influence of this block on the rest of the circuit will be discussed.

Concerning the APFC, the simplification is a replacement by its Fourier series (sum of current sources at different frequencies). Section 5.2 will provide a theoretical approach of the Fourier series (for a triangular waveform) while section 5.3 will apply it to the complete APFC current wave.

The EMI filter must be kept as it is to be sure to model correctly the interactions between different devices interacting together because the EMI filter is the block directly connected to the grid.

5.1 CFL block

5.1.1 Half-bridge equivalent model

The half-bridge can be considered as a current source toward its input and a voltage source toward its output (see figure 5.1), therefore separating the model in 2.

Voltage source: the input of the half-bridge is a DC voltage source (V_{APFC}), and the half-bridge is only able to output 2 voltage values: V_{APFC} or 0V. This means the half-bridge always outputs the same pulsating voltage (between 0 and V_{APFC}).

Current source: 2 situations must be considered.

- Transistors M1 is ON and M2 is OFF: no path to neutral, so no current can flow into the APFC.
- Transistors M1 is OFF and M2 is ON: V_{APFC} and the load are fixed, so the current variation is also fixed.

As the current is imposed in both situations, the half-bridge can be considered as a current source toward its input.

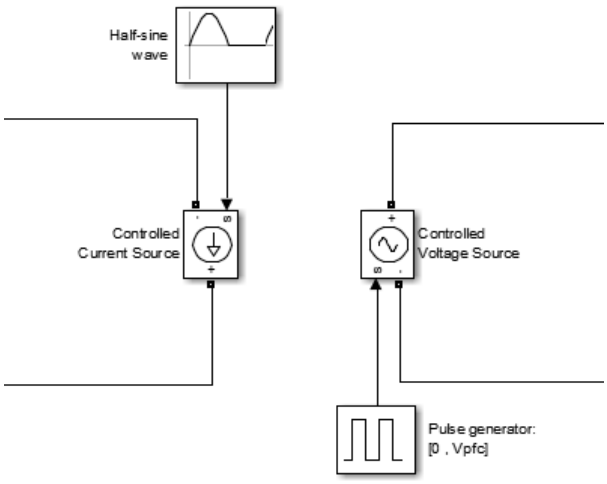

Figure 5.1: Half-bridge equivalent

5.1.2 Influence of the half-bridge

In this section, the influence of the half-bridge working at frequency f_{hb} on the input current of the device is analyzed. This frequency being of some tenth of kHz, it could appear in the 2-150kHz range of the input current of the device.

Two cases have to be distinguished: one where f_{hb} is higher than f_s and one where it is lower than f_s.

Frequency order: $f_{hb} >> f_s$

The small signal equivalent model of a boost converter is shown in Figure 5.2 . The capital letters represents a given DC point and the small ones the AC variations.
The half-bridge is replaced by its equivalent model (see previous section) and the left side (current source) is connected to the boost. It also has two components: an average current I_{hb} and an AC current i_{hb} at frequency f_{hb}.
D' is defined as : $D' = 1 - D$ with D, the "DC" duty-cycle of the converter.

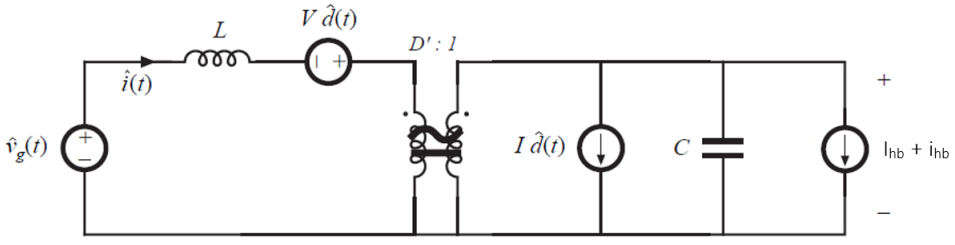

Figure 5.2: Small signal equivalent model of a boost converter connected to a half-bridge

For the case $f_{hb} >> f_s$, the half-bridge is operating at a frequency higher than the APFC bandwidth and so its controller does not react on the current variation due to the half-bridge. Thus,

$$\hat{d}(t) \approx 0 \tag{5.1}$$

Moreover, we also have $f_{hb} >> f_{line}$ with $f_{line} = 100Hz$ (rectified voltage), so :

- $\hat{v}(t) \approx 0$ (variation of the input voltage around a DC point is almost null.

- $I_{hb}(t) \approx 0$

The equivalent model can now be represented as follow (fig. 5.3):

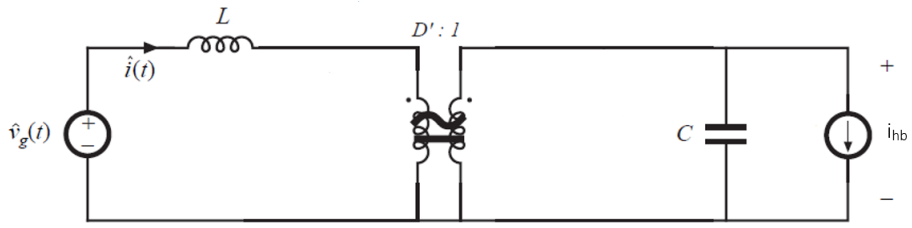

Figure 5.3: Simplified small signal equivalent model for $f_{hb} >> f_s$

The components at the right side can be placed to the left side taking into account the transformer ratio. This is illustrated in Figure 5.4 .

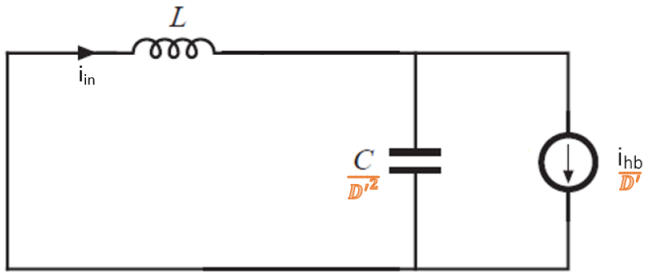

Figure 5.4: Simplified small signal equivalent model for $f_{hb} >> f_s$

This is a simple LC circuit and its transfer function is given by:

$$\boxed{\frac{\hat{i_{in}}}{\hat{i_{hb}}}(j\omega) = \frac{1}{D'} \cdot \frac{1}{(j\omega^2)\frac{CL}{D'^2} + 1}} \tag{5.2}$$

As shown in Figure 5.5, we have an attenuation of the half-bridge current for the frequency range considered (more than 10 kHz). When the duty-cycle increases, the attenuation becomes more important. This comes from the fact that when the duty-cycle is high (long t_{on}), the switch is closed for a longer time preventing the disturbance from entering into the input of the device. For the worst case (null duty-cycle) at 10kHz an attenuation of about 85dB is observed which is very important.

Non-idealities

Equation 5.2 can be improved taking the non-idealities of the boost into account.
For a boost with the following parameters: $P = 150W$, $V_o = 700V$ and $f_s = 30kHz$, typical non-ideality values are:

- $R_L = 5\Omega$

- $R_C = 1\Omega$

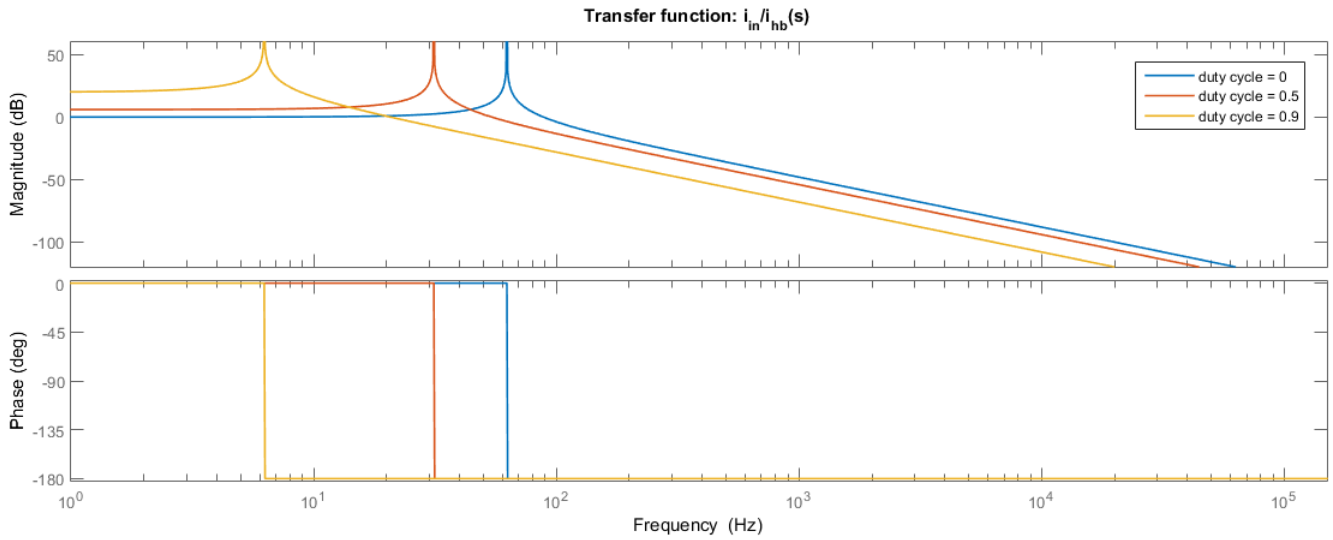

Figure 5.5

The transfer function can now be expressed as:

$$\boxed{\frac{\hat{i_{in}}}{\hat{i_{hb}}}(j\omega) = \frac{1}{D'} \cdot \frac{(j\omega)CR_C + 1}{(j\omega^2)\frac{CL}{D'^2} + (j\omega)C(R_C + \frac{R_L}{D'^2}) + 1}} \tag{5.3}$$

Figure 5.6 shows the transfer function with and without non-idealities for the worst case (duty-cycle=0). The attenuation with the non-idealities will be lower than the ideal case. However it stays important (around -65dB at 10kHz).

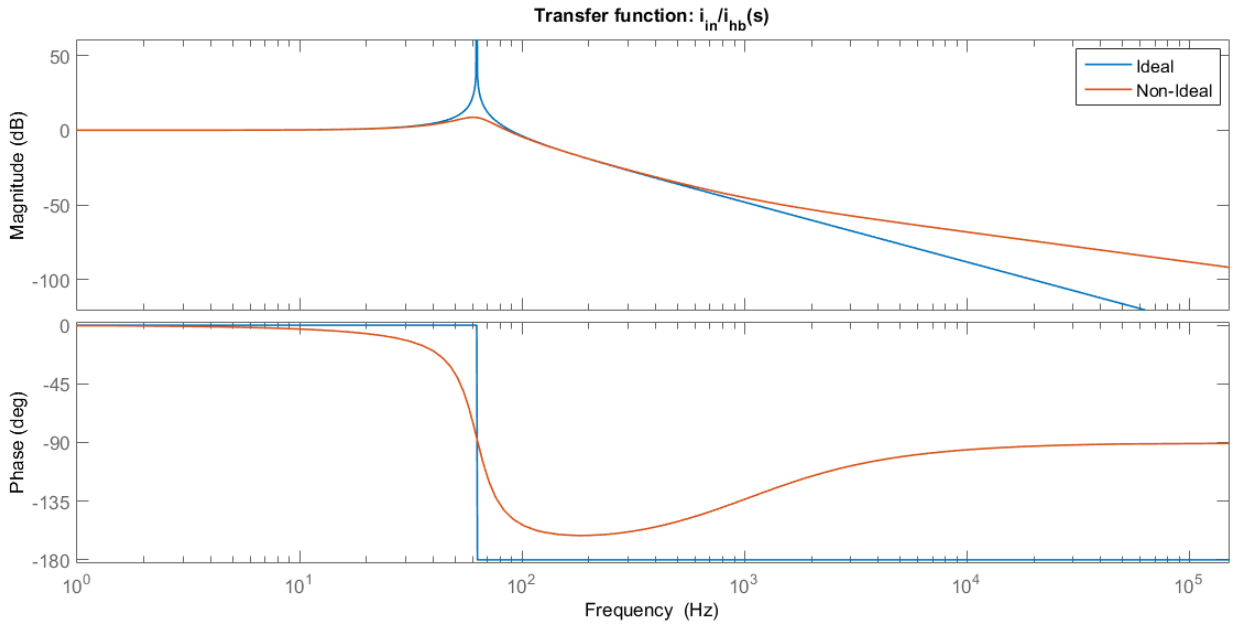

Figure 5.6

We can conclude that for the case $f_{hb} >> f_s$, the impact of the half-bridge can be neglected on the input current of the device.

Frequency order: $f_{hb} << f_s$

The APFC controller will now try to adapt and counter-act the impact of the CFL current variation and this reaction will depend on the half-bridge frequency. The half-bridge will now go through the APFC with an attenuation dependent on the half-bridge frequency and this attenuation can be estimated by computing the transfer function based on the state-space equations (i_{out} = load current).
The equation is computed directly with internal resistance of the inductor and of the capacitor (r_L and R_c).

$$sLi_L = V_{in} - i_L r_L - (1-D)V_{out} \tag{5.4}$$

$$V_{out}\left(\frac{sC}{1+sR_cC}\right) = (1-D)i_L - i_{out} \tag{5.5}$$

To compute the dependency, the transfer function between transient of i_L and i_{out} must be computed. As the impact of V_{in} on i_L transient will be independent of i_{out} impact, it can already be discarded from the equation.

From equation 5.4:

$$\frac{\hat{v}_{out}}{\hat{i}_L} = -\frac{sL + r_L}{1-D}$$

And when combining this result with equation 5.5, this gives:

$$\begin{aligned} \hat{i}_L\left(-\frac{sL+r_L}{1-D}\frac{sC}{1+sR_cC}\right) &= (1-D)\hat{i}_L - \hat{i}_{out} \\ \Rightarrow \frac{\hat{i}_L}{\hat{i}_{out}} &= \frac{(1-D)(1+sR_cC)}{s^2LC + s(r_LC + (1-D)^2R_cC) + (1-D)^2} \end{aligned} \tag{5.6}$$

We get the same result than the previous case (see equation 5.3). In fact we just use another method to get the same result. The only difference in this case is that the controller is fast enough to counter the output disturbance. The controller reaction will be seen at the input but attenuated a lot (left part of the transfer function). And in the previous case ($f_{hb} >> f_s$), the disturbance will just go through the boost (controller not fast enough) but attenuated much more (right part of the transfer function).

In Figure 5.7, the input current of the APFC is shown for different half-bridge frequencies (f_{hb}). As expected the attenuation gets more important when the resonant frequency of the tank circuit increases.
For $f_{hb} = 300Hz$ the "simulated" ratio between the frequency component at 300Hz of the current at the APFC input and at the tank circuit input is -31.53dB. This seems to be like the calculated transfer function.
For the other cases, the attenuation is so important that it is difficult to get a precise ratio value.

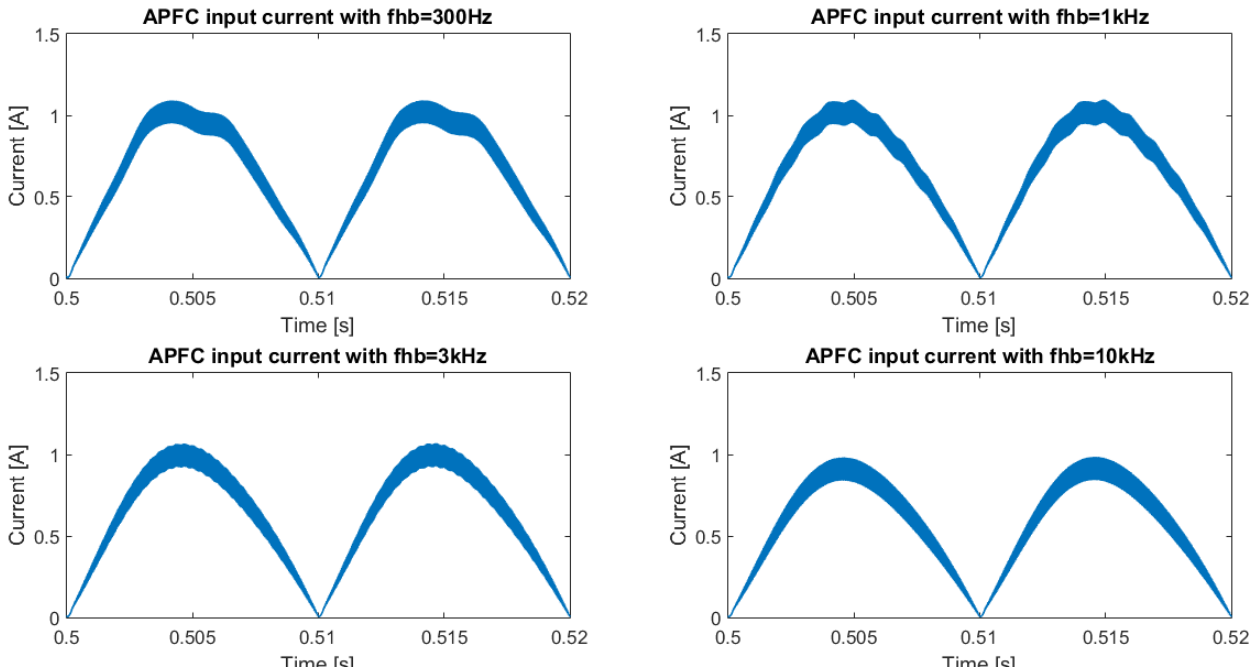

Figure 5.7: Input current of the APFC for different half-bridge frequencies (f_{hb})

5.2 Fourier series: theoretical analysis

The input current of the APFC is composed of triangles varying over time with an overall period of 10ms ($\frac{1}{100Hz}$), so the Fourier series analyses will be done through the following steps:
first an isosceles triangle waveform is analyzed, then a general triangle waveform of a given slope and finally in the next section, the Fourier series of the APFC input current waveform is computed.

A comparison between the theoretical results and simulations will be done at each of the different steps to validate the models.
The goal is to simplify the whole system by current sources and therefore speed up the simulations.

5.2.1 Mathematical definition

A Fourier series is an expression of a periodic function $f(t)$ in terms of an infinite sum of sines and cosines. It allows us to get the harmonic contain of a periodic function.
The Fourier series of the function $f(t)$ is given by the following expression [38]:

$$f(t) = \frac{1}{2}a_0 + \sum_{n=1}^{\infty} a_n cos(n\omega t) + \sum_{n=1}^{\infty} b_n sin(n\omega t) \tag{5.7}$$

with

$$a_0 = \frac{1}{T}\int_{-T}^{T} f(t)dt \tag{5.8}$$

$$a_n = \frac{1}{T}\int_{-T}^{T} f(t)cos(n\omega T)\ dt \tag{5.9}$$

$$b_n = \frac{1}{T}\int_{-T}^{T} f(t)sin(n\omega T)\ dt \tag{5.10}$$

We can notice the following:

- a_0 is the mean value of the function f(t),
  $a_1 cos(1\omega t) + b_1 sin(1\omega t)$ is the fundamental ,
  $a_2 cos(2\omega t) + b_2 sin(2\omega t)$ is the second harmonic,
  $a_3 cos(3\omega t) + b_3 sin(3\omega t)$ is the third harmonic,
  ...
  The amplitude of the harmonics can be computed as: $\sqrt{a_i^2 + b_i^2}$.
- For odd functions ($f(t) = -f(-t)$), $a_n = 0 \quad \forall n$
- For even functions ($f(t) = f(-t)$), $b_n = 0 \quad \forall n$

5.2.2 Isosceles triangle wave

In this section the Fourier series of a simple 30 kHz isosceles triangle wave is derived and the harmonic content is analyzed. The results are finally compared with the harmonics computed on Simulink© using the *FFT analysis tool*.

The waveform is represented in the figure below (fig 5.8).
It is an odd function, thus $a_n = 0$.
Moreover, it has a half-wave symmetry defined as : $x(t + \frac{T}{2}) = -x(t)$. This interesting property can be used to simplify the computation of the Fourier series on only a half-period:

$$b_n = \frac{2}{T} \int_0^T f(t) sin(n\omega t) dt \tag{5.11}$$

The factor b_n can then be computed as described in [39]:

$$b_n = \frac{2}{T} \left[\int_0^{\frac{T}{2}} \frac{t}{T/2} sin\left(\frac{n2\pi t}{2T}\right) dt \; + \int_{\frac{T}{2}}^T \left[1 - \frac{2}{T}\left(t - \frac{1}{2}T\right)\right] sin\left(\frac{n2\pi t}{2T}\right) dt \right] \tag{5.12}$$

$$= \frac{32}{\pi^2 n^2} cos\left(\frac{1}{4}n\pi\right) sin^3\left(\frac{1}{4}n\pi\right) \tag{5.13}$$

$$= \frac{8}{\pi^2 n^2} \begin{cases} (-1)^{\frac{n-1}{2}} & \text{n odd} \\ 0 & \text{n even} \end{cases} \tag{5.14}$$

Using the FFT analysis tool of Matlab Simulink, we can analyze the harmonic content:

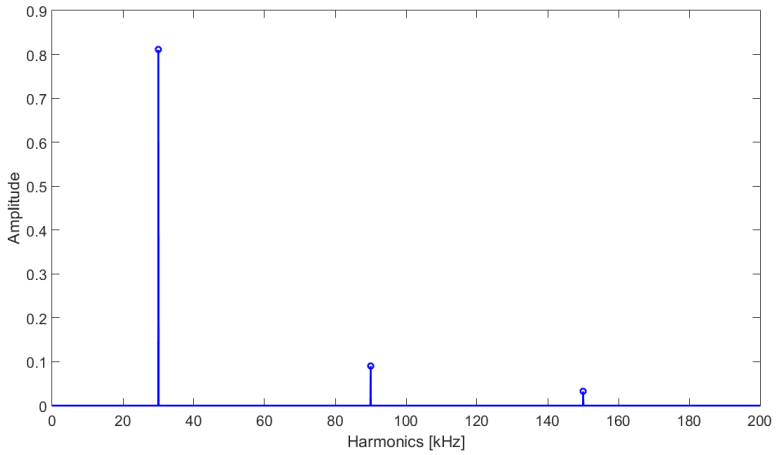

Figure 5.8: Spectrum of the triangle wave

As expected we only have odd harmonics (30kHz, 90kHz, 150kHz,...) and they decrease with n due to the $\frac{1}{n^2}$ term in equation 5.14 .

5.2.3 General triangle wave

We can go one step further and analyze a wave with triangles of a given slope m (of the rising part of the triangle). This case is illustrated in Figure 5.9 for different slopes ($m = 2, 3, 4, 5$).

N.B: slope and duty-cycle of the triangle are directly linked: $d = \frac{1}{m}$.

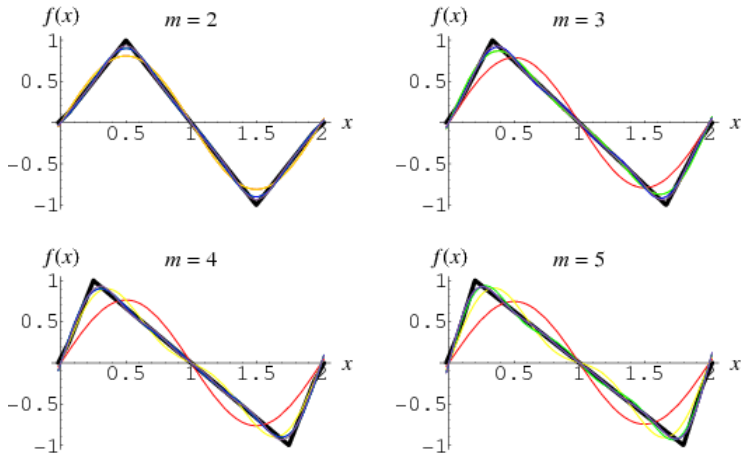

Figure 5.9: General triangle waveforms of slope m [39]

The function can be expressed as : [39]

$$f_m(t) = \begin{cases} \frac{mt}{T} & \text{for } 0 \leq t \leq \frac{T}{m} \\ 1 - \frac{m}{(m-1)T}(t - \frac{T}{m}) & \text{for } \frac{T}{m} \leq t \leq 2T - \frac{T}{m} \\ \frac{m}{T}(t - 2T) & \text{for } 2T - \frac{T}{m} \leq t \leq 2T \end{cases} \tag{5.15}$$

The function is odd again, and has a zero mean: $a_0 = 0$ and $a_n = 0$.
After some calculations, we get:

$$b_n = -\frac{2(-1)^n m^2}{n^2(m-1)\pi^2} sin\left(\frac{n(m-1)\pi}{m}\right) \tag{5.16}$$

Now, we will compute the coefficients for $m = 4$ and $m = 1.5$ and compare the values with the simulated waveforms (see table 5.1). We can notice that for m=2, we have an isosceles triangle wave and equation 5.16 becomes: $b_n = -\frac{2(-1)^n 2^2}{n^2\pi^2}$, the same expression than equation 5.14.

As shown in Table 5.1, the coefficients calculated theoretically and obtained by simulation are exactly the same.
Comparing the three first cases, increasing the slope from 2 to 6, decreases the fundamental (from 0.81 to 0.73) and increases the first higher harmonics (order 2,3,4).
The first effect can be explained graphically: when the slope changes (increase here), the triangles get less symmetrical and thus the 30kHz sine will play a lower role in the Fourier series (see figure 5.9, red waveform)

When we compare the 0.25 and 0.75 duty-cycle case (m=4 and m=1.33), that are the "symmetric" cases compared to the isosceles triangles, we get the same coefficients but with different signs for some of them (sine shifted by 180°).

		Theory	Simulation
$m = 2$			
	b_1	0.8106	0.8106
	b_2	0	0
	b_3	(-) 0.0901	0.0901
	b_4	0	0
	b_5	(-) 0.0324	0.0324
$m = 4$			
	b_1	0.7642	0.7642
	b_2	0.2702	0.2702
	b_3	0.0849	0.0849
	b_4	0	0
	b_5	(-) 0.0306	0.0306
$m = 6$			
	b_1	0.7295	0.7295
	b_2	0.3159	0.3159
	b_3	0.1621	0.1621
	b_4	0.0790	0.0790
	b_5	0.0292	0.0292
$m = 1.333$			
	b_1	0.7642	0.7642
	b_2	(-) 0.2702	0.2702
	b_3	0.0849	0.0849
	b_4	0	0
	b_5	(-) 0.0306	0.0306

Table 5.1: Fourier series coefficients b_n calculated and obtained by simulations.

It should be noted that for the simulation part, only the absolute value of the different coefficients are computed.

Effect of an offset

Considering an offset c on the triangular wave will lead to:

$$f(t) = c + f_0(t) \tag{5.17}$$

Calculating the coefficients:

$$a_0 = \frac{1}{T}\int_{-T}^{T} f(t)dt = \frac{1}{T}\int_{-T}^{T} c\ dt + 0 = 2c \tag{5.18}$$

$$a_n = \frac{1}{T}\int_{-T}^{T} f(t)cos(n\omega t)\ dt \tag{5.19}$$

$$= \frac{1}{T}\int_{-T}^{T} c\ cos(n\omega t)\ dt + \frac{1}{T}\int_{-T}^{T} f_0(t)cos(n\omega t)\ dt \tag{5.20}$$

$$= 0 + a_{n_0} \tag{5.21}$$

$$b_n = ... \tag{5.22}$$

$$= b_{n_0} \tag{5.23}$$

As expected the offset will only change the a_0 coefficient and from equation (5.7), $\frac{1}{2}a_0 = c$ will also be the offset of the Fourier series.
Of course this offset will correspond to the 0Hz component of the signal.

Effect of the amplitude

Until now a wave with an amplitude of 1 was considered.
For a general triangular wave of amplitude A, the equations of the waveform (equation 5.15) will now be:

$$f_m(t) = \begin{cases} \mathbf{A} \cdot \frac{mt}{T} & \text{for } 0 \leq t \leq \frac{T}{m} \\ \mathbf{A} \cdot \left(1 - \frac{m}{(m-1)T}(t - \frac{T}{m})\right) & \text{for } \frac{T}{m} \leq t \leq 2T - \frac{T}{m} \\ \mathbf{A} \cdot \frac{m}{T}(t - 2T) & \text{for } 2T - \frac{T}{m} \leq t \leq 2T \end{cases} \tag{5.24}$$

Using a similar approach as for the offset, we simply get:

$$b_n = \mathbf{A} \cdot \frac{-2(-1)^n m^2}{n^2(m-1)\pi^2} sin\left(\frac{n(m-1)\pi}{m}\right) \tag{5.25}$$

The effect of the offset and of the amplitude are shown in the table below. We consider an offset of 1 and an amplitude of 2.
We can observe that the results obtained previously are confirmed:

- Only a_0 is modified by the offset.

- The amplitude multiplies the a_n and b_n factors.

		Theory	Simulation
$m = 6$			
	a_0	1	1
	b_1	1.4590	1.4590
	b_2	0.6318	0.6318
	b_3	0.3242	0.3242
	b_4	0.1579	0.1579
	b_5	0.0584	0.0584

Table 5.2: Fourier series coefficients b_n calculated and obtained by simulations.

5.3 Fourier series: APFC replacement

The replacement of the APFC by its Fourier series in the complete model is represented in figure 5.10.

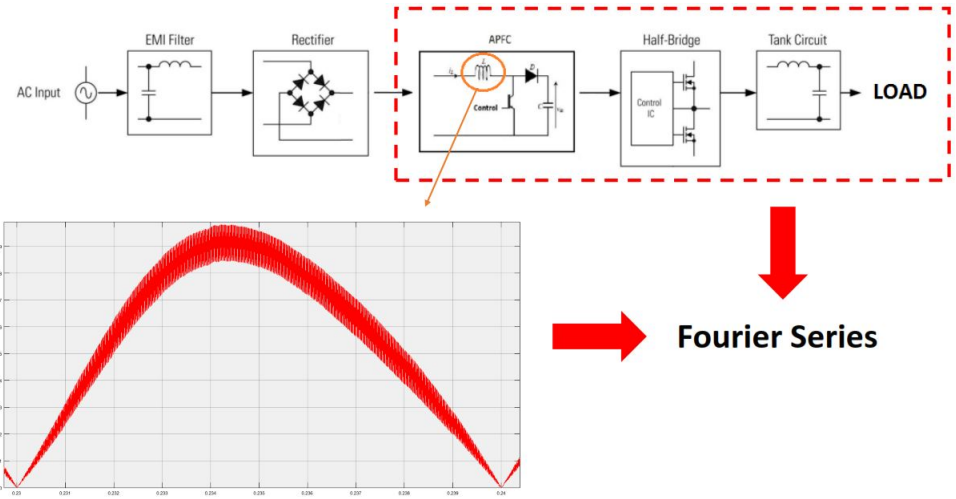

Figure 5.10

Only the APFC will be modeled by the Fourier Series in this section, but computations will be extended in section 5.4 to include the effect of the rectifier in it.

The Fourier coefficients cannot be computed over the all period directly as in equations 5.9 and 5.10 because the signal is discontinuous. Instead the integration is divided over many subintervals defined on the switching frequency (see figures 5.11 and 5.12).

$$\begin{aligned} a_n &= \frac{1}{L_{fund}} \int_0^{L_{fund}} f(t)\cos(n\omega t)\ dt \\ &= \frac{1}{L_{fund}} \sum_{k=0}^{K-1} \int_{k*2L_{pfc}}^{(k+1)*2L_{pfc}} f_{tri}(t-(k*2L_{pfc}))\cos(n\omega t)\ dt \end{aligned}$$

L_{fund} and L_{pfc} are the half-period of the fundamental signal and the APFC ripple respectively.

$f_{fund} = 100\ Hz$
$\Rightarrow L_{fund} = \frac{1}{2f_{fund}} = 5\ ms$

$f_{pfc} = 30\ kHz$
$\Rightarrow L_{pfc} = \frac{1}{2f_{pfc}} = 16.67\ \mu s$

$f_{tri}(t)$ is the function of a triangle which was given in equation 5.15. It can be made more general by defining it over two intervals only:

$$f_{tri}(t) = \begin{cases} \frac{A}{2}\frac{mt}{L_{pfc}} & \text{for } 0 \le t \le \frac{2L_{pfc}}{m} \\ \frac{A}{2}\left[2 - \frac{m}{(m-1)L_{pfc}}(t - \frac{2L_{pfc}}{m})\right] & \text{for } \frac{2L_{pfc}}{m} \le t \le 2L_{pfc} \end{cases} \tag{5.26}$$

So the total integration can be rewritten like this:

$$\begin{aligned} a_n = \frac{1}{T}\sum_{k=0}^{K-1} \Bigg\{ & \int_{k*2L_{pfc}}^{k*2L_{pfc}+\frac{2L_{pfc}}{m}} \frac{A}{2}\frac{m(t-(k*2L_{pfc}))}{L_{pfc}}\cos(n\omega t)\ dt \\ & + \int_{k*2L_{pfc}+\frac{2L_{pfc}}{m}}^{(k+1)*2L_{pfc}} \frac{A}{2}\left[2 - \frac{m}{(m-1)L_{pfc}}\left(t-(k*2L_{pfc}) - \frac{2L_{pfc}}{m}\right)\right]\cos(n\omega t)\ dt \Bigg\} \end{aligned}$$

First integral is for the rising edge (part 1 in figure 5.11) and the second one is for the falling edge (part 2 in figure 5.11). The integration over the complete period is represented in figure 5.12.

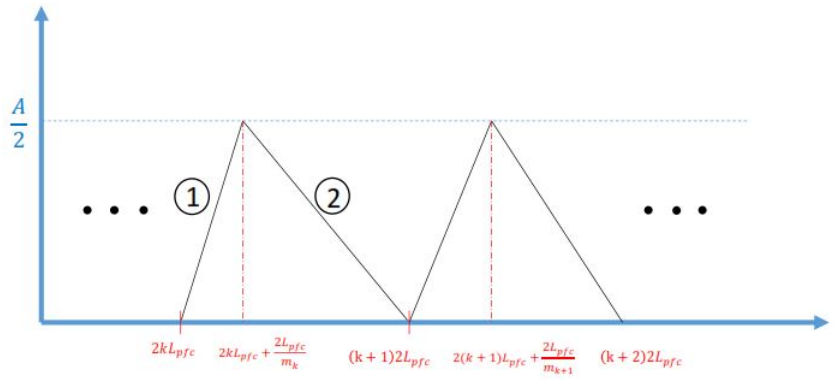

Figure 5.11: Integration on sub-interval

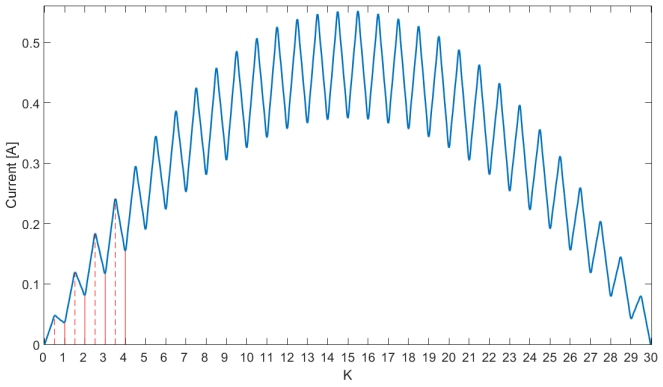

Figure 5.12: Integration over all period for Fourier Serie

The computations give the following coefficients for the rising and falling part (see complete development in appendix C)

Rising part:

$$P_1 = k * 2L_{pfc} \quad P_2 = \frac{2L_{pfc}}{m}$$
$$P_{dn} = P_1 \quad P_{up} = P_1 + P_2$$

$$a_{n,rise} = \frac{1}{L_{fund}} \sum_{k=0}^{K-1} \frac{A}{P_2} \left\{ P_2 \frac{L_{fund}}{n\pi} \sin\left(\frac{n\pi P_{up}}{L_{fund}}\right) + \left(\frac{L_{fund}}{n\pi}\right)^2 \left[\cos\left(\frac{n\pi P_{up}}{L_{fund}}\right) - \cos\left(\frac{n\pi P_{dn}}{L_{fund}}\right)\right]\right\} \tag{5.27}$$

$$b_{n,rise} = \frac{1}{L_{fund}} \sum_{k=0}^{K-1} \frac{A}{P_2} \left\{ -P_2 \frac{L_{fund}}{n\pi} \cos\left(\frac{n\pi P_{up}}{L_{fund}}\right) + \left(\frac{L_{fund}}{n\pi}\right)^2 \left[\sin\left(\frac{n\pi P_{up}}{L_{fund}}\right) - \sin\left(\frac{n\pi P_{dn}}{L_{fund}}\right)\right]\right\} \tag{5.28}$$

Falling part: $P_1 = 2L_{pfc}$ $P_2 = \frac{2L_{pfc}}{m}$
$P_{dn} = k * P_1 + P_2$ $P_{up} = (k+1) * P_1$

$$a_{n,fall} = \frac{1}{L_{fund}} \sum_{k=0}^{K-1} \frac{A}{(m-1)} \left\{ \sin\left(\frac{n\pi P_{up}}{L_{fund}}\right) \frac{L_{fund}}{n\pi} \left[m(1+k) - \frac{P_{up}}{P2} \right] + \right.$$
$$\sin\left(\frac{n\pi P_{dn}}{L_{fund}}\right) \frac{L_{fund}}{n\pi} \left[-m(1+k) + \frac{P_{dn}}{P2} \right] +$$
$$\left. \frac{1}{P_2} \left(\frac{L_{fund}}{n\pi}\right)^2 \left[-\cos\left(\frac{n\pi P_{up}}{L_{fund}}\right) + \cos\left(\frac{n\pi P_{dn}}{L_{fund}}\right) \right] \right\} \quad (5.29)$$

$$b_{n,fall} = \frac{1}{L_{fund}} \sum_{k=0}^{K-1} \frac{A}{(m-1)} \left\{ \cos\left(\frac{n\pi P_{up}}{L_{fund}}\right) \frac{L_{fund}}{n\pi} \left[-m(1+k) + \frac{P_{up}}{P2} \right] + \right.$$
$$\cos\left(\frac{n\pi P_{dn}}{L_{fund}}\right) \frac{L_{fund}}{n\pi} \left[m(1+k) - \frac{P_{dn}}{P2} \right] +$$
$$\left. \frac{1}{P_2} \left(\frac{L_{fund}}{n\pi}\right)^2 \left[-\sin\left(\frac{n\pi P_{up}}{L_{fund}}\right) + \sin\left(\frac{n\pi P_{dn}}{L_{fund}}\right) \right] \right\} \quad (5.30)$$

5.3.1 Ripple amplitude and slope (duty-cycle)

Ripple amplitude (A) and slope (m) must vary depending on V_{in} to keep V_{out} constant. A and m are computed for each sub-interval depending on V_{in} at the beginning of the sub-interval. They are modified only once per sub-interval to maintain the hypothesis of steady-state.

Slope: the slope of the signal depends on its amplitude and duration: $m' = \frac{A}{dL}$. But amplitude and period are already taken into account in the general equation, so it becomes only: $m = \frac{1}{d} = \frac{V_{out}}{V_{out} - V_{in}}$.

Ripple amplitude: as steady-state is considered over one sub-interval, the ripple amplitude can be computed as the current variation during step 1 (inductance charging, see equation 4.8): $A = \frac{V_{in} d}{L f_s}$

It can be observed in figure 5.13 the effect on the signal when adding these variations.

- Signal 1: Constant ripple and duty-cycle
- Signal 2: Varying ripple and constant duty-cycle
- Signal 3: Varying ripple, constant duty-cycle and the average ripple value is added to get a lower bound = 0 (the average ripple is basically the a_0 term of our *Fourier serie* and the integral of the entire signal would stay at 0 without it).
- Signal 4: Varying ripple and duty-cycle, average ripple value added [1].

Finally, the signal is added on the fundamental current, giving the result that was shown in figure 5.12.

[1] switching frequency is lowered to be able to observe the variation of duty-cycle

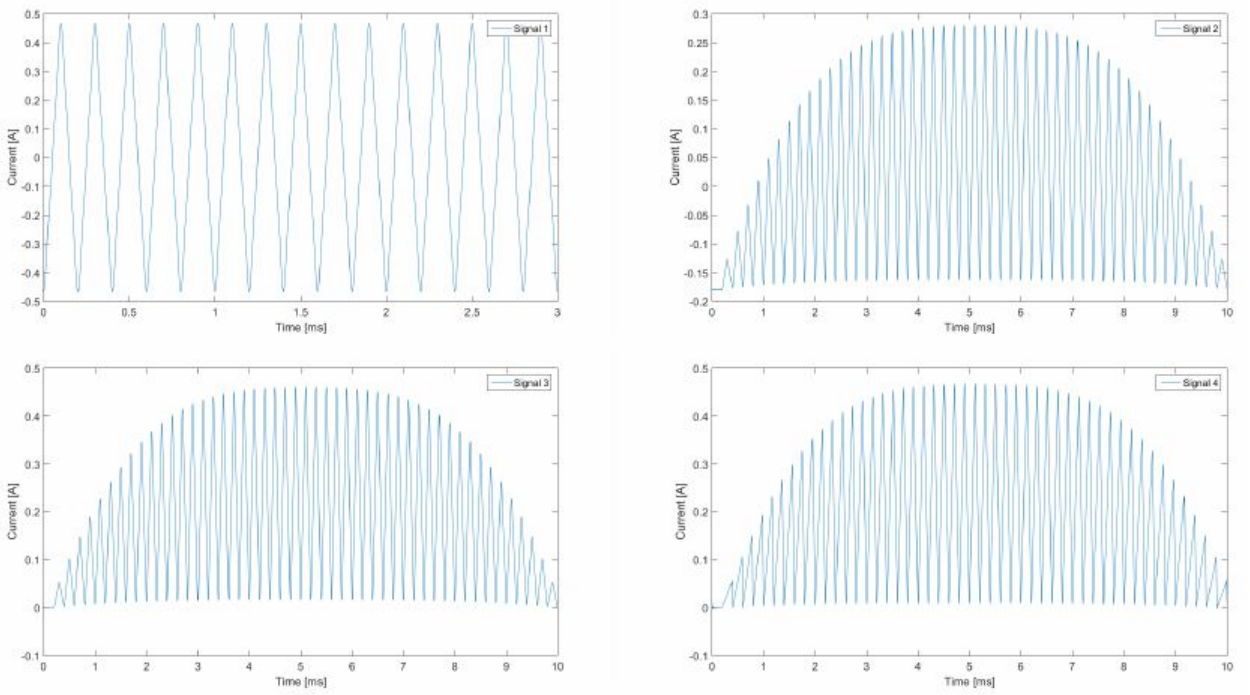

Figure 5.13

5.3.2 Output voltage impact

The ripple depends both on input voltage and duty-cycle. As defined in equation 4.7, duty-cycle comes close to 0 when V_{in} approaches V_{out}. This happens for $V_{out} = 400V$ when $V_{in,max}$ is reached ($V_{in,max} \approx 325V$) and this has a strong decreasing impact on the ripple (see figure 5.14, left) . This topic will be further described in section 5.3.4, but the difference in ripple can already be observed in figure 5.14.

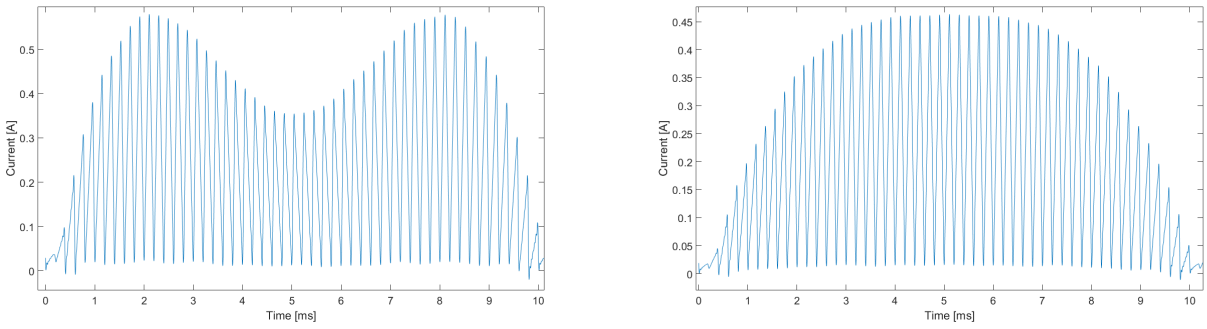

Figure 5.14: Ripple amplitude for $V_{out} = 400V$ (left) and $V_{out} = 700V$ (right)

5.3.3 Harmonics: modulation and choice

Accuracy of the *Fourier Serie* representation depends on how many harmonics we use, but many can be considered as negligible.
If the ripple was constant, there would be non-zero harmonics only on exact multiple of the switching frequency, but the variation of ripple both in magnitude and duty-cycle modulate the signal around the switching frequency multiples (see figure 5.15): harmonic order multiple of 50, i.e. ratio $\frac{f_s}{f_{fund}} = \frac{5e3}{100}$.

The harmonics are defined at frequencies $m \cdot f_s \pm k \cdot f_{fund} = m \cdot f_s \pm k \cdot 100$.
These side-lobe harmonics ($\pm k \cdot 100$) are decaying pretty fast and so it is arbitrarily defined to neglect the ones which are at least 10 times lower than the main lobe harmonic (see figure 5.15).

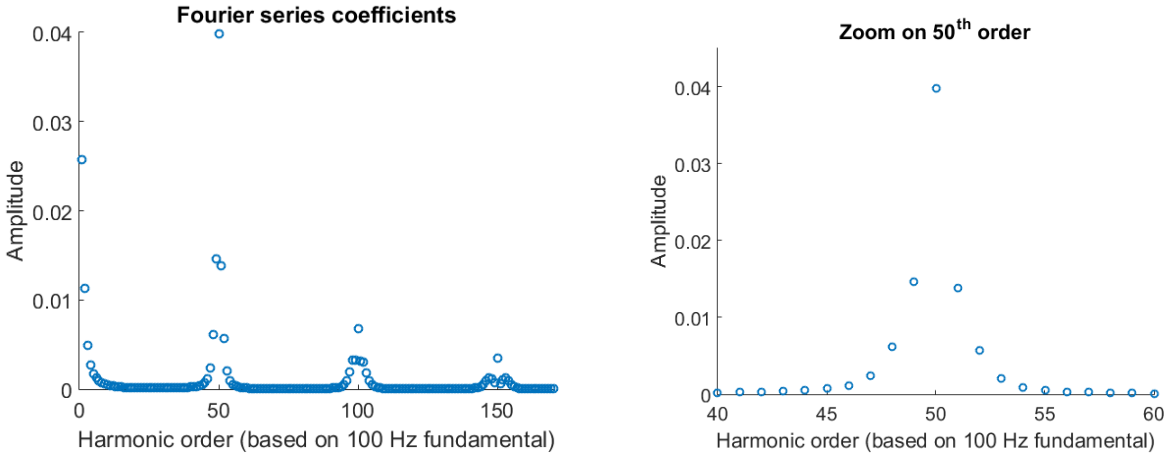

Figure 5.15: Modulation around the main harmonic

Error ratio

Ratio between harmonic content of the APFC input current in the complete ideal model and the simplified model.
Computed for one device, the error stays in the range [0.9 1.1], for any output power or frequency of the device.

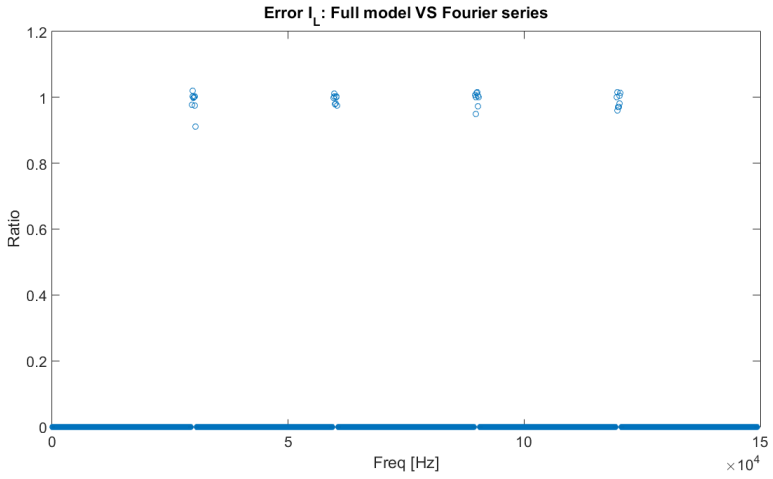

Figure 5.16

5.3.4 Spectrogram analysis

Input current of the APFC

In this subsection, we will analyze the harmonic content of the current wave during the time. The visualization of these combined time and frequency analysis is called a spectrogram. They are generally two-dimensional graphs containing the time, the frequency and finally the amplitude or energy of the signal. The latter can be represented by colors.
The spectrogram is computed, by dividing the signal in sections of a given length (with some

overlap tolerated). Each section is then windowed and the power spectrum is computed [13]. In Simulink©, a block named *Spectrum Analyzer* can be used to get a spectrogram of a signal. In figure 5.17, the spectrogram of the input current after the rectifier is shown for an output voltage of 700 and 400V. To have a better color range for the harmonics, we will not display the 100Hz component here.

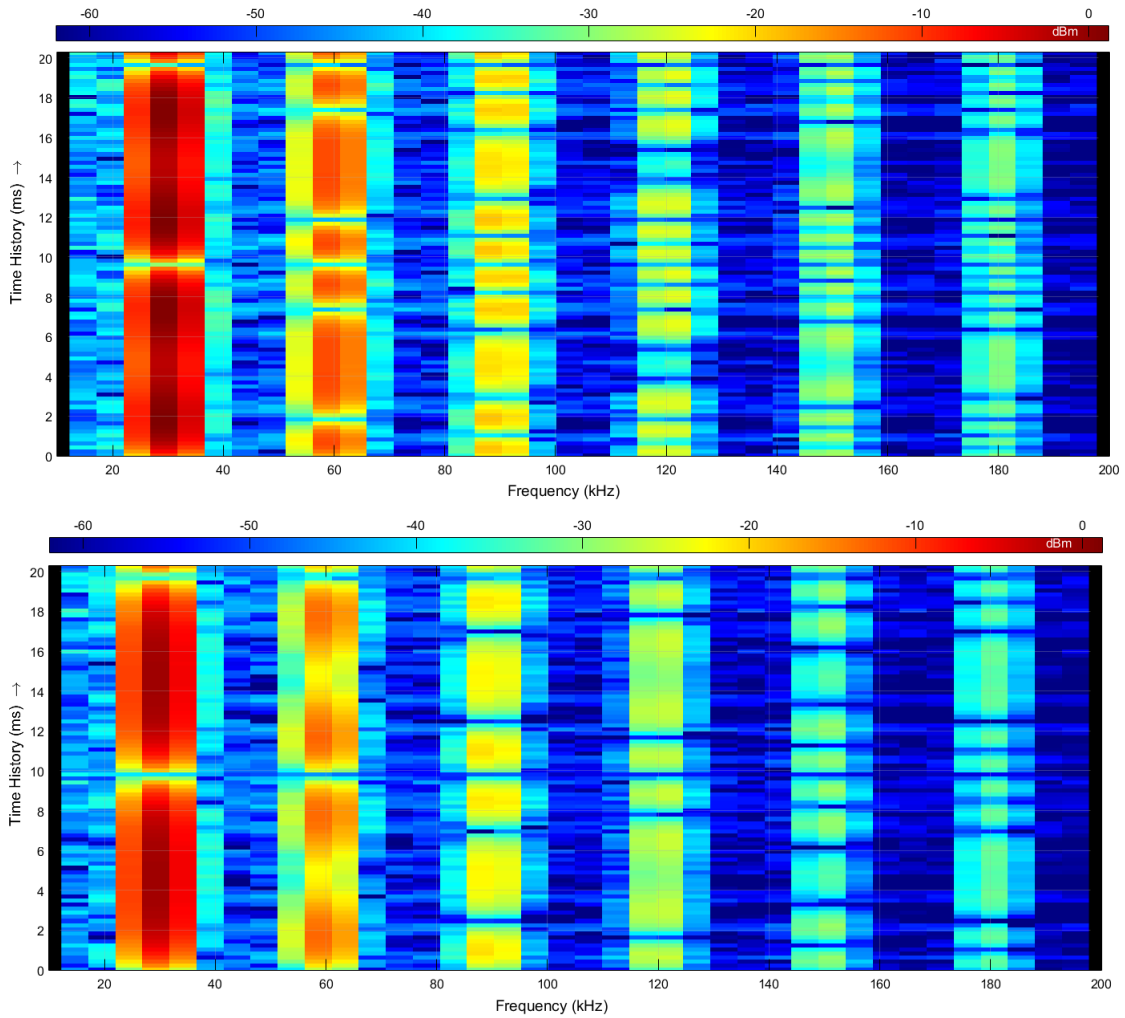

Figure 5.17: Spectrogram of the input current (after rectifier) for $Vo = 400V$ (top) and $700V$ (bottom)

As seen in figure 5.17, the 30kHz and its harmonics (60kHz,90kHz,...) are present. Their amplitude varies during the time and the number of peaks are different in both cases (400V and 700V):

We will now try to determine the number of peaks theoretically using a simple approach. We will consider that at a given time t, we have a periodic triangular wave of duty-cycle $1/m(t)$ and amplitude $A(t)$. Of course it is an important simplification because as explained earlier, the FFT is computed on windowed sections of the signal, so the FFT is not computed on:

- an infinite periodic signal.

- a signal of constant duty-cycle.

However, applying a window on a signal in a time domain is equivalent to applying a convolution with a sinc function in the frequency domain and so the result is this sinc function (depending

Frequency [kHz]	Number of peaks	
	$Vo = 400V$	$Vo = 700V$
30	2	1
60	4	2
90	5	3
120	7	4
150	8	5

Table 5.3: Fourier series coefficients b_n calculated and obtained by simulations.

on the window type and size) around the different deltas of the triangular wave. The maximal values of the windowed signal will so be around the initial frequency components. Because we just want to have the trend of the frequency evolution of the signal it can be acceptable.
The second approximation is also acceptable because the time resolution of our Spectrogram is only $150.28\mu s$. During this time interval the duty-cycle do not change a lot.

From equation 5.25, considering a varying amplitude ($A(t)$) and duty-cycle ($1/D(t) = m(t)$) we get:

$$b_n = A(t) \cdot \frac{-2(-1)^n m(t)^2}{n^2(m(t)-1)\pi^2} sin\left(\frac{n(m(t)-1)\pi}{m(t)}\right) \tag{5.31}$$

These two parameters were computed in section 4.2 as :

$$D(t) = 1 - \frac{V_{in}(t)}{V_o} \tag{5.32}$$

$$A(t) = \frac{D(t) \cdot T_s}{L} \cdot V_{in}(t) \tag{5.33}$$

The evolution of the b_n coefficients and thus the harmonic amplitudes (because $a_n = 0$) for $V_o = 400V$ and $V_o = 700V$ are shown respectively in Figure 5.18 and 5.19.
The number of peaks are exactly the same than those obtained by the spectrogram of the simulation (see table 5.3). The highest coefficient is the 30kHz component ($b_{n=1}$) and has the same shape than the ripple of the input current. The output voltage has an important impact on the shapes of the coefficients:
When the voltage increases, the number of variations, peaks decreases. The coefficient amplitude range for both voltage cases are not as much different because the inductance is designed for a maximal current ripple. So when the output voltage increases, the inductance is also increased to maintain approximatively a constant ripple.

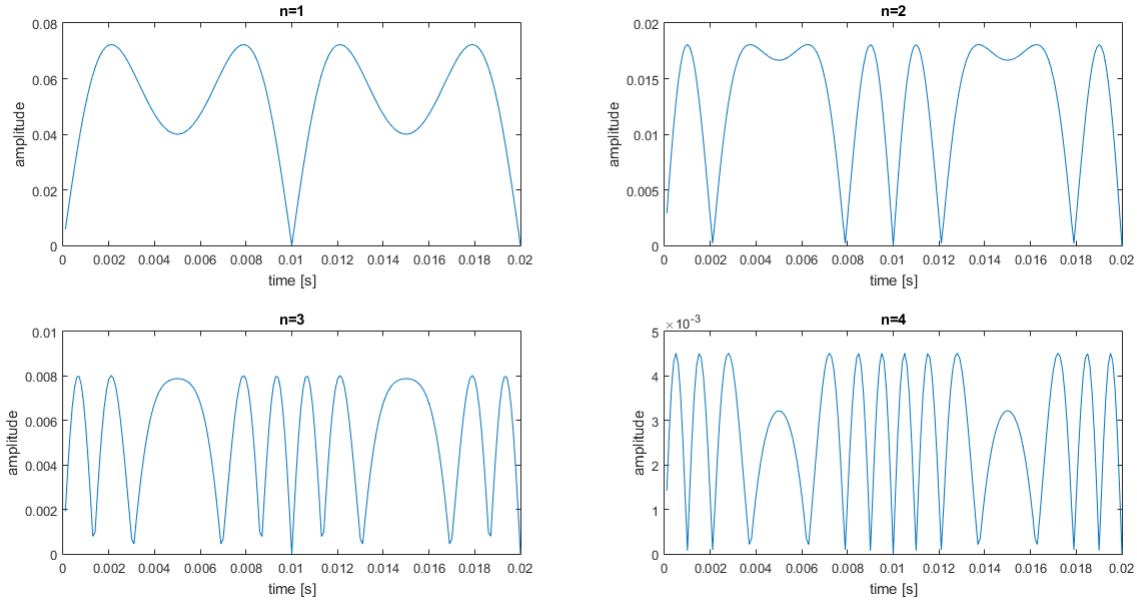

Figure 5.18: $b_n(t)$ coefficient for $V_o = 400V$

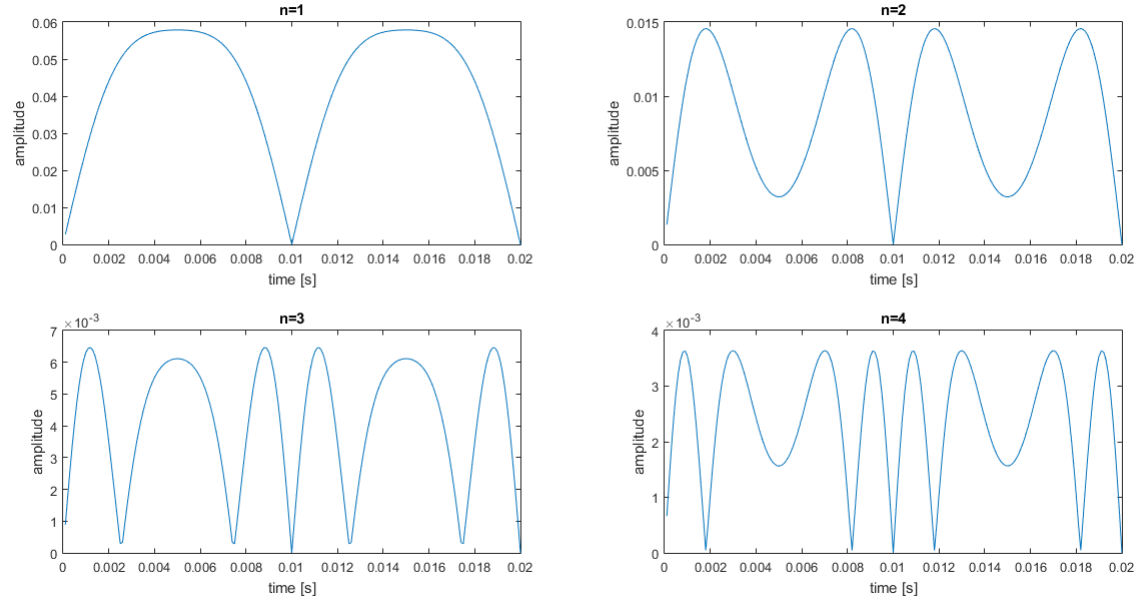

Figure 5.19: $b_n(t)$ coefficient for for $V_o = 700V$

Input current of the device (EMI included)

The spectrogram of the current at the input of the device (EMI included) is shown in Figure 5.20 . It is like the spectrogram in the previous case (after the rectifier, fig. 5.17) except that due to the the EMI filter with a cut-off frequency around 20kHz, the harmonics amplitudes will be attenuated.

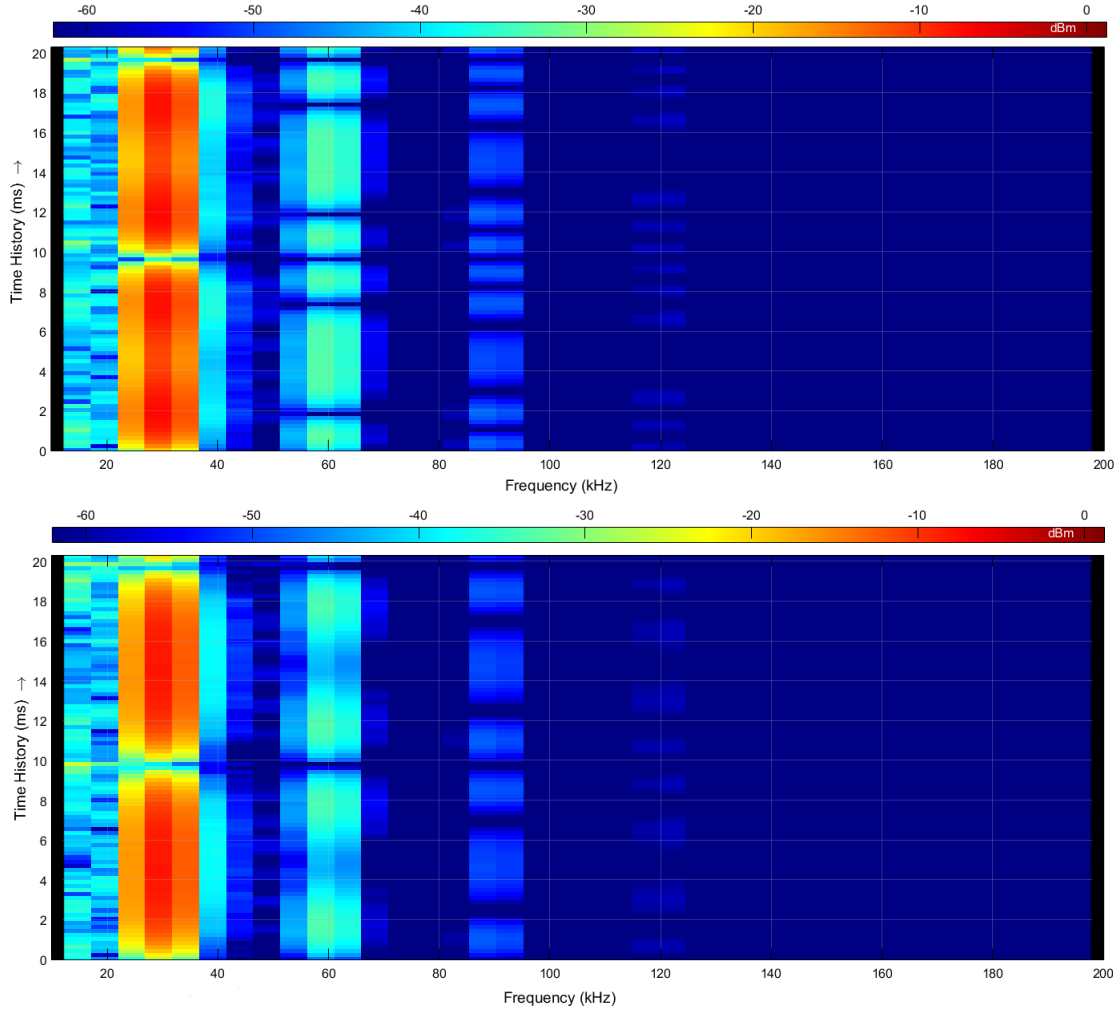

Figure 5.20: Spectrogram of the input current at the input of the device for $Vo = 400V$ (top) and $700V$ (bottom).

5.4 Fourier series: APFC+rectifier replacement

The objective is now to replace both the APFC and the rectifier by a single Fourier Series. The equations 5.27, 5.28, 5.29 and 5.30 found in section 5.3 to compute the Series coefficient are still valid as the ripple is still the same. The signal shape can be seen in figure 5.21 and is equivalent to taking the one used for the Fourier Series of the APFC, multiplied by a [+1 -1] rectangular window.

There are 3 values that we must eventually modify to perform the computation:

- L_{fund}: We are now taking a complete period of the grid voltage.

  $f_{fund} = 50\ Hz \Rightarrow L_{fund} = \frac{1}{2f_{fund}} = 10\ ms$

- m (ripple slope): identical for both half-periods.

- A (ripple amplitude): same in amplitude for the 2^{nd} half-period, but with a negative sign.

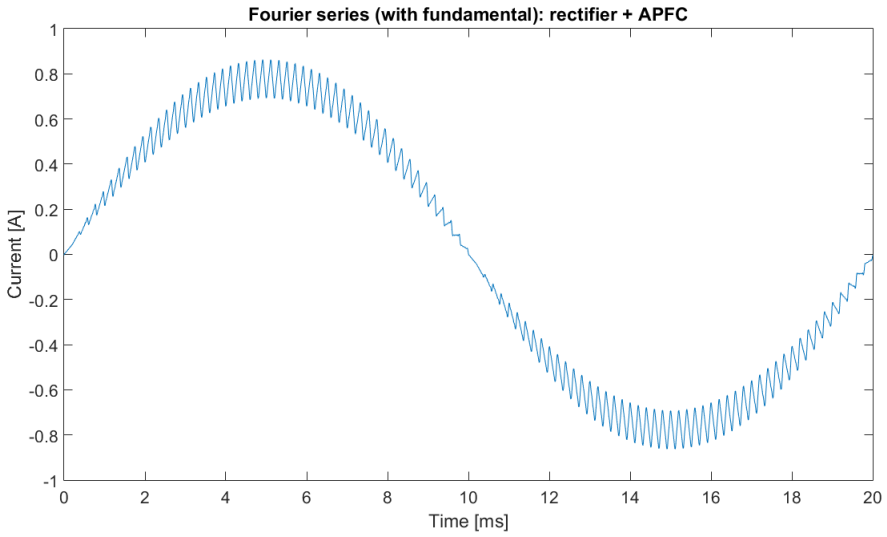

Figure 5.21: Fourier series for 50 Hz signal

	APFC	rectifier + APFC
L_{fund}	L_1	$2 * L_1$
m	m_1	$[m_1,\ m_1]$
A	A_1	$[A_1,\ -A_1]$

Table 5.4: Summary of variable modifications

5.4.1 Harmonics: modulation and choice

The modulation by the rectangular window of the rectifier lead to a displacement of the harmonics which are now at frequencies (see figure 5.22): $m \cdot f_s \pm (50 + k \cdot 100)$.

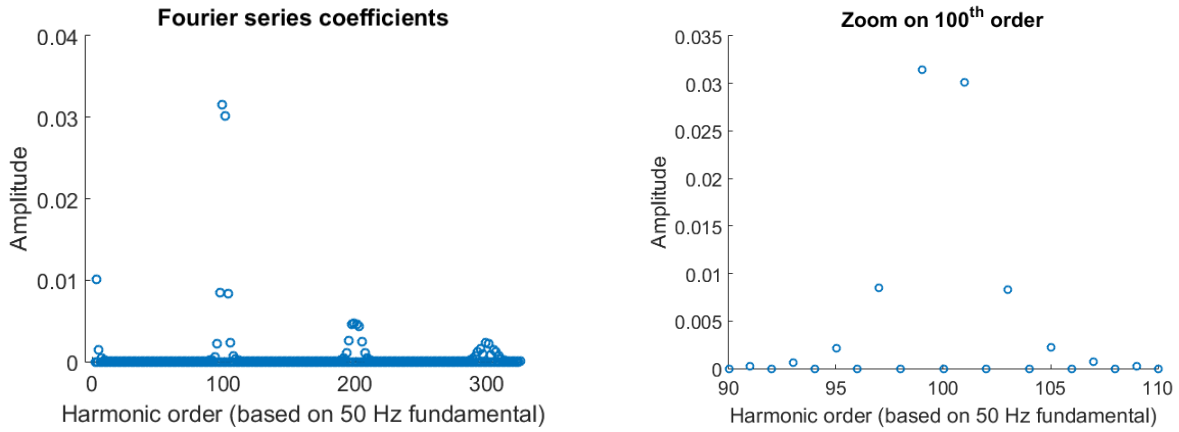

Figure 5.22: Modulation around the main harmonic

5.5 Simplified model conclusion

In this chapter a simplified model of an equipment using an APFC has been obtained.

Despite the fact that the CFL block is producing supraharmonics, they are attenuated by the APFC and are therefore considered as negligible.

The APFC and the rectifier can both be replaced by a single Fourier series representing the input current frequency distribution. This Fourier series is composed of harmonics around multiple of the APFC switching frequency. The modulation due to ripple and duty-cycle variation over a fundamental period ($2L_{fund}$) and the rectifier produce harmonics[2] at $m \cdot f_{pfc} \pm k \cdot 50$. But the decaying around $m \cdot f_{pfc}$ is important making harmonics usually negligible for $k > 4$.

The comparison between the full model and the simplified one gives satisfying results ($<$ $\pm 10\%$ error). Thus a device of given parameters can be replaced by only a current source (a sum of current sources) and the EMI filter. The EMI filter is kept because it is the block directly connected to the grid and will thus play a major role in the primary and secondary emissions of several devices interacting together.

[2] $m \in \mathbb{N}$
$k \in \mathbb{Z}_{impair}$

CHAPTER 6

PRIMARY AND SECONDARY EMISSIONS

In this chapter, the entire system (couple of devices in parallel) will be represented by a set of analytical equations. This is possible because everything after the EMI filter in a CFL model can be replaced by a Fourier series which can easily be inserted in the set of equations.

These simplifications enable to make simulation in frequency-domain (which are therefore much faster) and to make easier analyses of interaction between different equipment: especially the primary and secondary emissions.

In the CIRED paper [33], the analysis of several equipments on the same grid using an active power factor correction is done. The equipment including the EMI filter is modeled by a current source and the capacitor of the filter at grid side (see figure 6.1). The grid is modeled by a resistance because in low-voltage, the grid is more resistive. As we analyze the high harmonics currents (due to the APFC) and that we assume that the grid voltage is a pure $50Hz$ source (without higher harmonic content), we have a zero grid current/voltage source for harmonics above 50Hz.

We will not only consider equipments working around a same switching frequency f_s but also at completely different switching frequency thus also different EMI filters.

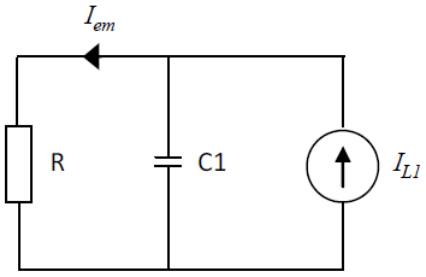

Figure 6.1: Simplified model of one device connected to the grid given in [33]

6.1 Two devices connected to the grid

The model of two devices connected to the grid is shown in Figure 6.2 . Each equipment is modeled by a current source determined in the Fourier Series section 5.3 and 5.4 and an EMI filter, both depending on the design parameters (power, boost switching frequency (f_s), output voltage (V_o), ...).

The EMI filter is an important block that has to be considered because it is directly connected to the grid and will play an important role in the interaction between equipments.
Of course, our equipment is connected between the line and the neutral and so the current sources will only impact the differential mode currents in the EMI filter; (the topology of the simplified DM filter is shown in section 4.4.1).

I_{em} is the current flowing at the interface of one of the equipment and will take into account the primary emission and secondary emission of the device defined as:

- Primary emissions: Emission coming from the device depending on its "output" impedance. This impedance includes the grid impedance, the EMI impedance of the device but also impedance of other connected devices (their EMI filter).

- Secondary emission: Emission generated elsewhere (from other devices, the grid) and that propagates into the device due to its low impedance at its terminal.

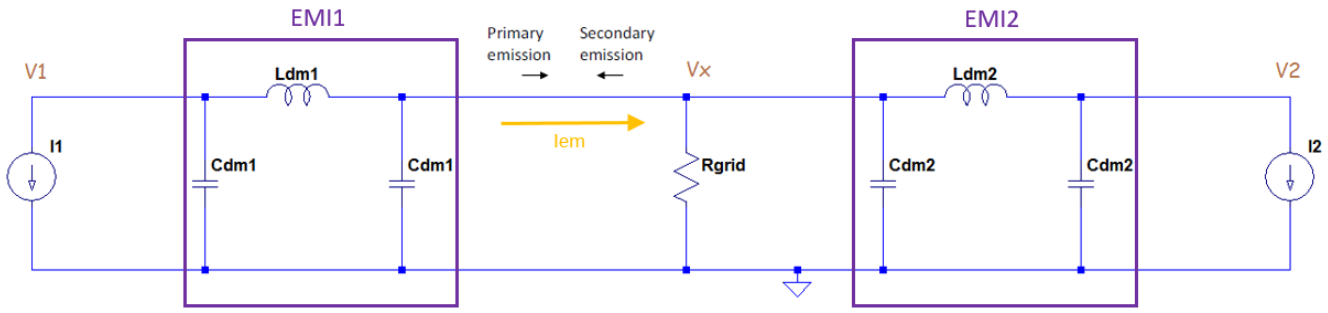

Figure 6.2: Simplified model of two devices connected to the grid (R_d not represented)

The interface current can be computed using Kirchhoff's current law at the different nodes of the circuit. The system of equations obtained is:

$$\begin{cases} I_1 - V_1 \cdot s \cdot C_{dm1} = \dfrac{V_1 - V_x}{(sL_{dm1} + R_d)} & \text{(I)} \\ \dfrac{V_1 - V_x}{sL_{dm1} + R_d} = V_x \cdot s \cdot C_{dm1} + I_{em} & \text{(II)} \\ Iem + \dfrac{V2 - Vx}{sL_{dm2} + R_d} = \dfrac{V_x \cdot (s \cdot R_{grid} \cdot C_{dm2} + 1)}{R_{grid}} & \text{(III)} \\ I_2 - V_2 \cdot s \cdot C_{dm2} = \dfrac{V_2 - V_x}{(sL_{dm2} + R_d)} & \text{(IV)} \end{cases}$$

where $R_d = 2 \cdot R_{dm} (= 16\Omega)$ are the damping resistors of the EMI filters.
Note: In our design, C_{DM} is fixed, thus $C_{DM1} = C_{DM2} = C_{DM}$.

This linear system of 4 equations with 4 unknown is hard to solve by hand. An efficient function in Matlab named `linsolve()` can be used to solve linear systems.

The solution of the current flowing at the interface of device 1 (I_{em}) is [1] :

$$\begin{aligned} I_{em}(s) &= I1(s) \cdot H1(s) - I2(s) \cdot H2(s) \\ &= I1 \cdot \frac{C^2 L_2 R s^3 + (C^2 R R_d + C L_2) s^2 + (2CR + CR_d)s + 1}{As^5 + Bs^4 + Cs^3 + Ds^2 + Es + 1} \\ &- I2 \cdot \frac{C^2 L_1 R s^3 + C^2 R R_d s^2 + 2CRs + 1}{As^5 + Bs^4 + Cs^3 + Ds^2 + Es + 1} \end{aligned} \tag{6.1}$$

with

$$\begin{aligned} A &= 2C^3 L_1 L_2 R \\ B &= (2C^3 L_1 R R_d + 2C^3 L_2 R R_d + C^2 L_1 L_2) \\ C &= (3C^2 L_1 R + 3C^2 L_2 R + C^2 L_1 R d + C^2 L_2 R_d + 2C^3 R R_d^2) \\ D &= (C^2 R_d^2 + C L_1 + C L_2 + 6C^2 R R_d) \\ E &= (4CR + 2CR_d) \end{aligned}$$

The first term of the equation ($I_1 \cdot H_1$) represents the primary emissions (I_{em} when $I_2 = 0$) and the second term represents the secondary emissions and the current at the interface is the difference between the primary and the secondary emissions.
An important point has to be noticed here:
The current I1(s) and I2(s) have their harmonic content that depends on the switching frequency f_s of their APFC. It is absolutely possible that for some given frequency, only primary emissions or even only secondary emissions are present. Moreover because we are working in the frequency domain and the current sources are sum of sines and cosines (Fourier series) we can just work at a given frequency f_i and have:

$$I_{em}(j\omega_i) = I1(j\omega_i) \cdot H1(j\omega_i) - I2(j\omega_i) \cdot H2(j\omega_i) \quad (\omega_i = 2\pi f_i) \tag{6.2}$$

Obviously this model can be extended to more than 2 devices following the same methodology, but the resulting expression would therefore become too long to be written in a synthetic manner.

6.1.1 Effect of the grid resistance

The grid impedance will have a big impact on the primary and the secondary emissions because it impacts the output impedance seen at the terminal of the devices.
First the primary transfer function $H1$ is plotted for different grid resistances ($R_{grid} = 1,\ 10,\ 25,\ 50\Omega$). The 2 devices used here are two identical devices with $P = 150W$, $V_o = 700V$ and $f_s = 30kHz$:

[1] To make the equations more readable, L_{dm} will be replaced by L and C_{dm} by C .

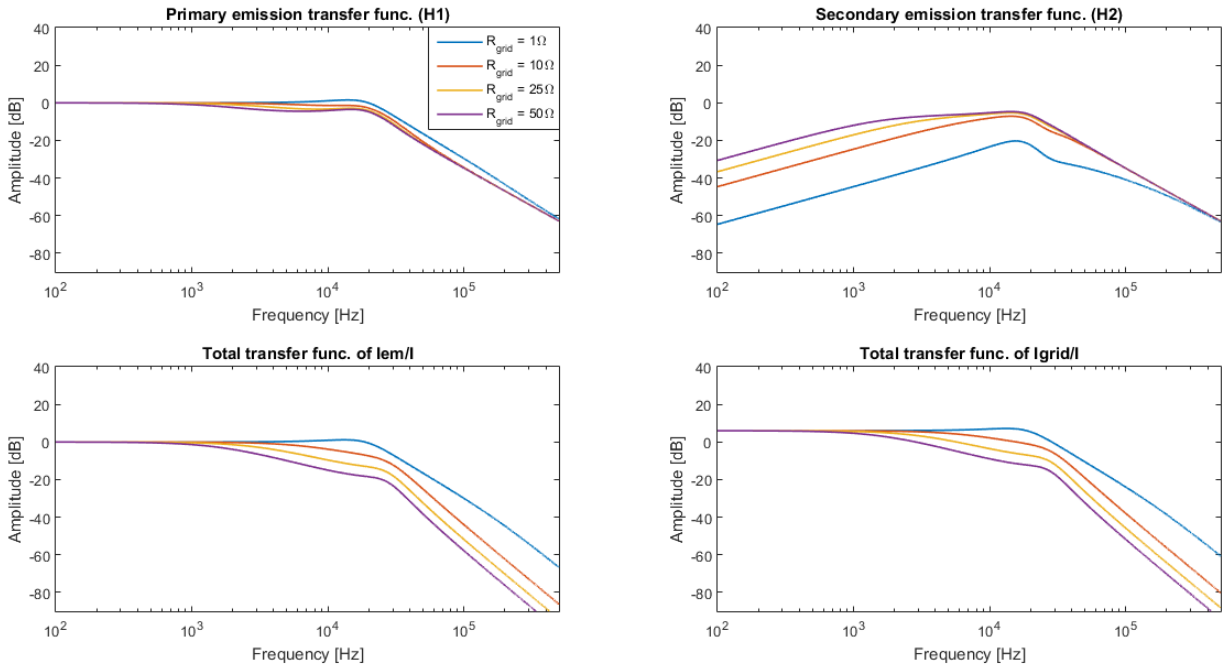

Figure 6.3

The following can be observed:

- Primary emission: the grid resistance value will have an impact on the damping (at the resonance frequency of the EMI filter) of the primary emission. When the resistance increases, the damping gets more important.

- Secondary emission: When the grid resistance increases, the secondary emission increases as well. This can simply be explained by the fact that when the resistance increases, less current from device 2 will flow into the grid and will instead flow into device 1.
  Nb. The secondary emission increases with the frequency until the resonance frequency but decreases after. This can be explained as follow:
  At low frequencies ($f < f_s$), the primary emission of device 2 is approximatively constant. When the frequency increases, the reactance of the EMI filter inductance of device 1 will be more important and the reactance of the capacitor at the grid side will be less important. Thus more current will flow into the capacitor of device 1.
  After the switching frequency ($f > f_s$), the primary emission of device 2 will decrease a lot and so, the secondary emission of device 1 as well.

Because two identical devices were used, it is possible to get a transfer function between the interface current I_{em} and the current of one equipment I and the same for the current entering into the grid I_{grid}. (For different devices I_{em} and I_{grid} will depend on both current I_1 and I_2.) For identical devices, the grid current is simply the sum of the interface currents at each device.

Before the cut-off frequency ($\pm 20kHz$) of the EMI-filter in the 2-20kHz band, the primary emissions are approximately constant, the secondary emissions increases and the grid transfer function is already decreasing. This shows that the higher harmonics stays more inside the low voltage network than flowing into the grid.

6.1.2 Effect of the number of devices

Figure 6.4 shows the impact of the number of identical devices on the primary and secondary emission. As for the grid resistance effect, the parameters of the devices are the following: $P = 150W$, $V_o = 700V$ and $f_s = 30kHz$ and the grid resistance is set to 5Ω.

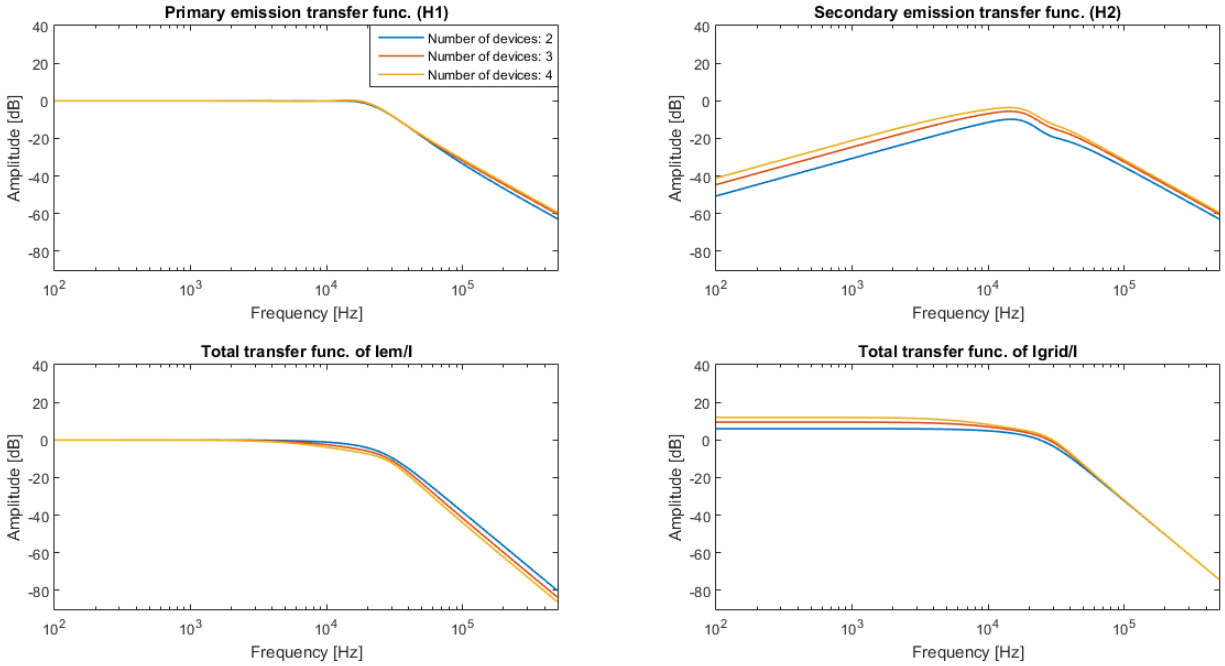

Figure 6.4

The following can be observed:

- Primary emission: The number of devices has not a big impact on the primary emission. They are a little bit increased with the number of devices due to the lower impedance at high frequency (more EMI filters in parallel).
- Secondary emission: They will obviously increase with the number of devices (more current sources from the other devices in parallel).

6.2 Model accuracy

Simulations that ran for a couple of minutes with the complete model are being performed in only a few seconds with this approach. But is the accuracy provided by this simplified model enough? This will be verified in this section while making further analysis of the primary and secondary emissions. In terms of equations, both types of emissions are defined by the followings:

$$I_{prim}(j\omega_i) = I_{em}(j\omega_i)]_{I_2(j\omega_i)=0} = I_1(j\omega_i) \cdot H_1(j\omega_i)$$
$$I_{sec}(j\omega_i) = I_2(j\omega_i) \cdot H_2(j\omega_i) = I_{prim}(j\omega_i) - I_{em}(j\omega_i)$$

As for the Fourier series analysis, the complete model of the APFC will be used to compare with the simplified transfer function and assess its accuracy: error ratio $= |\frac{I_{em,complete\ model}}{I_{em,simplified\ model}}|$ with I_{em} computed relative to device 1. In the mean time, we also want to observe the evolution of secondary emissions in relation with the situations.

3 different situations (with 3 devices every time) will be implemented to test the accuracy of this simplified model:

- All 3 devices have a different frequency with no common multiple below 150 kHz
- All 3 devices have a different frequency with 1 common multiple below 150 kHz
- All 3 devices have the same frequency

6.2.1 Different frequencies with no common multiple below 150 kHz

3 devices with the following switching frequencies: 25 kHz, 35 kHz and 45 kHz.
The error is maintained pretty stable, staying most of the time in the range [0.9; 1.1] (see figure 6.5). The secondary emissions are non-existant because no device is active in the same bandwidth as any other device.

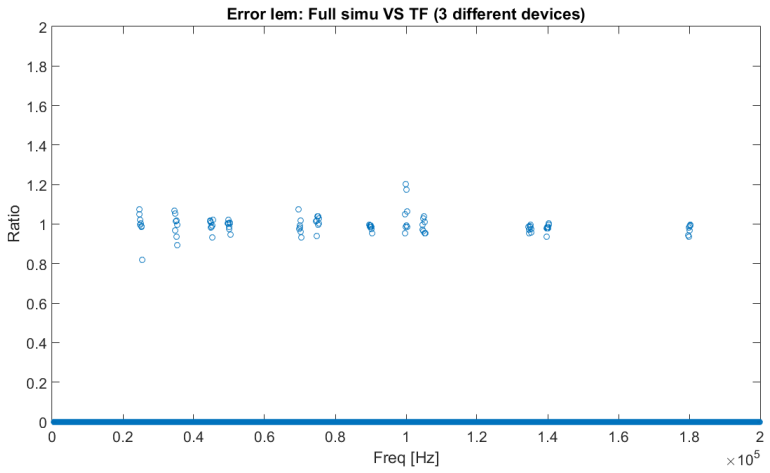

Figure 6.5: Error ratio: I_{em} from complete model over simplified model

6.2.2 Different frequencies with 1 common multiple below 150 kHz

3 devices with the following switching frequencies: 30 kHz, 37 kHz and 45 kHz.
Once again the error ratio for I_{em} is kept mostly in the range [0.9; 1.1] (see figure 6.6), but high secondary emissions are only observed around 90 kHz (see figure 6.7) because it is a common harmonic to 30 kHz and 45 kHz switching frequencies.
At 90 kHz, this is the 3^{rd} harmonic of the 30kHz-device and the 2^{nd} harmonic from the 45kHz-device. And so the harmonics from the 45kHz-device are a bit higher than the ones from the 30kHz-device because both devices were set to work with the same power. Therefore the secondary emissions from the 45kHz-device are also higher, explaining the ratio higher than 100% in figure 6.7.
If the computations had been done based on $I_{em,device3}$, as shown in Figure 6.8, the ratio would have been lower than 100% because secondary emissions would come from the 30kHz-device and the primary emissions from the 45kHz-device.

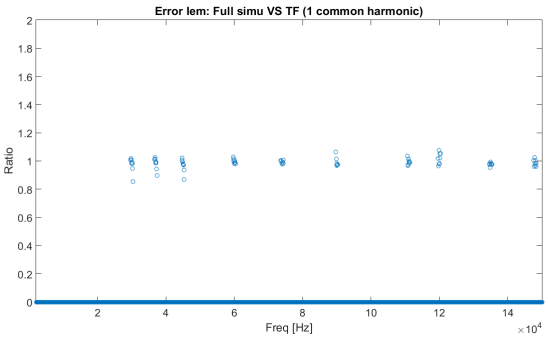

Figure 6.6: Error ratio: I_{em} from complete model over simplified model

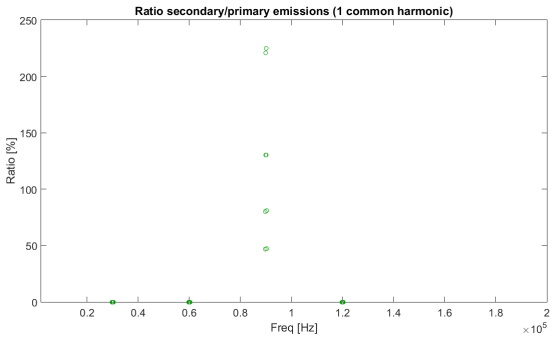

Figure 6.7: Ratio I_{sec}/I_{prim} simplified model

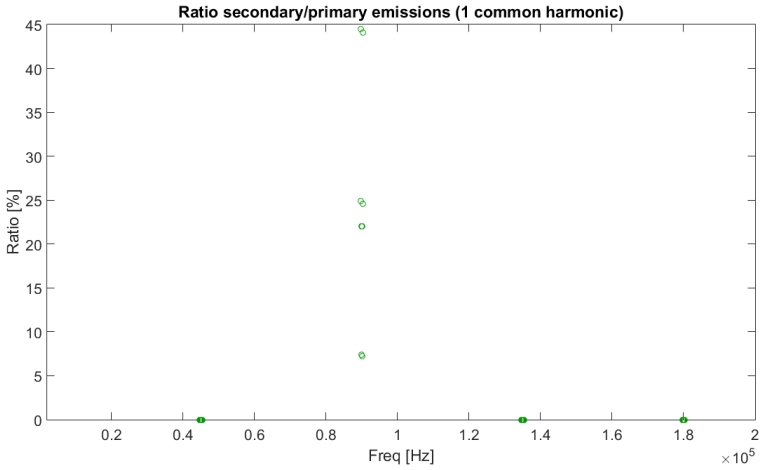

Figure 6.8: Ratio I_{sec}/I_{prim} from simplified model: I_{em} defined relatively to the third device

6.2.3 Same frequency

3 devices with the following switching frequencies: 30 kHz.

As was explained in the previous section, until the resonant frequency of the system (and a bit afterwards depending on the quality factor of the resonance), secondary emissions are increasing while primary emissions stay constant. This explains the sharp increase in the ratio I_{sec}/I_{prim} until 60 kHz as seen in figure 6.10.

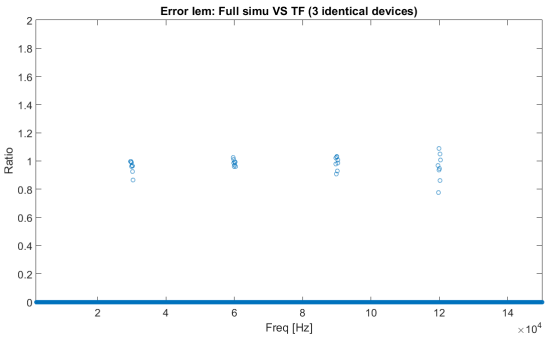

Figure 6.9: Error ratio: I_{em} from complete model over I_{em} from simplified model

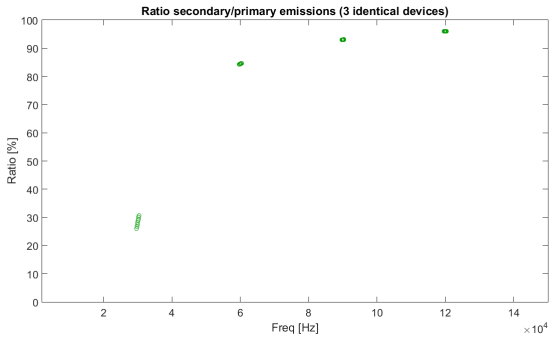

Figure 6.10: Ratio I_{sec}/I_{prim} (defined from simplified model)

6.2.4 Power/voltage variation and non-idealities

Tests were also executed with different devices to validate the model accuracy and 2 records will be shown here. Moreover both tests have been executed with the ideal model and with non-idealities.

Power variation only

This first test (see figures 6.11 and 6.12) is done for 3 devices with the following output power: 200W, 50W and 50W. It was realized with different frequencies having one common harmonic (30kHz, 37kHz and 45kHz). Other characteristics are the same as for previous examples: $V_{out} = 700V$ and $f_{hb} = 80kHz$.

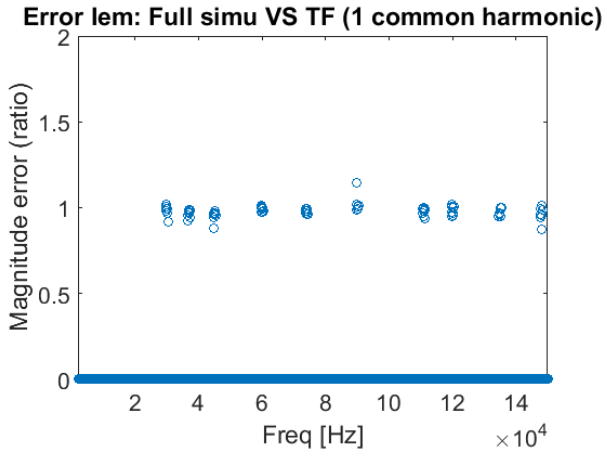

Figure 6.11: Error ratio of $I_{em,device1}$ with $P_1 = 200W$, $P_2 = 50W$, $P_3 = 50W$

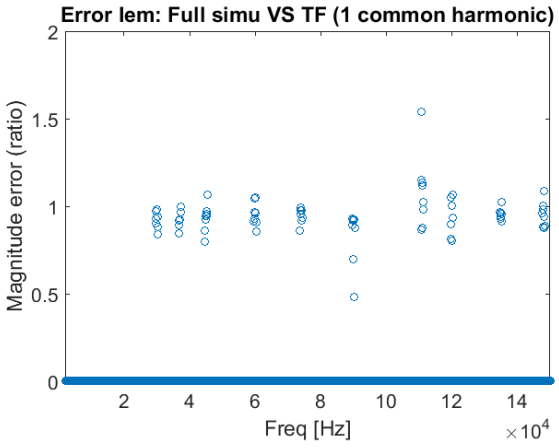

Figure 6.12: Error ratio of $I_{em,device1}$ with non-idealities: $r_L = 5\Omega$, $V_d = 0.7\Omega$, $ESR = 1.5\Omega$

Power and voltage variation

The second test (see figures 6.13 and 6.14) is done for 3 devices with 3 different power and output voltages. It was also realized with different frequencies having one common harmonic (30kHz, 37kHz and 45kHz). The half-bridge is kept constant at $f_{hb} = 80kHz$.

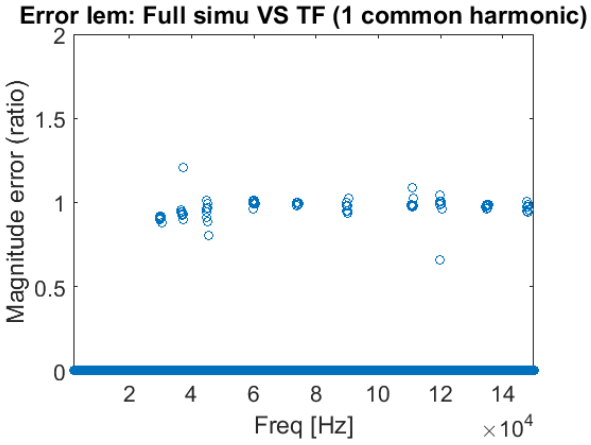

Figure 6.13: Error ratio of $I_{em,device1}$ with $P_1 = 50W$, $P_2 = 200W$, $P_3 = 500W$ $V_{o,1} = 500V$, $V_{o,2} = 600V$, $V_{o,3} = 700V$

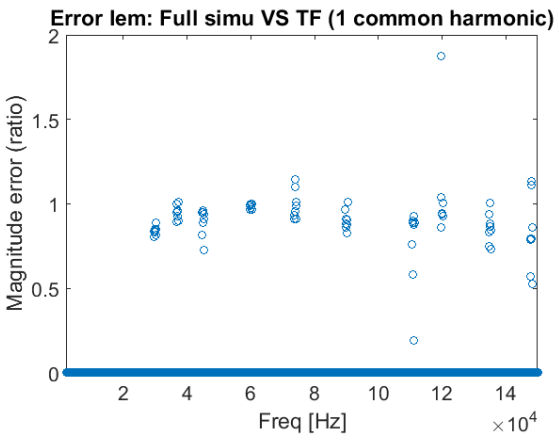

Figure 6.14: Error ratio of $I_{em,device1}$ with non-idealities: $r_L = 5\Omega$, $V_d = 0.7\Omega$, $ESR = 1.5\Omega$

Conclusion

In both tests, results were quite accurate for the ideal model

CHAPTER 7

CONCLUSION

The objective of this work was to propose a simulation model for equipment creating harmonics in the frequency range from 2kHz to 150 kHz. It was decided to focus on a *Compact Fluorescent Lamp* for its generic model with the central APFC.

The initial objective was to implement a complete model running in a time-domain simulation to give the most accuracy. Unfortunately, this model proved to be far too slow to be practical, requiring several minutes of computation time to simulate only a few devices in parallel for 1 second. This model would have to run for hours to be able to simulate an entire house.

Therefore it was proposed to break down the APFC model to only the harmonics of its input current and replace these harmonics by a Fourier series. In steady-state, the input current can be considered as periodic with a 1/50Hz period (imposed by the grid) and this was the period used to compute the Fourier series. This enabled to speed up the harmonics computation time, but they could only be calculated at the input of the device and furthermore for an isolated device.

This led to a second simplification: breaking down the network from the complete simulation to its Kirchhoff's current equations. So the all system could be represented by current equations and the APFC by a current source (derived through the Fourier series). This enables to compute the current harmonics everywhere in the system, making the distinction at a device input between current coming from the device itself or from another one, and all this with a computation time of a few seconds only. The relative error was kept between 0.9 and 1.1 compared to the complete model.

A summary of the computation time for the different models and relative to the number of devices simulated is given in table 7.1.

	Complete model [s]	Simulink with FS [1] [s]	Analytical model[2] [s]
1 device	195	81.4	2.2
3 devices	392	148	4.5
5 devices	657	205	5.1

Table 7.1: Simulations: computation time (run-time of 1 second)

Most of the tests were performed with an ideal model, but some non-idealities were also tested (parasitic capacitors and voltage drops) to assess the model validity. With strong non-idealities (up to 2 times the common values for the parasitic capacitors), the error between the ideal complete model and the complete model with non-idealities could reach up to 250%.
This variation could not be reproduced in the simplified model because the ripple amplitude

[1] Complete model, with APFC replaced by current source derived from Fourier series
[2] Last chapter simplification

is computed on the rising edge of the ripple and the non-idealities impact mostly the falling edge of the ripple. Therefore some adaptation of the model should be done to take them into consideration correctly.

The error ratios are based on the hypothesis that the complete model is our reference. This reference should be confronted to physical results of a real CFL lamp to validate the model.

This modeling procedure could be extended to other types of APFC converters (buck, buck-boost, flyback) and other types of contol modes (Discontinuous Conduction Mode, ...).

APPENDIX A

CROSS-OVER FREQUENCY: VOLTAGE LOOP

The cross-over frequency is defined as follow:

$$|G_{vOL}(j\omega_{cv})| = 1 \tag{A.1}$$

with G_{vOL} the voltage open loop transfer function and $\omega_{cv} = 2\pi f_{ci}$ where f_{ci} is the cross-over frequency.
From the voltage open loop transfer function (equation 4.26), a relation between K_p and K_i can be found:

$$\left|\frac{KRK_p(j\omega_{cv} + \frac{K_i}{K_p})}{RC(j\omega_{cv})^2 + 2j\omega_{cv}}\right| = 1 \tag{A.2}$$

$$\iff \frac{|KRK_p(j\omega_{cv} + \frac{K_i}{K_p})|}{|RC(j\omega_{cv})^2 + 2j\omega_{cv}|} = 1 \tag{A.3}$$

$$\iff \frac{\sqrt{(KRK_p\omega_{cv})^2 + (KRK_i)^2}}{\sqrt{(-RC\omega_{cv}^2)^2 + (2\omega_{cv})^2}} = 1 \tag{A.4}$$

$$\tag{A.5}$$

Squaring both side of the equation:

$$\frac{(KRK_p\omega_{cv})^2 + (KRK_i)^2}{(-RC\omega_{cv}^2)^2 + (2\omega_{cv})^2} = 1 \tag{A.6}$$

K_p can now be isolated as:

$$K_p = \sqrt{\frac{\omega_{cv}^2(R^2C^2\omega_{cv}^2 + 4) - K^2R^2K_i^2}{K^2R^2\omega_{cv}^2}} \tag{A.7}$$

APPENDIX B

TOTAL RMS NOISE CURRENT OF A CCM APFC

The first step to compute the total rms current ($I_{in,rms}$) on the 100Hz input waveform is to compute the local rms current $i_{in,rms}$ on a switching period of the APFC (T_s). It is defined as:

$$i_{rms}^2 = \frac{1}{T_s}\int_{T_s} i_{in}(t)^2 dt \tag{B.1}$$

$$= \frac{1}{T_s}\left(\int_0^{t_{on}} i_{on}(t)^2 dt + \int_0^{t_{off}} i_{off}(t)^2 dt\right) \tag{B.2}$$

The rising and falling parts of the current (i_{on} and i_{off}) are supposed to be linear (see 4.2) and can be expressed as [29]:

$$i_{on}(t) = \frac{\Delta I_L(\omega t)}{t_{on}(\omega t)} \cdot t + I_{in}(\omega t) - \frac{\Delta I_L(\omega t)}{2} \tag{B.3}$$

$$i_{off}(t) = -\frac{\Delta I_L(\omega t)}{t_{off}(\omega t)} \cdot t + I_{in}(\omega t) + \frac{\Delta I_L(\omega t)}{2} \tag{B.4}$$

For an APFC the duty-cycle is adjusted such that the current follows the rectified voltage waveform. The on and off time intervals will thus depends on the 100Hz input voltage [29]:

$$t_{on}(\omega t) = T_s \cdot (1 - \alpha sin(\omega_{100} t)) \tag{B.5}$$

$$t_{on}(\omega t) = T_s \cdot \alpha \cdot sin(\omega_{100} t) \tag{B.6}$$

where $\alpha = \frac{V_{in}}{V_o}$.

Replacing i_{on} and i_{off} by their expressions leads to the following expression [29]:

$$i_{in,rms}^2(\omega t) = I_{in}^2(\omega t) + \frac{\Delta I_L^2(\omega t)}{12} \tag{B.7}$$

The first part represents the "average" input current and the second one the ripple current that represents the noise.
As shown in 4.2, the current ripple on an inductance is given by:

$$\Delta I_L = V_{in}(\omega t) \cdot \frac{t_{on}(\omega t)}{L} \tag{B.8}$$

The total rms current on a half-period (10 ms) can now be calculated:

$$i^2_{noise,rms} = \frac{1}{\pi}\int_0^{\pi}\left[\frac{V_{in}}{L}\cdot sin(\theta)\cdot T_s(1-\alpha sin(\theta))\right]^2 d\theta \tag{B.9}$$

$$= \frac{1}{\pi}\frac{V_{in}^2 T_s^2}{L^2}\int_0^{\pi}\left(\sin^2\theta + \alpha^2\sin^4\theta - 2\alpha\sin^3\theta\right)d\theta \tag{B.10}$$

$$= \frac{1}{\pi}\frac{V_{in}^2 T_s^2}{L^2}\left(\int_0^{\pi}\sin^2\theta d\theta + \alpha^2\int_0^{\pi}\sin^4\theta d\theta - 2\alpha\int_0^{\pi}\sin^3\theta d\theta\right) \tag{B.11}$$

$$= \frac{1}{\pi}\frac{V_{in}^2 T_s^2}{L^2}\left(\frac{\pi}{2} + \alpha^2\frac{3\pi}{8} - \frac{8}{3}\alpha\right) \tag{B.12}$$

APPENDIX C

FOURIER SERIES DEVELOPMENT

C.1 Rising part

The computation of both integrals is described separately: first one here and the second one in next section. To make the computations a bit easier and readable, the following variables are used:

$$\begin{array}{ll} P_1 = k * 2L_{pfc} & P_2 = \frac{2L_{pfc}}{m} \\ P_{dn} = P_1 & P_{up} = P_1 + P_2 \end{array}$$

$$\begin{aligned} a_{n,rise} &= \tfrac{1}{L_{fund}} \textstyle\sum_{k=0}^{K-1} \tfrac{A}{2} \tfrac{m}{L_{pfc}} \quad \left\{ \int_{P_{dn}}^{P_{up}} x \cos\left(\tfrac{n\pi x}{L_{fund}}\right) dx \; - \int_{P_{dn}}^{P_{up}} P_1 \cos\left(\tfrac{n\pi x}{L_{fund}}\right) dx \right\} \\ &= \tfrac{1}{L_{fund}} \textstyle\sum_{k=0}^{K-1} \tfrac{A}{2} \tfrac{m}{L_{pfc}} \quad \left\{ \left[x \tfrac{L_{fund}}{n\pi} \sin\left(\tfrac{n\pi x}{L_{fund}}\right) + \left(\tfrac{L_{fund}}{n\pi}\right)^2 \cos\left(\tfrac{n\pi x}{L_{fund}}\right) \right]_{P_{dn}}^{P_{up}} + \right. \\ &\qquad \left. \left[-P_1 \tfrac{L_{fund}}{n\pi} \sin\left(\tfrac{n\pi x}{L_{fund}}\right) \right]_{P_{dn}}^{P_{up}} \right\} \\ &= \tfrac{1}{L_{fund}} \textstyle\sum_{k=0}^{K-1} \tfrac{A}{2} \tfrac{m}{L_{pfc}} \quad \left\{ \sin\left(\tfrac{n\pi(P_1+P_2)}{L_{fund}}\right) \tfrac{L_{fund}}{n\pi} [\cancel{P_1} + P_2 - \cancel{P_1}] - \sin\left(\tfrac{n\pi P_1}{L_{fund}}\right) \tfrac{L_{fund}}{n\pi} [-\cancel{P_1} + \cancel{P_1}] + \right. \\ &\qquad \left. \left(\tfrac{L_{fund}}{n\pi}\right)^2 \left[\cos\left(\tfrac{n\pi P_{up}}{L_{fund}}\right) - \cos\left(\tfrac{n\pi P_{dn}}{L_{fund}}\right) \right] \right\} \\ &= \tfrac{1}{L_{fund}} \textstyle\sum_{k=0}^{K-1} \tfrac{A}{P_2} \quad \left\{ P_2 \tfrac{L_{fund}}{n\pi} \sin\left(\tfrac{n\pi P_{up}}{L_{fund}}\right) + \left(\tfrac{L_{fund}}{n\pi}\right)^2 \left[\cos\left(\tfrac{n\pi P_{up}}{L_{fund}}\right) - \cos\left(\tfrac{n\pi P_{dn}}{L_{fund}}\right) \right] \right\} \end{aligned}$$

$$b_{n,rise} = \tfrac{1}{L_{fund}} \textstyle\sum_{k=0}^{K-1} \tfrac{A}{P_2} \quad \left\{ -P_2 \tfrac{L_{fund}}{n\pi} \cos\left(\tfrac{n\pi P_{up}}{L_{fund}}\right) + \left(\tfrac{L_{fund}}{n\pi}\right)^2 \left[\sin\left(\tfrac{n\pi P_{up}}{L_{fund}}\right) - \sin\left(\tfrac{n\pi P_{dn}}{L_{fund}}\right) \right] \right\}$$

C.2 Falling part

Once again, variables are used for integral bounds to make the computation easier.

$$\begin{array}{ll} P_1 = 2L_{pfc} & P_2 = \frac{2L_{pfc}}{m} \\ P_{dn} = k * P_1 + P_2 & P_{up} = (k+1) * P_1 \end{array}$$

$$
\begin{aligned}
a_{n,fall} &= \tfrac{1}{L_{fund}} \textstyle\sum_{k=0}^{K-1} \tfrac{A}{2} && \int_{P_{dn}}^{P_{up}} 2 - \tfrac{m}{(m-1)L_{pfc}} \left[x - k*2L_{pfc} - \tfrac{2L_{pfc}}{m}\right] \cos\left(\tfrac{n\pi x}{L_{fund}}\right) dx \\
&= \tfrac{1}{L_{fund}} \textstyle\sum_{k=0}^{K-1} \tfrac{A}{2} && \int_{P_{dn}}^{P_{up}} \tfrac{2(m-1)L_{pfc} - mx + mk*2L_{pfc} + \cancel{m}\cancel{\frac{2L_{pfc}}{m}}}{(m-1)L_{pfc}} \cos\left(\tfrac{n\pi x}{L_{fund}}\right) dx \\
&= \tfrac{1}{L_{fund}} \textstyle\sum_{k=0}^{K-1} \tfrac{A}{2(m-1)} && \left\{ -\tfrac{m}{L_{pfc}} \int_{P_{dn}}^{P_{up}} x \cos\left(\tfrac{n\pi x}{L_{fund}}\right) dx + \int_{P_{dn}}^{P_{up}} \tfrac{2(m-1)\cancel{L_{pfc}} + mk*2\cancel{L_{pfc}} + 2\cancel{L_{pfc}}}{\cancel{L_{pfc}}} \cos\left(\tfrac{n\pi x}{L_{fund}}\right) dx \right\} \\
&= \tfrac{1}{L_{fund}} \textstyle\sum_{k=0}^{K-1} \tfrac{A}{2(m-1)} && \left\{ -\tfrac{2}{P_2} \int_{P_{dn}}^{P_{up}} x \cos\left(\tfrac{n\pi x}{L_{fund}}\right) dx + \int_{P_{dn}}^{P_{up}} 2m(1+k) \cos\left(\tfrac{n\pi x}{L_{fund}}\right) dx \right\} \\
&= \tfrac{1}{L_{fund}} \textstyle\sum_{k=0}^{K-1} \tfrac{A}{2(m-1)} && \left\{ -\tfrac{2}{P_2} \left[x \tfrac{L_{fund}}{n\pi} \sin\left(\tfrac{n\pi x}{L_{fund}}\right) + \left(\tfrac{L_{fund}}{n\pi}\right)^2 \cos\left(\tfrac{n\pi x}{L_{fund}}\right) \right]_{P_{dn}}^{P_{up}} + \right. \\
& && \left. \left[2m(1+k) \tfrac{L_{fund}}{n\pi} \sin\left(\tfrac{n\pi x}{L_{fund}}\right) \right]_{P_{dn}}^{P_{up}} \right\} \\
&= \tfrac{1}{L_{fund}} \textstyle\sum_{k=0}^{K-1} \tfrac{A}{2(m-1)} && \left\{ \sin\left(\tfrac{n\pi P_{up}}{L_{fund}}\right) \tfrac{L_{fund}}{n\pi} \left[2m(1+k) - \tfrac{2P_{up}}{P2} \right] + \right. \\
& && \sin\left(\tfrac{n\pi P_{dn}}{L_{fund}}\right) \tfrac{L_{fund}}{n\pi} \left[-2m(1+k) + \tfrac{2P_{dn}}{P2} \right] + \\
& && \left. \tfrac{2}{P_2} \left(\tfrac{L_{fund}}{n\pi}\right)^2 \left[-\cos\left(\tfrac{n\pi P_{up}}{L_{fund}}\right) + \cos\left(\tfrac{n\pi P_{dn}}{L_{fund}}\right) \right] \right\} \\
&= \tfrac{1}{L_{fund}} \textstyle\sum_{k=0}^{K-1} \tfrac{A}{(m-1)} && \left\{ \sin\left(\tfrac{n\pi P_{up}}{L_{fund}}\right) \tfrac{L_{fund}}{n\pi} \left[m(1+k) - \tfrac{P_{up}}{P2} \right] + \right. \\
& && \sin\left(\tfrac{n\pi P_{dn}}{L_{fund}}\right) \tfrac{L_{fund}}{n\pi} \left[-m(1+k) + \tfrac{P_{dn}}{P2} \right] + \\
& && \left. \tfrac{}{P_2} \left(\tfrac{L_{fund}}{n\pi}\right)^2 \left[-\cos\left(\tfrac{n\pi P_{up}}{L_{fund}}\right) + \cos\left(\tfrac{n\pi P_{dn}}{L_{fund}}\right) \right] \right\}
\end{aligned}
$$

$$
\begin{aligned}
b_{n,fall} &= \tfrac{1}{L_{fund}} \textstyle\sum_{k=0}^{K-1} \tfrac{A}{2(m-1)} && \left\{ \cos\left(\tfrac{n\pi P_{up}}{L_{fund}}\right) \tfrac{L_{fund}}{n\pi} \left[-2m(1+k) + \tfrac{2P_{up}}{P2} \right] + \right. \\
& && \cos\left(\tfrac{n\pi P_{dn}}{L_{fund}}\right) \tfrac{L_{fund}}{n\pi} \left[2m(1+k) - \tfrac{2P_{dn}}{P2} \right] + \\
& && \left. \tfrac{2}{P_2} \left(\tfrac{L_{fund}}{n\pi}\right)^2 \left[-\sin\left(\tfrac{n\pi P_{up}}{L_{fund}}\right) + \sin\left(\tfrac{n\pi P_{dn}}{L_{fund}}\right) \right] \right\}
\end{aligned}
$$

BIBLIOGRAPHY

[1] https://www.audioasylum.com/cgi/vt.mpl?f=amp&m=195943.

[2] Active pfc for electronic power supplies. *VICOR CORPORATION*.

[3] CENELEC Frequency Bands | Band A,Band B,Band C,Band D. http://www.rfwireless-world.com/Terminology/CENELEC-frequency-bands.html.

[4] CISPR guide. http://www.iec.ch/emc/iec_emc/iec_emc_players_cispr.htm.

[5] EN 55011:2009. http://rfemcdevelopment.eu/en/emc-emi-standards/en-55011-2009.

[6] EN 55015:2006. http://www.rfemcdevelopment.eu/en/emc-emi-standards/en-55015-2006.

[7] How fluorescent lamps work. http://sound.whsites.net/lamps/fluoro-lamps.html.

[8] IEC 61000-4-16 Conducted Immunity Testing Lab with EMC / EMI Experts. http://www.keystonecompliance.com/iec-61000-4-16/.

[9] IEC 61000-4-19:2014 | IEC Webstore | electromagnetic compatibility, EMC, smart city. https://webstore.iec.ch/publication/4188#additionalinfo.

[10] Noise suppression by emi filtering: Basics of emi filters, murata manufacturing co., ltd.

[11] Q factor vs bandwidth in octaves band filter -3 dB pass calculator calculation formula quality factor Q to bandwidth BW width octave convert filter BW octave vibration mastering slope dB/oct steepness EQ filter equalizer cutoff freqiency - sengpielaudio Sengpiel Berlin.

[12] Resonant RLC Circuits. http://hyperphysics.phy-astr.gsu.edu/hbase/electric/serres.html.

[13] Spectrogram using short-time Fourier transform - MATLAB spectrogram - MathWorks Benelux.

[14] Power factor correction converter design with fan6982. *Fairchild Semiconductor Corporation*, 2010.

[15] Digital control unveils a new epoch in PFC design, July 2014.

[16] CENELEC. Electromagnetic interference between electrical equipment/systems in the frequency range below 150 khz. *CENELEC SC205A: Mains Communicating Systems*.

[17] Shamim Choudhury. Average current mode controlled power factor correction converter using TMS320LF2407A, TEXAS INSTRUMENTS. July 2005.

[18] S. Galli, A. Scaglione, and Z. Wang. For the grid and through the grid: The role of power line communications in the smart grid. *Proceedings of the IEEE*, 99(6):998–1027, June 2011.

[19] S.A.Mahmoud H.Z.Azazi, E. E. EL-Kholy and S.S.Shokralla. Review of passive and active circuits for power factor correction in single phase, low power acdc converters. *Proceedings of the 14th International Middle East Power Systems Conference*, December 2010.

[20] Challa Mohana Krishna and others. Computationally efficient models for simulation of non-ideal DC–DC converters operating in continuous and discontinuous conduction modes. *Sadhana*, 40(7):2045–2072, 2015.

[21] Anders Larsson. High frequency distortion in power grids due to electronic equipment. 2006.

[22] Anders Larsson. *On high-frequency distortion in low-voltage power systems*. PhD thesis, Luleå University of Technology, Luleå, 2011. OCLC: 727046859.

[23] Bollen M.H.J. Wahlberg M.G. Lundmark C.M Rönnberg S.K. Larsson E.O.A. Measurements of high-frequency (2-150 khz) distortion in low-voltage networks. *IEEE Transactions on Power Delivery, Volume. 25, No. 3, July 2010*.

[24] Caroline Leroi, Emmanuel De Jaeger, and U. C. L. UCL–Belgium. Conducted disturbances in the frequency range 2–150 kHz: influence of the LV distribution grids. In *Proceedings of the 23th CIRED International Conference on Electricity Distribution, Lyon, France*, pages 15–18, 2015.

[25] C. M. Lundmark, E. O. A. Larsson, and M. H. J. Bollen. Required changes in emission standards for high-frequency noise in power systems. *International Journal of Energy Technology and Policy*, January 2006.

[26] C. M. Lundmark, S. K. Ronnberg, M. Wahlberg, E. O. A. Larsson, and M. H. J. Bollen. Emc filter common mode resonance. In *2009 IEEE Bucharest PowerTech*, pages 1–6, June 2009.

[27] Jonas Mühlethaler, Hirofumi Uemura, and Johann W. Kolar. Optimal design of EMI filters for single-phase boost PFC circuits. In *IECON 2012-38th Annual Conference on IEEE Industrial Electronics Society*, pages 632–638. IEEE, 2012.

[28] Asst. Lect. Raed F. Abbas Prof. Dr. Jafar H. Alwash, Asst. Prof. Dr. Turki K. Hassan. Design and implementation of single-phase boost pfc converter. *Journal of Engineering*, December 2013.

[29] Klaus Raggl, Thomas Nussbaumer, and Johann W. Kolar. Guideline for a Simplified Differential-Mode EMI Filter Design. *IEEE Transactions on Industrial Electronics*, 57(3):1031–1040, March 2010.

[30] S. K. Rönnberg, M. H. J. Bollen, and M. Wahlberg. Harmonic emission before and after changing to led and cfl; part i: Laboratory measurements for a domestic customer. In *Proceedings of 14th International Conference on Harmonics and Quality of Power - ICHQP 2010*, pages 1–7, Sept 2010.

[31] Sarah Rönnberg. *Emission and interaction from domestic installations in the low voltage electricity network, up to 150 kHz*. PhD thesis, Luleå University of Technology, Luleå, 2013. OCLC: 940849558.

[32] Sarah Rönnberg and Math Bollen. primary and secondary emission of a pv inverter in the frequency range 2 to 150 khz. *International Journal of Electrical Power and Energy Systems*.

[33] Sarah Rönnberg, Anders Larsson, Math Bollen, and Jean-Luc Schanen. A simple model for interaction between equipment at a frequency of some tens of kHz. In *International Conference on Electricity Distribution: 06/06/2011-09/06/2011*, 2011.

[34] Fu-Yuan Shih, Dan Y. Chen, Yan-Pei Wu, and Yie-Tone Chen. A procedure for designing EMI filters for AC line applications. *IEEE transactions on power electronics*, 11(1):170–181, 1996.

[35] Chris Swartz. The causes and impact of emi in power systems; part 1. *Vicor*.

[36] P. Tenti and G. Spiazzi. Harmonic limiting standards and power factor correction techniques. In *EPE'95*, 1995.

[37] Philip C. Todd. UC3854 controlled power factor correction circuit design. *Unitrode Application Note U-134*, page 278, 1999.

[38] Eric W. Weisstein. Fourier Series. http://mathworld.wolfram.com/FourierSeries.html.

[39] Eric W. Weisstein. Fourier Series–Triangle Wave. http://mathworld.wolfram.com/FourierSeriesTriangleWave.html.

[40] Tim Williams. *EMC for Product Designers: Meeting the European EMC Directive*. Newnes, 2014.

Rue Archimède, 1 bte L6.11.01, 1348 Louvain-la-Neuve **www.uclouvain.be/epl**